University of Genoa
Department of Earth, Environment and Life Sciences

Doctorate School in Science and Technologies for the Environment and Territory
Ph.D. Thesis, XXXIV Cycle

Ph.D. in Earth Science

Title of Ph.D. Thesis

Spatial prediction of landslide susceptibility/intensity through advanced statistical approaches implementation: applications to the *Cinque Terre* (Eastern *Liguria*, Italy)

Advisor:
Prof. Andrea Cevasco (*University of Genoa*)

Co-Advisor:
Prof. Luigi Lombardo (*University of Twente*)

Coordinator of Doctorate School:
Prof. Marco Firpo

Ph.D. candidate:
Mariano Di Napoli

Academic Year 2020/2021

DECLARATION OF ORIGINALITY

I confirm that the work described in this dissertation is my work unless otherwise cited or acknowledged. The thesis is of my composition and has not been submitted for any other degree at the University of Genoa or any other institution.

Mariano Di Napoli

April 2022

Thesis citation: Di Napoli M., 2022. *Spatial prediction of landslide susceptibility/intensity through advanced statistical approaches implementation: applications to the Cinque Terre (Eastern Liguria, Italy)*. Ph.D. thesis, University of Genoa, Department of Earth, Environment and Life Sciences, Genoa, Italy.

ACKNOWLEDGEMENTS

First and foremost, I would like to express my greatest and sincerely thanks to my supervisors Prof. Andrea Cevasco and Prof. Marco Firpo, for giving me this opportunity. They always provided me with a clear guidance, constructive criticism, continuous questions, and trust throughout my Ph.D. study.

Furthermore, I would like to thank my co-tutor, Prof. Luigi Lombardo, because he gave me something priceless: his time. Despite we have worked remotely for more than a year, he guided me through my research project, introducing me to a "completely new world" and always giving me advices and constructive suggestions.

I would further like to thank Prof. Domenico Calcaterra and Dott. Ing. Diego Di Martire for guiding and suggesting me from the beginning of this fantastic adventure.

The list of people to whom saying thank is very long. During my Ph.D. project, I have met more people who gave me useful advice. First of all, a great thank you to Dott. Francesco Carotenuto, who helped me with R programming and performing advanced statistical analyses. Simply, without him, his time, his patience, his help, I would not be here, writing the acknowledgment, because there would not be a thesis at all.

Moreover, I address heartfelt thanks to my colleagues of the group of Geomorphology and Engineering Geology of DiSTAV, in particular to my two "desk-neighbors" Giacomo and Andrea.

Additionally, a dutiful thanks to *Cinque Terre* National Park and, in particular, its Director, Eng. Patrizio Scarpellini, for providing funding and logistic support during field operations.

Then I would like to express my gratitude to my "UNINA" colleagues, and in particular to Pierluigi, who helped and supported me from the first day and during these three years of Ph.D. project, with his advices and discussions. A special thanks also to Alessandro, who gave me useful suggestions with multi-spectral images especially by using Google Earth Engine, and also for engaging me in “foreign” experiences.

Lastly, a special thank goes to Federica for her love and constant support, without which I wouldn’t have achieved this result. Finally, I owe my deepest gratitude to all my family, for their constant and essential support.

LIST OF FIGURES

LIST OF TABLES

LIST OF ACRONYMS

ALS	Airborne Laser Scanning
ANN	Artificial Neural Network
AUC	Area Under Curve
AVI	Areas affected by landslides or floods in Italy
CA	Committee Averaging
CLC	Corine Land Cover
C_n	Detachment point
CRED	Centre for Research on the Epidemiology of Disasters
CTNP	Cinque Terre National Park
CV	Coefficient of Variation
DHE	Damaging Hydrogeological Events
DEM	Digital Elevation Model
DTM	Digital Terrain Model
EM	Ensemble Method
EM-DAT	Emergency Events Database
EPOCH	European Programme On Climate and Natural Hazards
FS	Factor of Safety
GAM	Generalized Additive Model
GAMM	Generalized Additive Mixed Model
GBM	Generalized Boosting Model
GC	Grid Cell
GIS	Geographic Information System
GLM	Generalized Linear Models
GLMM	Generalized Linear Mixed Model
GMRF	Gaussian Markov Random Field
GNSS	Global Navigation Satellite Systems
H	slope Height
IID	Independent and Identically Distributed
IFFI	Inventario dei Fenomeni Franosi – Landslide Inventory in Italy
INLA	Integrated Nested Laplace Approximation

ISPRA	Superior Institute for the Environmental Protection and Research
InSAR	Interferometric Synthetic Aperture Radar
L	runout distance
L1O	Leave-One-Out
LDS	Landslide Detachment Susceptibility
LDTRS	Landslide Detachment, Transit and Runout Susceptibility
LGCP	Log-Gaussian Cox Process
LGM	Latent Gaussian Model
LiDAR	Light Detection And Raging
LIM	Landslide Inventory Map
LR	Likelihhod Ratio
LRS	Landslide Runout Susceptibility
LSE	Latent Spatial Effect
LSM	Landslide Susceptibility Map
MaxEnt	Maximum Entropy
MI	Maximum Invasion
ML	Machine Learning
MCMC	Markov Chain Monte Carlo
PA	Presence-Absence
PC	Penalized Complexity
P-Bg	Presence-Background
PO	Presence Only
PDF	Probability Density Function
PF	Predisposing Factor
PIFF	Punto Identificativo Fenomeno Franoso (Landslide Phenomenon Identification Point)
PM	Mean of Probabilities
PME	Median of Probabilities
PMW	Weighted Mean of Probabilities
PS	Permanent Scatter
RK	Regression Kriging
RW1	Random Walk of the first order

RSP	Relative Slope Position
SDM	Spatial Distribution Model
SPI	Stream Power Index
SU	Slope Unit
TLS	Terrestrial Laser Scanning
TPI	Topographic Position Index
TWI	Topograhic Wetness Index
UCU	Unique Condition Unit
UNESCO	United Nations Educational, Scientific and Cultural Organization
WP/WLI	Working Party on World LandslIde
VIF	Variance Inflation Factor
Y'_n	Maximum invasion point

CHAPTER 1: INTRODUCTION

1.1. Problem statement

Landslides are frequently responsible for considerable huge economic losses and casualties in mountainous regions especially nowadays as development expands into unstable hillslope areas under the pressures of increasing population size and urbanization (Di Martire et al. 2012). People are not the only vulnerable targets of landslides. Indeed, mass movements can easily lay waste to everything in their path, threatening human properties, infrastructures and natural environments.

Italy is severely affected by landslide phenomena and it is one of the most European countries affected by this kind of phenomena. In this framework, Italy is particularly concerned with forecasting landslide effects (Calcaterra et al. 2003b), in compliance with the National Law n. 267/98, enforced after the devastating landslide event of *Sarno* (*Campania*, Southern Italy). According to the latest Superior Institute for the Environmental Protection and Research (*ISPRA*, 2018) report on "hydrogeological instability" of 2018, it emerges that the population exposed to landslides risk is more than 5 million and in particular almost half-million falls into very high hazard zones. The slope stability can be compromised by both natural and human-caused changes in the environment. The main reasons can be summarised into heavy rainfalls, earthquakes, rapid snow-melts, slope cut due to erosions, and variation in groundwater levels for the natural cases whilst slopes steepening through construction, quarrying, building of houses, and farming along the foot of mountainous zone correspond to the human component.

This Ph.D. thesis was carried out in the *Liguria* region, inside the *Cinque Terre* National Park. This area was chosen due to its abundance of different types of landslides and its geological, geomorphological and urban characteristics. The *Cinque Terre* area can be considered as one of the most representative examples of human-modified landscape. Starting from the early centuries of the Middle Ages, local farmers have almost completely modified the original slope topography through the construction of dry-stone walls, creating an outstanding terraced coastal landscape (Terranova 1984, 1989; Terranova et al. 2006; Brandolini 2017). This territory is extremely dynamic since it is characterized by a complex geological and geomorphological setting, where many surficial geomorphic processes coexist, along with peculiar weather conditions (Cevasco et al. 2015). For this reason, part of this research focused on analyzing the disaster that hit the *Cinque Terre* on October, 25th, 2011. Multiple landslides took place in this occasion, triggering almost simultaneously hundreds of shallow landslides in the time-lapse of 5-6 hours, causing 13 victims, and severe structural and economic damage (Cevasco et al. 2012; D'Amato Avanzi et al. 2013). Moreover, this artificial landscape experienced important land-use changes over the last century (Cevasco et al. 2014; Brandolini 2017), mostly related to the abandonment of agricultural activity.

It is known that terraced landscapes, when no longer properly maintained, become more prone to erosion processes and mass movements (Lesschen et al. 2008; Brandolini et al. 2018a; Moreno-de-las-Heras et al. 2019; Seeger et al. 2019).

Within the context of slope instability, the international community has been focusing for the last decade on recognising the landslide susceptibility/hazard of a given area of interest. Landslide susceptibility predicts "where" landslides are likely to occur, whereas, landslide hazard evaluates future spatial and temporal mass movement occurrence (Guzzetti et al., 1999). Although both definitions are incorrectly used as interchangeable. Such a recognition phase becomes crucial for land use planning activities aimed at the protection of people and infrastructures. In fact, only with proper risk assessment governments, regional institutions, and municipalities can prepare the appropriate countermeasures at different scales. Thus, landslide susceptibility is the keystone of a long chain of procedures that are actively implemented to manage landslide risk at all levels, especially in vulnerable areas such as *Liguria*. The methods implemented in this dissertation have the overall objective of evaluating advanced algorithms for modeling landslide susceptibility.

1.2. Structure of the thesis

The thesis has been structured in six chapters. The first chapter introduces and motivates the work conducted in the three years of the project by including information about the research objectives. The second chapter gives the basic concepts related to landslides, definition, classification and causes, landslide inventory, along with the derived products: susceptibility, hazard and risk zoning, with particular attention to the evaluation of landslide susceptibility. The objective of the third chapter is to define the different methodologies, algorithms and procedures applied during the research activity. The fourth chapter deals with the geographical, geological and geomorphological features of the study area. The fifth chapter provides information about the results of the applied methodologies to the study area: Machine Learning algorithms, runout method and Bayesian approach. Furthermore, critical discussions on the outcomes obtained are also described. The sixth chapter deals with the discussions and the conclusions of this research, critically analysing the role of such work in the general panorama of the scientific community and illustrating the possible future perspectives.

1.3. State-of-the-art

Cinque Terre is a terraced coastal landscape that is unique worldwide for its geological, geomorphological and landscape characteristics. At the same time, singular are the issues that the area experiences as a result of: *i*) social and economic changes that have taken place since the

middle of the last century, *ii*) changes due to anthropogenic modification, resulting in river culverts in the terminal stretch of the main water bodies, *iii*) the massive tourist increment which, starting from 2000, has led to a marked increase of risk conditions.

The construction, over the centuries, of dry-stone walls, initially has made it possible to obtain new lands useful for vineyards and olive groves cultivations. Since the First World War, and definitely after the end of the Second World War, the development and encouragement of industrial activities accelerated the progressive abandonment by local farmers. The abandonment of terraced territories determine erosion processes and land degradation. The outcome is the increase of hazards with diffuse problems of instability and huge solid transport in the rivers (Brancucci and Paliaga 2006), especially following abundant/intense rainfalls (Tarolli et al. 2019).

In recent decades, phenomena with high intensity are manifested much more frequently also due to a recognized climate change phase taking place on a planetary level (Seneviratne et al. 2012; Watts et al. 2021). One of the most important events that profoundly marked this territory and the local population was the event of October 2011. This event triggered hundreds of shallow landslides which, once channelled, evolved into flows hitting the *Monterosso* and *Vernazza* hamlets.

From 2011 onwards, several researchers have been accomplished with a substantial increase in scientific production. In particular, in ten years, about 35 papers have been published and two Ph.D. theses on landslides susceptibility have been carried out. In particular, following the October 25th, 2011 event, a detailed inventory of geo-hydrological processes occurred in the *Vernazza* catchment has been implemented and the relations between rainfall-induced shallow landslides and land-use (with specific focus on the degree of abandonment of terraced areas) have been analysed (Cevasco et al. 2012, 2013a). Afterwards, field surveys and engineering geological investigations, including laboratory and in situ tests, were executed at various sites to assess the stratigraphic, hydraulic and geotechnical features of the soil slope covers (Cevasco et al. 2013b). The distribution of the shallow landslides was analysed with respect to the slopes, the bedrock lithology, the land uses and the engineering geological setting. It was firstly noticed that the time since abandonment of terraces played an important role in the occurrence of shallow landslides induced by rainfall (Cevasco et al. 2014).

A first susceptibility model was developed in the *Vernazza* catchment by using the Likelihood Ratio (LR) function and simulation of landslide occurrence as response to land-use change was performed (Galve et al. 2015). Results allowed to define guidelines for reducing landslide risk at short term (applying structural measures over potentially unstable slopes) but also highlighted the need for a long-term programme (promoting the development of agricultural or forestry practices on terraced slopes). The issues related to the choice of proper geo-hydrological risk mitigation

measures and land management were also dealt with in a study performed in the *Vernazza* catchment by Brandolini and Cevasco (2015). At the same time, efforts were made for enhancing landslide susceptibility models at *Vernazza* applying, in particular, data-driven methods (Bordoni et al. 2015). Thank to the availability of pre- and post-event Light Detection And Ranging (LiDAR) data, it was possible to analyze in great detail the role played by human embankments (located along channels, completely or partially destroyed during the event) in worsening the effects of the flash flood that affected the *Vernazza* hamlet (Cevasco and Brandolini 2015).

However, identification and mitigation of landslide risk is still a challenging task for local administrations and policy-makers, being the spatial-temporal prediction of such phenomena still affected by large uncertainties. To this aim, landslide susceptibility assessment is fundamental to improve the understanding of the occurrence of such phenomena (Brabb 1985; Gigli et al. 2014; Lagomarsino et al. 2017). Many methodologies aim at assessing landslide susceptibility maps and in recent years, a significant boost has been gained thanks to robust scientific advances, both among numerical (Baum et al. 2008; Schilirò et al. 2018; Park et al. 2019) and statistical approaches (van Westen et al. 2003; Yalcin et al. 2011; Goetz et al. 2015; Lombardo et al. 2016; Xiao et al. 2019). The inventories employment of past landslides coupled with environmental factors can be used to train statistical models (Ermini et al. 2005; Vorpahl et al. 2012; Segoni et al. 2015). No standard susceptibility procedure has ever been established, hence making possible the exploitation of numerous different algorithms and methodologies. Statistical landslide susceptibility methods have been extensively applied in different settings, models and spatial scales (Felicísimo et al. 2013; Trigila et al. 2015; Kornejady et al. 2017; Arabameri et al. 2019, 2021; Novellino et al. 2021). Among the new statistical approaches, Machine Learning algorithms are more and more recurrent, gaining new consideration. Many algorithms have been applied to landslide susceptibility maps, as testified by wide scientific literature, such as Artificial Neural Network (Lee et al. 2004; Abbaszadeh Shahri et al. 2019), Random Forest (Catani et al. 2013; Chen et al. 2019) and MaxEnt (Lombardo et al. 2016; Kim et al. 2018).

Addittionally, with the aim of contributing to a better understanding of the relationships between extreme events, climate change and geomorphic phenomena, in view of the risks that such phenomena represent for both people and tourists, the response of coastal basins of easternmost *Liguria* to severe rainfall over time and the time-scale at which changes on extreme rainfall events occur was investigated (Cevasco et al., 2015). In particular, changes in storm erosivity and their relationships with the occurrence and severity of DHEs (Damaging Hydrogeological Events) for the period 1954-2011 were analysed. This study confirmed that the values of the October 25th 2011 event, both in terms of cumulative precipitation and rainfall intensity records, have never been

achieved in the reference period. Furthermore, a more pronounced impulsive storminess was observed after 1991, with erosivity exceeding in various years the one standard deviation in the last two decades, and evidence of more frequent extreme events in recent times, with two rainfall events with return periods higher than 100 years since 1980, indicated a potential increase in the frequency of DHEs.

Effectively, rainfall-triggered landslides are notoriously dangerous phenomena capable of causing serious damage and a notable death toll as well as important economic losses worldwide. Shallow landslides usually occur on steep soil-mantled slopes (Dietrich et al. 1995; Guzzetti et al. 2008; Cevasco et al. 2014) as a consequence of heavy or intense rainfalls and often may evolve into potentially catastrophic flow-like movements. The consequences of shallow landslides and flow-like phenomena are typically more dangerous in inhabited centres located at the foot of slopes, where the hydrographic network is well developed, which can impact buildings and infrastructure located in lowland areas, threatening people's safety. Moreover, the consequences of incorrect urban and land-use planning can be disastrous (Di Martire et al. 2012). These natural disasters undoubtedly suggest the importance of improving existing urban planning tools, including also runout analyses. The spatial and temporal hazard posed by flow-like movements is determined by both source-related features (e.g., location and volume) and subsequent runout dynamics (e.g., travelled paths and distances; Fan et al. 2017). Therefore, in addition to the identification of potential landslide source areas, it is crucial to investigate landslide runout (i.e., travel distance) and incorporate it into landslide hazard or susceptibility assessments. For this reason, landslide susceptibility zoning should include information about landslide source areas as well as downslope areas that might be affected by mobilized materials. Unfortunately, most of the available landslide zoning maps only examine susceptibility to landslide detachment, not considering transit and runout analyses. These shortcomings have a great impact on final hazard models and urban planning.

In addition, researches in the *Vernazza* catchment progressed investigating the relationships between landslide magnitude and land use conditions of agricultural terraced slopes. In particular, LiDAR elevation data, coupled with aerial photo interpretation, were used for the computation of shallow landslide mobilized volumes on terraced slopes affected by the intense rainfall event of October 25th, 2011. It was found that abandoned terraced slopes have been affected by a higher amount of mobilized debris volumes than still-cultivated terraces. In particular, terraces abandoned for a short time (less than 25–30 years) resulted the most hazardous land-use class, showing erosion rates that were approximately 2 and 3 times higher than terraced slopes abandoned a long time ago (more than 25–30 years) and still-cultivated terraces, respectively (Brandolini et al. 2018a). New researches on landslide susceptibility were performed in the *Vernazza* catchment by applying a

data-driven method (Generalized Additive Model) and the elaboration of different land-use scenarios were used to assess the influence of the land-use change on the landslides occurrence (Persichillo et al. 2016, 2017a).

An original methodology, which enables risk assessments to be accomplished in fully quantitative terms, integrating both physical and economic science techniques was then proposed and applied to the *Vernazza* catchment (Galve et al. 2016). This risk assessment combined geomorphological studies, probabilistic modelling and cost-benefit analyses. The cost-effectiveness of several landslide mitigation measures applying the proposed procedure was analysed. The results demonstrate that measures previously considered as suitable for mitigating shallow landslides were inappropriate from the economic viewpoint. The applied techniques also served to optimize economically the most appropriate mitigation measure for the study area.

Researches on landslide susceptibility developed also in the area of *Monterosso*, which was heavily affected by the effects of the October 25th, 2011 event. In particular, after compiling a detailed shallow landslide inventory and a specific land-use map for the *Monterosso* and some neighbouring basins, a physically-based stability model (TRIGRS) was applied to reproduce the landslide event was applied (Schilirò et al. 2017, 2018). Data from the October 25th, 2011 event at *Cinque Terre* were included in a study which the main purpose was the comparison of three different statistical techniques (least-squares linear fit, quantile regression and logistic regression) used to determine the rainfall thresholds for shallow landslides occurrence in the *Riviera Spezzina* area (Galanti et al. 2018). New studies on landslide susceptibility assessment through probabilistic/statistical and physically-based methods were developed in the *Vernazza* catchment (Raso et al. 2020a, Raso, Ph.D. thesis; Raimondi Ph.D. thesis). Other studies in the same area, using data from the October 25th, 2011 allowed (*i*) to develop a new approach for defining and computing a sediment connectivity index (Zingaro et al. 2019); (*ii*) to confirm the role played by the degree of abandonment of terraces on shallow landslides distribution (Pepe et al. 2019); (*iii*) to evaluate the influence of the choices made when compiling a rainfall-induced shallow landslide inventory on the determination of susceptibility obtained by using generalized additive models (Persichillo et al. 2017b; Bordoni et al. 2020).

As regards the area of the *Cinque Terre* National Park, a lot of studies were conducted to produce: (*i*) a comprehensive landslide inventory map (Raso et al. 2019a) and its interaction with the trail network (Raso et al. 2019a); (*ii*) a new procedure for effective management of geo-hydrological risks across the "*Sentiero Verde-Azzurro*" (Giordan et al. 2020); (*iii*) a comprehensive geomorphological map (Raso et al. 2020b). Furthermore, this dissertation discusses the different advanced statistical techniques for landslide susceptibilities, such as Machine Learning and

Bayesian models. In addition, being the current literature lacking and in the study region completely unexplored, the landslide runout evaluation has been performed in order to predict areas potentially concerned (further information in the next section).

1.4. Research objectives

The main objective of this study is to increase the slope instability state of knowledge. The different outcomes were achieved through the implementation of advanced statistically-based methods and the acquisition of new input data.

In particular, the research will focus on three case studies:

The first one is represented by the *Monterosso al Mare* case study, an area of about 5.5 km^2. Landslide susceptibility maps were produced using three different Machine Learning algorithms, namely Artificial Neural Network, Generalized Boosting Model and Maximum Entropy. These methods were subsequently "ensembled" to assess the proneness instability of the area. Moreover, in order to compare the results obtained from all the ensemble models and to asses model uncertainty, the coefficient of variation has been computed. In this way, the reliability of ensemble models has been evaluated.

The second case study will consider the whole *Cinque Terre* National Park territory. In this case, the adoption of a combined approach allowed to estimate shallow landslide susceptibility to both detachment and potential runout. At first, landslide triggering susceptibility was assessed using Machine Learning techniques. Then, a Geographical Information System-based procedure was applied to estimate the potential landslide runout using the "reach angle" method. Information from such analyses were combined to obtain a susceptibility map related to detachment, transit, and runout.

Lastly, the *Monterosso* and *Vernazza* catchments were taken into account. In these case studies, the Bayesian approach was investigated in order to examine the relation between landslide intensity (how many landslides may occur per mapping unit) and the extent of landslides to generate maps that predict the aggregated size of landslides per mapping unit, and the portion they may affect.

CHAPTER 2: LANDSLIDES

2.1. Landslide definition and classifications

Landslides are one of the main natural hazards, for extent, impact on man-made infrastructures and properties and number of casualties. Since 1988, the Centre for Research on the Epidemiology of Disasters (CRED) has preserved the Emergency Events Database (EM-DAT) and every year it publishes an "Annual Disaster Statistical Review". In 2020, 389 natural disasters have been recorded with 15080 deaths, 98.4 million people affected and 171.3 billion US$ in economic losses worldwide. Apart from the COVID-19 pandemic, the year 2020 was dominated by climate-related disasters. In comparison to the previous two decades (2000-2019), 2020 had a higher impact in terms of several recorded events and economic losses. Floods were the most common disaster worldwide, often associated with landslides. Obviously, landslides represent one of the most impactful events affecting human activities and, globally, the costs of their exposure to hazard are quite significantly relevant (Guzzetti, 2000; Battistini et al., 2013; Froude & Petley, 2018).

Although a large number of definition and classifications has been given in the literature for landslides (Nemčok et al. 1972; Varnes 1978; Hutchinson 1988; Cruden 1991; WP/WLI 1991; Cruden and Varnes 1996), a very simple one was proposed by (Varnes 1978): *a downward and outward movement of a mass of rock, debris, or earth down a slope, under the influence of gravity*. Considering the noteworthy increase of devastating landslide events, the UNESCO Working Party on World Landslide Inventory claimed for an establishment of a detailed list of the World's landslides. One of the first assignments has been to establish a Working Party, to propose methods of classifying the rates of landslides movement, their causes, the geology and activity and distribution of movement within landslides (WP/WLI 1993). One of the most common classifications for landslides is based on two terms: *i*) the first concerns the material involved, *ii*) the second describes the type of movement (Varnes 1978). The landslide materials may be geotechnically described as either rock (a solid and cemented aggregate of particles), soil (a cohesionless aggregate of coarse-grained particles, *i.e.* debris, or fine-grained particles, *i.e.* earth). As regards the movements, seven different types have been classified and depicted (Fig. 2.1):

- **Falls**: abrupt displacements of geologic materials, such as rocks and boulders, that become detached from steep slopes or cliffs. Separation occurs along discontinuities such as fractures, joints, and bedding planes, and movement develops by free-fall, bouncing, and rolling. Falls are strongly influenced by gravity, mechanical weathering, and the presence of interstitial water.
- **Topples**: mass movements of different materials consisting in a forward rotation about a fulcrum point.

- **Rotational slides**: a slide in which the surface of rupture is curved concavely upward and the slide movement is roughly rotational about an axis that is parallel to the ground surface and transverses across the slide.
- **Translational slides**: the landslide mass moves along a roughly planar surface with little rotation or backward tilting.
- **Spreads**: they usually occur on very gentle slopes or flat terrain. The dominant mode of movement is lateral extension accompanied by shear or tensile fractures. When coherent material, either bedrock or soil, rests on materials that liquefy, the upper units may undergo fracturing and extension and may then subside, translate, rotate, disintegrate, or liquefy and flow.
- **Flows**: mass movements characterized by five basic categories that differ from each other.
    a) Debris flow: is a form of rapid mass movement in which a combination of loose soil, rock, organic matter, air, and water mobilize as a slurry that flows downslope. The main characteristic of these phenomena is the presence of an established channel. Debris flows are commonly caused by intense surface-water flow, due to heavy precipitation or rapid snowmelt, that erodes and mobilizes loose soil or rock on steep slopes. Debris-flow source areas are often associated with steep gullies, and debris-flow deposits are usually indicated by the presence of debris fans at the mouths of gullies. Moreover, fires that denude slopes of vegetation intensify the slopes susceptibility to debris flows.
    b) Debris avalanche: is a very rapid to extremely rapid shallow flow of partially or fully saturated debris on a steep slope without confinement in an established channel. The depositional landform constructed by debris avalanche is a laterally unconstrained colluvial apron, difficult to interpret in terms of individual paths. Therefore, debris avalanche term should be reserved for events that remain poorly channelled and without a laterally bounded deposition landform. Moreover, also the water content is spatially variable. Often, a relatively dry mass of debris may move on a thin, saturated basal layer liquefied by over-riding.
    c) Earthflow: have a characteristic “hourglass” shape. The slope material liquefies and runs out, forming a bowl or depression at the head. The flow itself is elongated and usually occurs in fine-grained materials or clay-bearing rocks on moderate slopes and under saturated conditions. However, dry flows of granular material are also possible.
    d) Mudflow: is an earthflow consisting of material that is wet enough to flow rapidly and that contains at least 50 per cent sand-, silt-, and clay-sized particles.

e) Creep: is the imperceptibly slow, steady, downward movement of slope-forming soil or rock. Movement is caused by shear stress sufficient to produce permanent deformation, but too small to produce shear failure. Creep is indicated by curved tree trunks, bent fences or retaining walls, tilted poles or fences, and small soil ripples or ridges.

- **Complex landslides**: consist of the composition of one or more types of movements, one following the others.

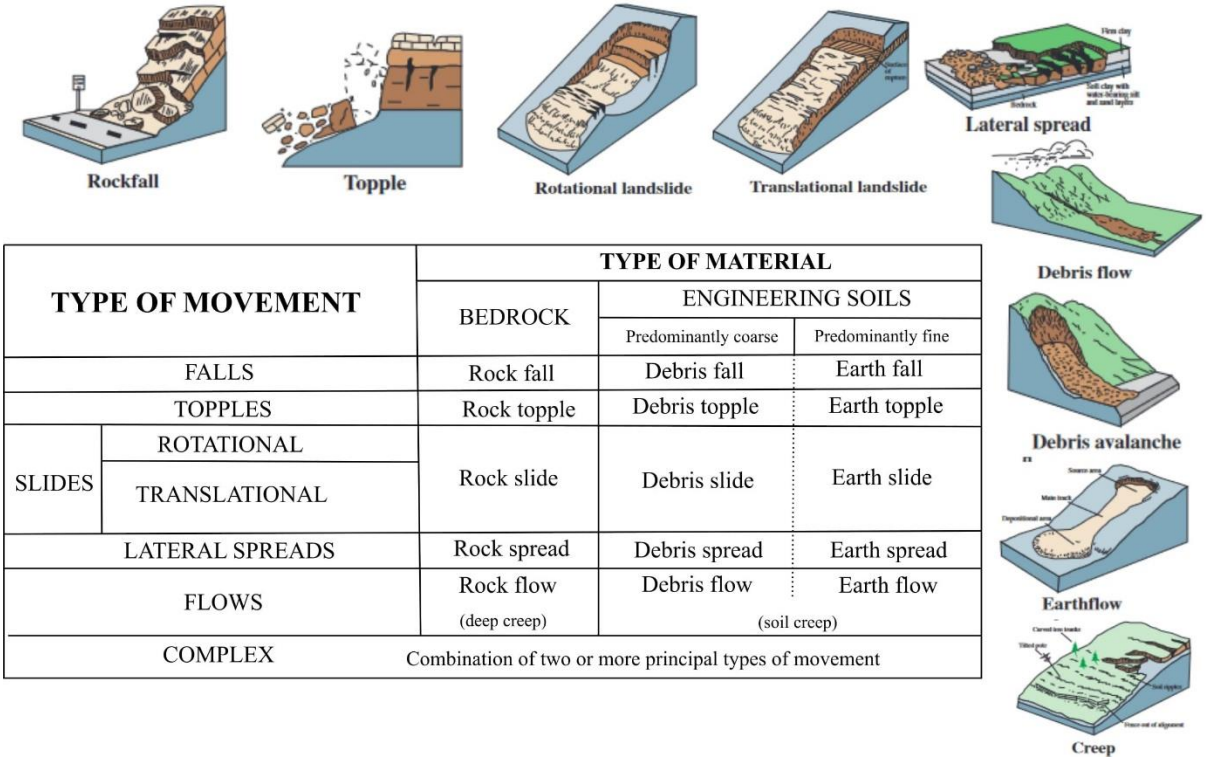

TYPE OF MOVEMENT		TYPE OF MATERIAL		
		BEDROCK	ENGINEERING SOILS	
			Predominantly coarse	Predominantly fine
FALLS		Rock fall	Debris fall	Earth fall
TOPPLES		Rock topple	Debris topple	Earth topple
SLIDES	ROTATIONAL	Rock slide	Debris slide	Earth slide
	TRANSLATIONAL			
LATERAL SPREADS		Rock spread	Debris spread	Earth spread
FLOWS		Rock flow (deep creep)	Debris flow (soil creep)	Earth flow
COMPLEX		Combination of two or more principal types of movement		

Figure 2.1 Abbreviated version of Varnes' classification of slope movements (Varnes 1978).

However, the importance of providing significant information concerning the age, the mechanism and the style of the movement has been more and more acknowledged by earth scientists and governments. Starting from the experiences of the various WP/WLI, and especially within the WP/WLI of 1993, a glossary was drawn up on the terminology to be used to unambiguously describe landslides. Such glossary provided a rationalization of the terms, starting from Varnes classification, and finalized into the Cruden and Varnes classification of 1996. First of all, just five of the former seven categories of typology of movement have been distinguished, referring only to falls, topples, slides, flows and spreads, then including rotational and translational slides into one category, and eliminating the complex typology.

Moreover, the ***state of activity***, which describes, through geomorphological information, the temporal evolution characteristics of a landslide, has been defined, selecting eight different types (Fig. 2.2). **Active** landslides (Fig. 2.2,1) are those that are currently moving, including first-time movements and reactivations (Fig. 2.2,3). Landslides that have moved within the last annual cycle

of the season but that are not moving at the present are described as **suspended** (Fig. 2.2,2). **Inactive** landslides (Figs. 2.2,5-8) are those whose last movement dates back to more than one annual seasonal cycle. The **inactive** landslides can be further subdivided into the following states: **dormant** (when reactivation is possible; Fig. 2.2,5), **abandoned** (when it is no longer influenced by its original triggers; Fig. 2.2,6), **stabilized** (after natural or artificial protective measures; Fig. 2.2,7) and **relict** (when it developed in a geomorphological and climatic condition completely different from the actual situation; Fig. 2.2,8).

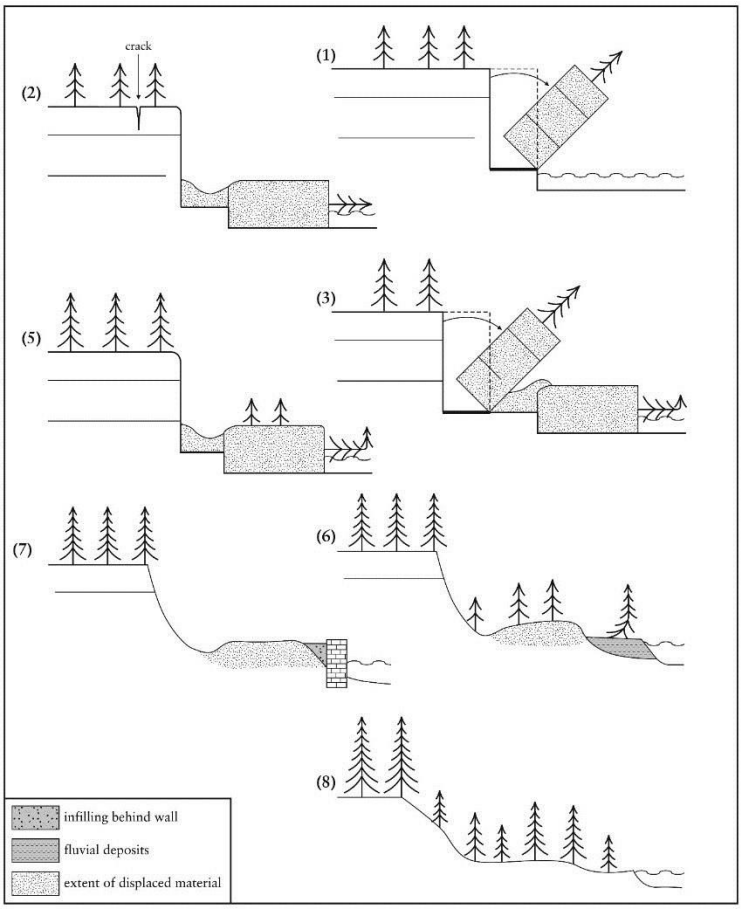

Figure 2.2 Scheme of the state of activity of a landslide, modified from (WP/WLI 1993). Profile section of topples with different states of activity: 1) active: erosion at the toe of the slope causes the block to topple; 2) suspended: cracking in the crown of topple; 3) re-activated: another block topples; 5) dormant: displaced mass begins to regain its tree cover and scarps are modified by weathering; 6) abandoned: the fluvial deposition has protected the toe of the slope; 7) stabilized: retaining wall protects the toe of the slope and 8) relict: uniform tree cover over a slope. State 4 (inactive) comprehends states 5-8.

Another important task that has been defined by the (WP/WLI 1993) is the delineation of the ***distribution of activity***, which refers to how and where the landslide is moving (Fig. 2.3). An **advancing** landslide (Fig. 2.3a) has the rupture surface extending in the direction of movement. In a **retrogressive** landslide (Fig. 2.3b) the rupture surface is extending in the opposite direction to the movement of the displaced material. If the rupture surface of the landslide is extending in two or more directions the landslide is **enlarging** (Fig. 2.3c). In a **diminishing** landslide (Fig. 2.3d) the

volume of displaced material is decreasing. The presence of a scarp, with no clearly visible rupture surface of the displaced mass, is defined as a **confined** landslide (Fig. 2.3e). In a **moving** landslide (Fig. 2.3f) the displaced material continues to move without any visible change in the rupture surface and the volume of the displaced material. Lastly, a **widening** landslide (Fig. 2.3g) has the rupture surface extending into one or both flanks of the landslide.

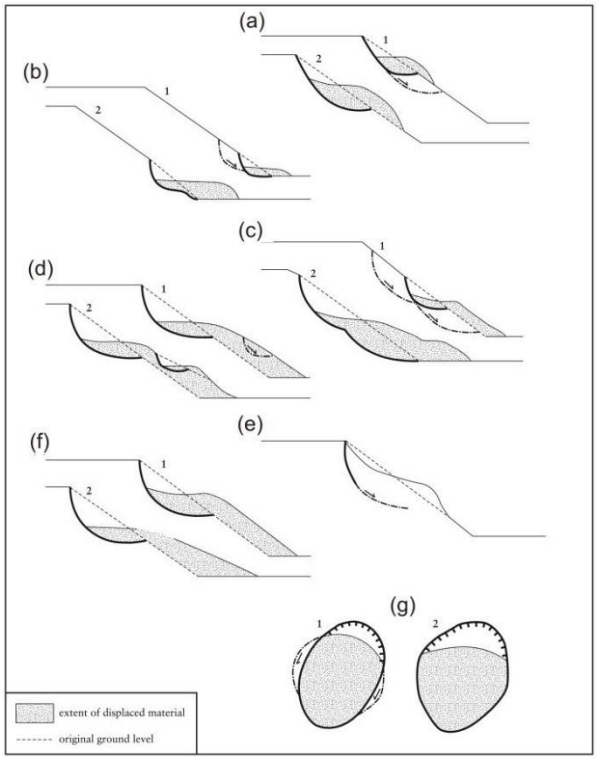

Figure 2.3 Profile section through landslides showing different distributions of activity: advancing (a); retrogressing (b); enlarging (c); diminishing (d); confined (e); moving (f) and widening (g); from (WP/WLI 1993).

To conclude, also the ***style*** of a landslide ***activity*** has been defined and described, consisting of the contribution of different movements within a single landslide and their relationship (Fig. 2.4). A complex landslide (Fig. 2.4a) exhibits at least two types of movement (falling, toppling, sliding, spreading and flowing) in temporal sequence. At least two types of movement simultaneously in different parts of the displacing mass characterize a **composite** landslide (Fig. 2.4b). A **successive** landslide (Fig. 2.4c) is the same as a nearby, earlier landslide, but does not share displaced material or rupture surface with it. In a **single** landslide (Fig. 2.4d) there is only a single movement of displaced material, whereas a **multiple** landslide (Fig. 2.4e) shows repeated development of the same type of movement.

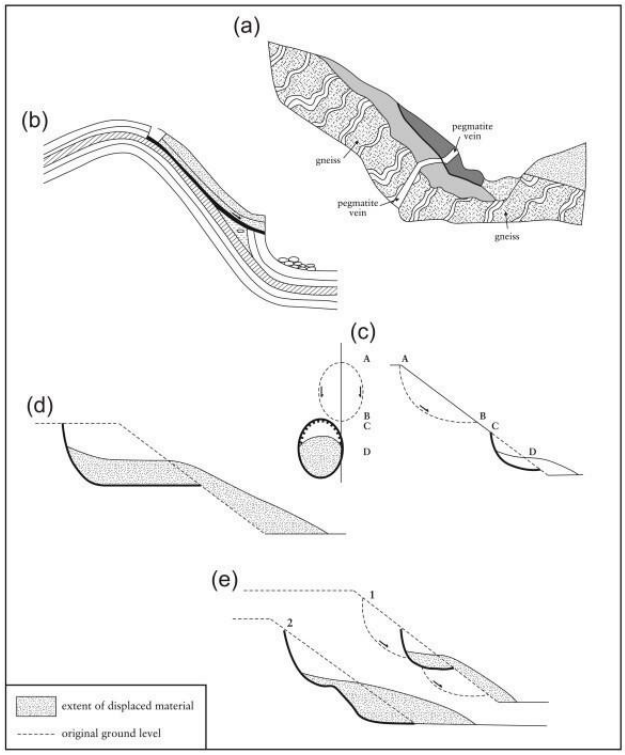

Figure 2.4 Section through landslides showing different styles of activity (WP/WLI 1993): complex (a); composite (b); successive (c); single (d) and multiple (e).

Finally, Cruden and Varnes (1996) introduced a velocity scale, rationalizing all the previous scales. For a landslide, velocity is intended as the highest speed attained after the slope failure. The velocity of mass movement is one of the most important aspects in landslide studies and it represents a very important parameter for the risk assessment in hazardous areas. In Figure 2.5 seven classes of velocity and the related probable destructive significance have been identified. They range from extremely rapid events the rate of which can exceed the speed of a running person (5 m/sec) to extremely slow events (below 16 mm/year) which can be imperceptible without appropriate instruments.

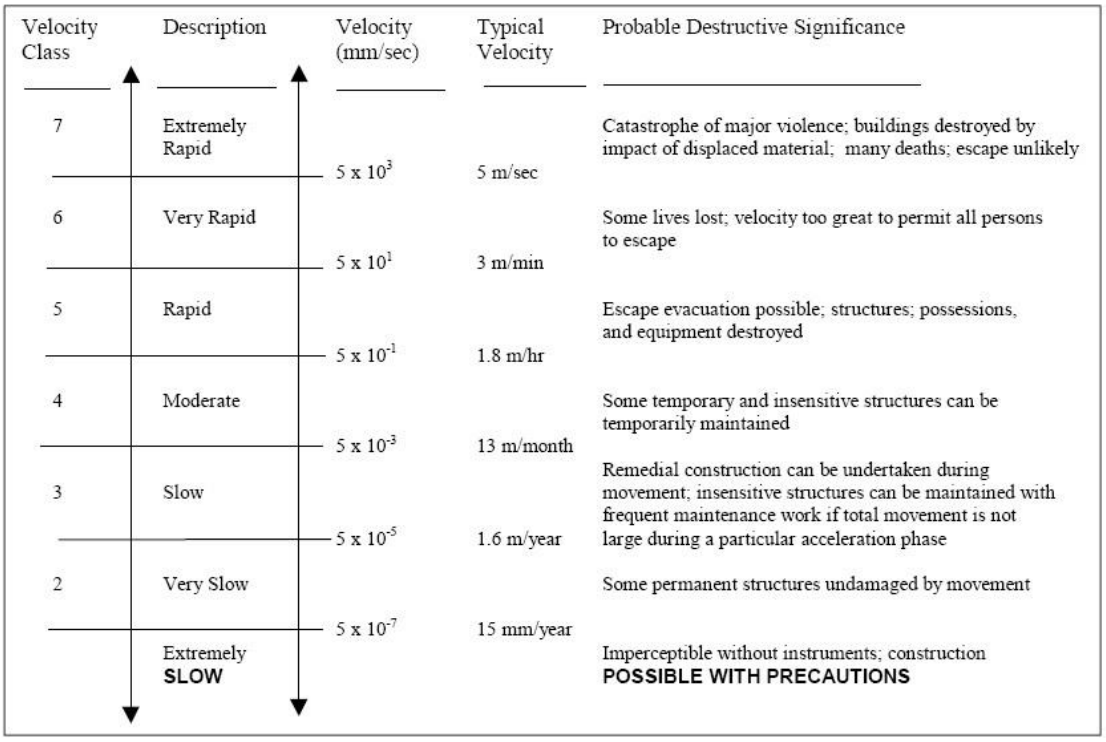

Figure 2.5 The landslide velocity classification and the corresponding potential damage (Cruden and Varnes 1996).

It is worth mentioning that other classifications have been proposed in engineering geological studies, starting from Balzer (1875) onward, but Varnes (1978), ideating a classification based on the type of material involved and type of movement, has given a first modern approach. Successively, Pierson and Costa (1987) focused their attention to classify the flow type landslide, based on velocity and sediment concentration. Hutchinson (1988) proposed a geomorphological and geotechnical approach, shown in Figure 2.6, and then the European Programme On Climate and Natural Hazards, (EPOCH 1993) focused their efforts on classifying landslides based on the European experiences and conditions. Dikau et al. (1996) suggested a classification of landslide mechanisms compatible with Hutchinson (1988) and (EPOCH 1993), and finally, Hungr (2001) analyzed and re-organized the flow-type landslides, based on the genetic and the morphological aspects, and in the year 2014 attempted to revise several aspects of the well-known classification of Varnes (1978), modifying the definition of landslide-forming materials and providing compatibility with accepted geotechnical and geological terminology of rocks and soils, and in conclusion, individuating 32 landslide types.

A	Rebound		
		1	Movements associated with man-made excavations
		2	Movements associated with naturally eroded valleys
B	Creep		
		1	Superficial, predominantly seasonal creep; mantle creep
		2	Deep-seated, continuous creep; mass creep
		3	Pre-failure creep; progressive creep
		4	Post-failure creep
C	Sagging of mountain slopes		
		1	Single-sided sagging associated with the initial stages of landsliding
		2	Double-sided sagging, associated with the initial stages of double landsliding, leading to ridge spreading
		3	Sagging associated with multiple toppling
D	Landslides		
		1	Confined failures
		2	Rotational slips
		3	Compound failures (markedly non-circular, with listric or bi-planar slip)
		4	Translational slides
E	Debris movements of flow-like form		
		1	Mudslides (non-periglacial)
		2	Periglacial mudslides (gelifluction of clays)
		3	Flow slides
		4	Debris flows, very to extremely rapid flows of wet debris
		5	Sturzstroms, extremely rapid flows of dry debris
F	Topples		
		1	Topples bounded by pre-existing discontinuities
		2	Topples released by tension failure at rear of mass
G	Falls		
		1	Primary, involving fresh detachment of material; rock and soil falls
		2	Secondary, involving loose material, detached earlier; stone falls
H	Complex slope movements		
		1	Cambering and valley-bulging
		2	Block-type slope movements
		3	Abandoned clay cliffs
		4	Landslides breaking down into mudslides or flows at the toe
		5	Slides caused by seepage erosion
		6	Multi-tiered slides
		7	Multi-storeyed slides

Figure 2.6 Hutchinson classification of landslides (modified from Hutchinson 1988).

In this thesis, the Cruden and Varnes (1996) classification has been followed.

2.2. Landslides features

Regardless of the exact definition used or the type of landslide under discussion, understanding the basic parts of a typical landslide is helpful. Figure 2.7 shows the position and the most common terms used to describe the unique parts of a landslide.

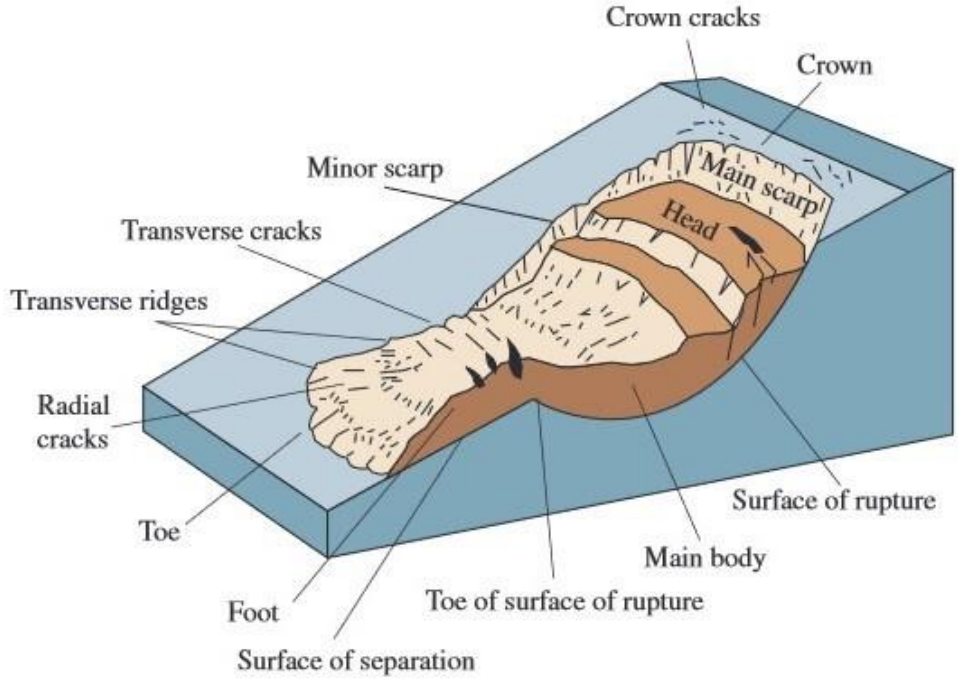

Figure 2.7 An idealized landslide showing commonly used nomenclature for labelling the parts of a landslide (from Highland and Bobrowsky 2008).

Crown: the non-mobilized material still in place and adjacent to the highest parts of the main scarp.

Main Scarp: a steep surface on the undisturbed ground at the upper edge of the landslide, caused by movement of the displaced material away from the undisturbed ground.

Top: the highest point of contact between the displaced material and the main scarp.

Head: the upper parts of the landslide along the contact between the displaced material and the main scarp.

Minor Scarp: a steep surface on the displaced material of the landslide produced by differential movements within the displaced material.

Main Body: the part of the displaced material of the landslide that overlies the surface of rupture between the main scarp and the toe of the surface of rupture.

Foot: the portion of the landslide that has moved beyond the toe of the surface of rupture and overlaid the original ground surface.

Tip: the point of the toe farthest from the top of the landslide.

Toe: the lower, usually curved margin of the displaced material of a landslide, it is the most distant from the main scarp.

Surface of Rupture: the surface which forms (or which has formed) the lower boundary of the displaced material below the original ground surface.

Toe of the Surface of Rupture: the intersection (usually buried) between the lower part of the surface of rupture of a landslide and the original ground surface.

Surface of Separation: the part of the original ground surface overlain by the foot of the landslide.

Displaced Material: material displaced from its original position on the slope by movement in the landslide. It forms both the depleted mass and the accumulation.

Zone of Depletion: the area of the landslide within which the displaced material lies below the original ground surface.

Zone of Accumulation: the area of the landslide within which the displaced material lies above the original ground surface.

Depletion: the volume bounded by the main scarp, the depleted mass and the original ground surface.

Depleted Mass: the volume of the displaced material, which overlies the rupture surface but underlies the original ground surface.

Accumulation: the volume of the displaced material, which lies above the original ground surface.

Flank: the undisplaced material adjacent to the sides of the rupture surface. Compass directions are preferable in describing the flanks but if left and right are used, they refer to the flanks as viewed from the crown.

Original Ground Surface: the surface of the slope that existed before the landslide took place.

Important as well is to define the landslide dimensions, as provided by WP/WLI (1993). In Figure 2.8 the main characteristics are illustrated.

1. **Width of the Displaced Mass**: the width of the displaced mass, Wd, is the maximum width of the displaced mass perpendicular to the length of the displaced mass, Ld.
2. **Width of the Rupture Surface**: the width of the rupture surface, Wr, is the maximum width between the flanks of the landslide, perpendicular to the length of the rupture surface, Lr.
3. **Total length**: the total length, L, is the minimum distance from the tip of the landslide to the crown.
4. **Length of the Displaced Mass**: the length of the displaced mass, Ld, is the minimum distance from the tip to the top.
5. **Length of the Rupture Surface**: the length of the rupture surface, Lr, is the minimum distance from the toe of the surface of rupture to the crown.
6. **Depth of the Displaced Mass**: the depth of the displaced mass, Dd, is the maximum depth of the displaced mass, measured perpendicular to the plane containing Wd and Ld.

7. **Depth of the Rupture Surface**: the depth of the rupture surface, Dr, is the maximum depth of the rupture surface below the original ground surface measured perpendicular to the plane containing Wr and Lr.

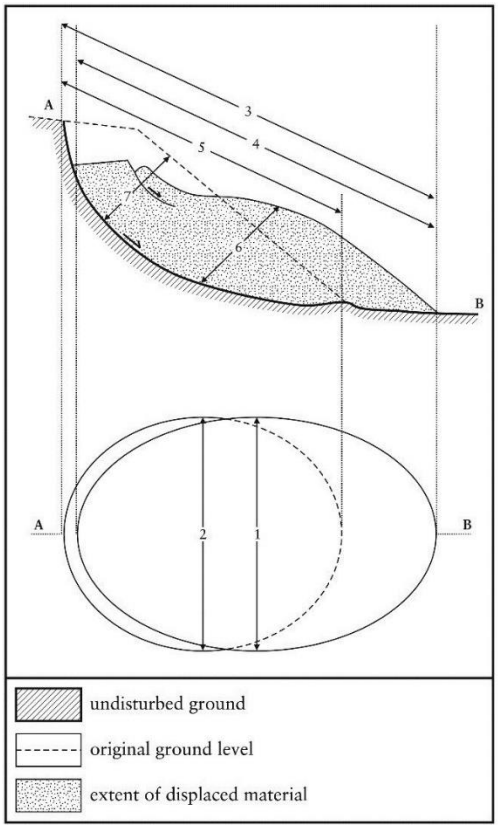

Figure 2.8 Landslide dimensions (modified from WP/WLI 1993).

2.3. Landslide causes

There are two primary categories of causes of landslides: natural and human-caused. Sometimes, landslides are caused, or made worse, by a combination of the two factors. The **natural occurrence** has three major triggering mechanisms that can occur either singly or in combination: 1) *water*, 2) *seismic activity* and 3) *volcanic activity*. Effects of all of these causes vary widely and depend on factors such as slope steepness, morphology or shape of the terrain, soil type, underlying geology, and whether there are people or structures in the affected areas.

Slope saturation by **water** represents the main trigger for landslide activation; in particular, the slope saturation by water is the primary reason (Iverson et al. 1997). Very often, this is an effect of prolonged and intense rainfalls (Iverson 2000), snowmelts (Cardinali et al. 2000) or generally changes in the groundwater levels, also along coastlines, earth dams, reservoirs and canals and rivers. Steep wildfire-burned slopes often are landslide-prone due to a combination of the burning and resultant denudation of vegetation on slopes, a change in soil chemistry due to burning, and subsequent saturation of slopes by water from various sources, such as rainfall.

Also, **seismic activity** increases the instability of mountainous areas, and consequently the likelihood of slopes to landslide occurrence (Lombardo et al. 2019a). Earthquakes in steep landslide-prone areas greatly increase the likelihood that landslides will occur, due to ground shaking alone, liquefaction of susceptible sediments, or shaking-caused dilation of soil materials, which allows rapid infiltration of water.

As a final point, the **volcanic activity** embodies one of the most destructive types of trigger for landslides, whereas the lava can melt snow and ice, and facilitate flooding on the slopes of volcanoes and surrounding mountains, generating the so-called lahars, volcanic debris flows (Scott et al. 2005).

Populations expanding onto new land and creating neighbourhoods, towns, and cities are the primary means by which **humans** contribute to the occurrence of landslides. Disturbing or changing drainage patterns, destabilizing slopes, and removing vegetation are common human-induced factors that may initiate landslides. Other examples include overstepping of slopes by undercutting the bottom and loading the top of a slope to exceed the bearing strength of the soil or other component material.

2.4. Landslide mapping and inventory

Landslide Inventory Map (LIM) is a fundamental tool for landslide hazard evaluation. Inventories denote areas that are identified as having failed by landslide processes. A faithful and detailed representation of landslide inventories is commonly reputed as an essential component to generate reliable susceptibility maps (Ardizzone et al. 2002; Galli et al. 2008; Guzzetti et al. 2012; Fressard et al. 2014; Steger et al. 2015, 2016).

To produce a reliable map that predicts the landslide hazard and risk in a certain area, it is crucial to have insight into the spatial and temporal frequencies of landslides, and therefore each landslide hazard or risk study should begin with a LIM that is as complete as possible in both space and time (Corominas et al. 2014). The level of detail of these maps ranges from simple reconnaissance inventory that only delineates broad area where landsliding appears to complex inventories that depict and classify each landslide and involve the location, classification, volume, travel distance, state of activity and date of occurrence of landsliding in an area (Fell et al. 2008).

For the aforementioned reasons, in recent literature, many researchers have examined the role of landslide inventories on landslide susceptibility analysis (Ardizzone et al. 2002; Galli et al. 2008; Guzzetti et al. 2012; Fressard et al. 2014). The latest innovative and interesting findings have been introduced by Steger et al. (2016) and Bordoni et al. (2020). Steger et al. (2016) examined how inventory-based positional inaccuracies affect the related landslide susceptibility maps. An increase

in the positional error leads to an increased distortion of modelling and validation results. This first study emphasizes how high predictive performance is necessary but not sufficient to obtain reliable landslide susceptibility maps. In fact, the authors have proved that high AUC values can be reached by susceptibility maps with poor geomorphic plausibility and the inclusion of a bias may enhance the apparent predictive performance of a model if a predictor describes this bias.

Detailed and complete work has been conducted by (Bordoni et al. 2020). The main objective of this study was to highlight possible differences in the reconstruction of susceptibility maps obtained for the same study area, using different shallow landslides inventories criteria. In particular, three scenarios were tested: *i*) maps created using inventories of events that occurred in different moments in the same area; *ii*) different methods to identify shallow landslides according to different detection techniques; *iii*) different criteria as regards shallow landslide inventories. The authors argue that, for each considered study area, susceptibility models prepared using different inventories have similar and good predictive capability, but the agreement between the models and the distribution of susceptibility classes is fair. These results highlight the importance of the type of input inventory used to create a susceptibility model, with consequent effects on the accuracy and reliability of the realized maps.

The representation of a landslide can be achieved through a point or a polygon, according to the scale of the map. An inventory can also include information on the past documented landslides activity but does not provide any information about their temporal evolution, or the changes that may have occurred with time (Parise 2001). This instrument embodies a good basis for the preparation of derivative maps, such as landslide susceptibility or hazard maps.

LIM can be carried out using a variety of techniques. A recent overview of the methods used for landslide inventory mapping is given by (Guzzetti et al. 2012). Visual interpretation of stereoscopic imagery (either aerial photographs or very high-resolution optical satellite images) remains the most widely used method and results in inventories of high resolution (van Westen et al. 2008) when specific local conditions (such as vegetation limitations) are met and when it is carried out by expert interpreters. Nowadays, the use of Google Earth data is a good alternative for many areas, and many parts of the world are covered by high-resolution images which can be downloaded and combined in GIS with a digital elevation model to generate stereoscopic images, which are essential in landslide interpretation. One of the most important developments is the use of shaded relief images produced from LiDAR DEMs, from which the objects (e.g. vegetation) on the Earth's surface have been removed, for the visual interpretation of landslide phenomena (Eeckhaut et al. 2007; Ardizzone et al. 2007; Jaboyedoff et al. 2012)

LIM using visual stereo image interpretation is a time-consuming task and requires extensive skills, training and perseverance. In many cases, such skilled interpreters are not available, or landslide inventories have to be produced within a short period after the occurrence of a triggering event, requiring the application of automated detection methods based on remote sensing. (Stumpf and Kerle 2011) provide complete overviews of the various remote sensing methods and tools that can be used for (semi-)automated landslide mapping and monitoring. A large number of methods make use of passive optical remote sensing tools, such as pixel-based classification or change detection from spaceborne images (Hervás et al. 2003; Mondini et al. 2011; Esposito et al. 2020), or object-oriented classification from spaceborne images (Martha et al. 2010; Rau et al. 2014).

Many methods used for landslide mapping and monitoring make use of digital elevation measurements that may be derived from a wide range of tools, such as terrestrial photographs (Travelletti et al. 2010), terrestrial videos, UAV-based aerial photographs (Niethammer et al. 2011), airborne stereophotogrammetry and spaceborne stereophotogrammetry (Martha et al. 2010b). Also, the application of LiDAR data from both airborne laser scanning (ALS) and terrestrial laser scanning (TLS) has proven very successful (Jaboyedoff et al. 2012). Apart from LiDAR, the most useful tool for landslide inventory mapping and monitoring using remote sensing is in the InSAR domain. Interferometric Synthetic Aperture Radar (InSAR) has been used extensively for measuring surface displacements. Multi-temporal InSAR analyses using techniques such as persistent scatterer (PS) InSAR (Ciampalini et al. 2016; Del Soldato et al. 2018; Guerriero et al. 2019) and small baseline InSAR (Hooper 2008; Zhao et al. 2016) can be used to measure the displacements of permanent scatterers such as buildings with millimetre accuracy, and allow the deformation history to be reconstructed (Farina et al. 2006; Infante et al. 2019).

2.5. Landslide susceptibility, hazard and risk zoning

The information reported within LIMs represents crucial and preparatory data for every landslide hazard or risk study since they facilitate the assessment of the spatial and temporal frequencies of landslides along with their intensity, susceptibility and vulnerability (Fell et al. 2008).

A *Landslide Susceptibility Map* (*LSM*) subdivides the terrain into zones with differing likelihoods that landslides of a certain type may occur. Landslide susceptibility assessment can be considered the initial step towards a landslide hazard and risk assessment, but it can also be an end product in itself that can be used in land-use planning and environmental impact assessment. As landslide susceptibility maps primarily provide a proposed ranking of terrain units in terms of spatial probability of occurrence, they do not explicitly convey information on landslide return periods (Corominas et al. 2014).

Landslide hazard refers to the probability of landslides occurrence of a particular type and magnitude in a given location within a reference period (Guzzetti et al. 1999). Here magnitude usually refers to size (volume) and velocity. Thus this concept differs from that of susceptibility in that the former considers the magnitude of the event and, more importantly, it also considers the frequency (temporal occurrence or recurrence) of landslides (Hervás and Bobrowsky 2009). Unfortunately, the terms susceptibility and hazard are often erroneously used as synonyms, and therefore many so-called landslide hazard maps are actually susceptibility maps, as they do not consider the temporal dimension along with the spatial aspects in the evaluation of the future landslide occurrence.

Landslide risk can be expressed as the probability of a hazardous phenomenon causing damage or losses produced by landslides (Hervás and Bobrowsky 2009). Generally, the estimation of risk involves the assessment of hazard (just defined), elements at risk (*i.e.*, the population, proprieties and economic activities in the area potentially affected by the landslides, Fell (1994) and their vulnerability (*i.e.*, degree of loss of an element or elements within the landslide-affected area, where elements are the structures or persons within such area (Fell 1994). This kind of map is far less common than susceptibility or hazard mapping. Evaluating landslide risk (particularly in a quantitative term) is still a complicated task, especially because the information needed to precisely estimate hazard and vulnerability may not be available (van Westen et al. 2006).

About the LSMs, in the past three decades, a large number of models have been proposed and tested. Since landslide susceptibility assessment is a spatial evaluation, differences arise in the way of selection of an appropriate terrain subdivision, namely of a "*mapping unit*" (Soeters and van Westen 1996; Guzzetti et al. 2005) (see paragraph 2.5.1). Overviews of the methods available for landslide susceptibility evaluation can be found in Fell et al. (2008) and Reichenbach et al. (2018). The methods can be subdivided into two groups: qualitative (inventory-based and knowledge-driven methods) and quantitative (data-driven methods and physically-based models).

In knowledge-driven or **heuristic** approaches, the LSM is based on the opinion of an expert geomorphologist who defines the weighted value for each environmental factor considered to be the input for the landslide susceptibility zonation. The method is direct, as the expert interprets the susceptibility of the terrain directly in the field, based on the observed phenomena and the geomorphological/geological setting, usually by using Geographic Information System (GIS) tools. Based on his/her expert knowledge on past landslide occurrences and their predisposing factors within a given area, an expert assigns particular weights to certain combinations of factors, in fact, these methods susceptibility is expressed in a qualitative form.

The **statistical** approach is based on the assumption that future landslides are more likely to occur under the same geological and geomorphological conditions that led to past slope instability, for this reason, are also termed "data-driven". The combination of these conditions are statistically determined and, based on similar existing conditions, quantitative estimation of landslide occurrences are generated for areas free of landslides (Soeters and van Westen 1996). The output may be expressed in terms of probability. The statistical approach is of two types: bivariate or multivariate. In bivariate statistical analysis, each causal factor map is combined with the landslide distribution map and weighed values based on landslide densities are calculated for each causal factor class (Süzen and Doyuran 2004; Yalcin 2008; Yalcin et al. 2011; Chen et al. 2018b). Bivariate statistical methods are a good learning tool that the analyst can use to determine which factors or a combination of factors play a role in the initiation of landslides. It does not take into account the interdependence of variables, and it has to serve as a guide when exploring the dataset before multivariate statistical methods are used (Corominas et al. 2014). On the other hand, multivariate statistical models evaluate the combined relationship between a dependent variable (landslide occurrence) and a series of independent variables (landslide controlling factors). In this type of analysis, all relevant factors are sampled either on a grid basis or in slope morphometric units. For each of the sampling units, the presence or absence of landslides is determined (Baeza and Corominas 2001; Guzzetti et al. 2006; Kavzoglu et al. 2015).

Lastly, **physically-based** stability models are based on the modelling of the slope failure process. The methods are only applicable over large areas when the geological and geomorphological conditions are fairly homogeneous and the landslide types are simple (Corominas et al. 2014). Most physically-based models that are applied at a local scale make use of the infinite slope model and are therefore only applicable for the analysis of shallow landslides (less than a few metres in depth). These models quantitatively produce a stability index by calculating the Factor of Safety (FS), namely the ratio of resisting forces to driving forces. If the resisting force of slope materials, whether consolidated bedrock or unconsolidated sediments, is considered as the shear strength of the materials and the driving forces are considered as the predisposing causes. If the FS is less than or equal to 1 (i.e., $FS \leq 1$), the slope will fail because driving forces will equal or exceed the resisting forces. If FS is significantly greater than 1, the slope will be quite stable. However, if FS is only slightly greater than 1, small disturbances may cause the slope to fail. The advantage of these models is that they are based on slope stability models, allowing the calculation of quantitative values of stability, but, at the same time, the main drawbacks of these methods are the degree of simplification involved, the need for large amounts of reliable input data and difficulties in getting access to critical parameters such as the distribution of soil depths, the spatial variability of

geotechnical and hydrological parameters (i.e., permeability, cohesion, etc.) or in simulating transient slope hydrological processes such as macropore flows and temporal changes in hydraulic properties.

2.5.1. Mapping units

A mapping unit is a portion of the earth surface that includes a set of properties different from those recognisable across a definable boundary in the adjacent units (Hansen 1984; van Westen et al. 1993, 1997). In susceptibility studies, the investigated area must be subdivided into mapping units and the functional areas before the modelling phase. The latter will be used to define the area where the stability prediction will be reproduced and estimated over each constituent mapping unit.

An important observation by Guzzetti et al. (1999) and Guzzetti et al. (2006) refines the definition of mapping unit as a domain that maximises internal homogeneity and between-unit heterogeneity. A large set of mapping units is proposed in the literature (Carrara et al. 1995; Soeters and van Westen 1996; Guzzetti et al. 1999), each depending on the criteria adopted in partitioning the area:

1) Grid cell
2) Terrain unit
3) Unique condition unit
4) Slope unit
5) Geo-hydrological unit
6) Topographic unit
7) Administrative boundary

Each of these units is characterised by advantages and disadvantages (van Westen et al. 1993; Carrara et al. 1995; Guzzetti et al. 1999, 2006; Van Den Eeckhaut et al. 2005). However, only limited literature is available on the influence of different partition units for susceptibility mapping purposes (Carrara et al. 1995; Van Den Eeckhaut et al. 2009). The most used mapping units in literature essentially pertain to the slope unit, unique condition unit, and grid cell types. Slope units subdivide the area of interest into hydrological zones limited by divide and drainage lines (Carrara 1988; Carrara et al. 1991, 1995; Guzzetti et al. 1999) and can be obtained either manually or automatically through specific programs. The automatic digitization of slope units is generally preferred because of the low computational time, the objectivity of the procedure and the reproducibility of the experiments. The first attempts in reproducing slope units from high-resolution Digital Elevation Models (DEMs) date back to Carrara (1988) and Fairfield and Leymarie (1991). Unique Condition Unit (UCU) represents a specific combination of different

classes corresponding to a set of factors that are thought to be related to the landslide activation. The procedure to obtain a UCU involves the primary selection of suitable predictors that are subsequently reclassified into classes and ultimately crossed together to generate a set of unique combinations. The literature is also plenty of studies that demonstrate the advantages of this mapping unit, particularly when it is used to apply specific statistic techniques (Clerici et al. 2002; Rotigliano et al. 2011; Poiraud 2014). The two aforementioned units partition the territory into irregular polygons. Conversely, grid cell units subdivide the whole study area into squared cells of a given side length. The applications of grid cell units are numerous and the principal reason for their success is to be related to the often coincident structure between the grid representing the discretised area and the raster structure of the predictors, making the research outcomes straightforward for the operators (Lombardo et al. 2014). The grid cell and slope unit are the mapping units adopted to carry out all the experiments described in this dissertation.

CHAPTER 3: METHODS AND PROCEDURES

3.1. Predisposing factors

The modelling procedures have been supported throughout this research by including independent variables obtained from terrain analysis. All morphometric variables were derived, in the first case study, from a detailed Digital Terrain Model (DTM) produced by *Friuli Venezia Giulia* Regional Administration a few days after the October, 2011 rainstorm event (5 x 5 m), while, for the second and third analyses, all data were processed from a 10 x 10 m DTM provided by the *Liguria* Region Administration in 2017 (https://geoportal.regione.liguria.it/). The landslide susceptibility literature is rich in articles that adopted topographic attributes as causative factors for shallow landslides. Below, a brief description of all environmental variables employed in this dissertation will be given.

- *Slope steepness* is one of the most relevant predisposing factors in landslide occurrence. Slope values are inversely related to stability if soil cover thickness is not adequate. Thus, the likelihood of a mass movement occurrence is positively correlated with slope, higher is slope steepness higher is the probability of landslides detachment;
- *Slope aspect* - indirectly impacts landslides because it influences hydrological processes (e.g. evapotranspiration), such as the weathering, vegetation and root development (Capitani et al. 2013; Abedini et al. 2017) and the concentration of water exposed to sunlight in the soil (Sadr et al. 2014). The slope aspect is cyclic, with values 0 and 360 being coincident degree measurements. A common way to treat cyclic data is to transform it by using trigonometric function. A trigonometric transformation of aspect data is rather 'pure' since it retains the continuity of aspect. For these data, a cosine transformation measures southerliness-to-northerliness (-1 to 1, respectively), while a sine transformation measures westerliness-to-easterliness (-1 to 1, respectively), obtaining as a result *northness* and *eastness* (Lombardo et al. 2020a);
- The curvature function displays the shape or curvature of the slope. A part of surface can be concave or convex, depending on the curvature value. The curvature is calculated by computing the second derivate of the elevation. The output of the curvature function can be used to describe the physical characteristics of a drainage basin to understand erosion and runoff processes. Curvature values can be used to find soil erosion patterns as well as the distribution of water on land. The *Planform curvature* (commonly called plan curvature) is perpendicular to the direction of the maximum slope. Planform curvature relates to the convergence and divergence of flow across a surface. A positive value indicates that the surface is laterally convex at that cell. A negative plan indicates that the surface is laterally

concave at that cell. A value of zero indicates that the surface is linear. On the other hand, *Profile curvature* is parallel to the slope and indicates the direction of maximum slope: it affects the acceleration and deceleration of flow across the surface. A negative value indicates that the surface is upwardly convex at that cell, and flow will be decelerated. A positive profile indicates that the surface is upwardly concave at that cell, and the flow will be accelerated while a value of zero indicates that the surface is linear (Peckham 2011);

- *Topographic Wetness Index* (TWI) is an important factor indicating the potential of runoff generation and it is a proxy for the thickness of the soil saturation zone. For shallow landslides, slope failure is facilitated by saturated soil conditions together with a soil layer of sufficient thickness. TWI was calculated as (Beven and Kirby 1979) (Eq. 3.1):

$$TWI = \ln\left(\frac{A}{\tan(Slope)}\right) \quad 3.1$$

  where *A* is the cumulative upslope area of a drainage basin through a point and *tan(Slope)* is the angle of the slope at the same point. High index values indicate the great potential of water accumulated due to low slope angles and high upslope contributing area;

- TPI stands for *Topographic Position Index*, which is defined as the difference between a central pixel and the mean of its surrounding cells (Wilson and Gallant 2000). The TPI compares the elevation of each cell in a DTM to the mean elevation of a specified neighbourhood around that cell. Positive TPI values represent locations that are higher than the average of their surroundings, as defined by the neighbourhood (i.e. ridges). Negative TPI values represent locations that are lower than their surroundings (i.e. valleys). TPI values near zero are either flat areas (where slope is near zero) or areas of constant slope (where the slope of the point is significantly greater than zero);

- *Stream Power Index* (SPI) is a measure of the erosive power of flowing water computed as (Moore and Wilson 1992) (Eq. 3.2):

$$SPI = \ln(A\tan(Slope)) \quad 3.2$$

  where *A* is the specific basin area, and the *tan(slope)* is the local slope gradient. SPI is a proxy variable for the stream power or the energy of the flowing water expanded on the bed and banks of a channel. As the catchment area and slope gradient increase, the amount of water contributed by upslope areas and the velocity of water flow increase, hence SPI and erosion risk increase. The units representing the SPI are dimensionless and the interpretation of this parameter distribution corresponds to a general increase of energy of the water flowing onto the topography as a function of the increase of the values that the parameter expresses across the area (*i.e.*, SPI shows the lowest values on and close to ridges, where the

contributing area is relatively small, while it reaches higher values at the bottom of steep valleys);

- *Relative Slope Position* (RSP) indicates the location of each cell relative to the ridge and valley of a hillslope. The slope position values ranging from 0 (bottom of the valley) and 1 (top of the ridge).
- *Distance to roads* and *distance to streams* have been both estimated by using the Euclidean distance method. Distance to stream is a crucial parameter that controls slope stability. In fact, the proximity of the drainage structures could erode the foot of the slope and streams are preferential ways where landslides can increase their mobility (Wistuba et al. 2015). Similarly, landslides may occur on the road and on the side of slopes affected by roads, representing a discontinuity in the slope profile. Also, ground excavation at the base and the material accumulation on top of the slope may represent a hazardous factor (van Westen et al. 2003);
- As different studies demonstrated, the *degree of abandonment of agricultural terraced* slopes represents an important landslide susceptibility factor in the study area, strongly influencing the magnitude of rainfall-induced mass movements (Cevasco et al. 2014; Pepe et al. 2019). In this thesis, special care has been paid to the recognition and mapping of both agricultural terraces and non-terraced areas. In particular, using data from the previous study (Cevasco et al. 2013a; Raso et al. 2020b), four classes were distinguished: *1*) cultivated terraced areas, *2*) abandoned terraces with poor vegetation cover (initial state of abandonment), *3*) abandoned terraces with dense vegetation cover (advanced state of abandonment), *4*) non-terraced areas (including either urban areas, outcropping rocks and woods);
- *Land-use*, because of its temporal and spatial variations, can greatly affect landslide occurrence (Glade 2003). In particular, it controls landslide hazards and influences the development of the spatial pattern of elements at risk (Promper et al. 2014; Gariano et al. 2018). The land-use role as a landslide PF is crucial for slope stability because the development and utilization of the land affect the infiltration, surface runoff and vegetation. The land-use map has been obtained from the Corine Land Cover project (CLC), released in 2018 by the European Environment Agency (https://land.copernicus.eu/pan-european/corine-land-cover);
- Lithological and structural variations often lead to a difference in strength and permeability of rocks and soils. The importance of lithology in slope failure occurrences has widely been accepted in the international literature (Ayalew and Yamagishi 2005; van Westen et al. 2008;

Trigila et al. 2015; Segoni et al. 2020). *Geo-lithological* map was obtained thanks to the *Liguria* region portal (https://geoportal.regione.liguria.it/catalogo/mappe.html);

- *Soil thickness*, unfortunately, used only for the first case study, is a key parameter when dealing with shallow landslides involving loose material and experiencing a sharp permeability contrast at the soil-bedrock interface (Ho et al. 2012; Segoni et al. 2012; Kim et al. 2015). The action of soil erosion, defined as the detachment and transportation of soil material from one place to another through the action of wind, water in motion, or by the beating action of the raindrops (Sharma et al. 2011), is also of primary importance. The soil thicknesses have been estimated interpolating about 200 points in the catchment using a Regression Kriging technique (RK, Hengl et al. 2007). These points were collected during the field investigations in the study area with direct field observation. RK is a spatial interpolation technique that combines the information derived by a deterministic description of the spatial variability of a variable (a Machine Learning algorithm) and the interpolation of the Machine Learning algorithm residuals with simple kriging to take into account the stochastic part of the variability (Hengl et al. 2007). The use of ML method frees from the responsibility of making specific assumptions about the response variable for linear prediction and provides a better fit for complex non-linear relationships in the *p+1-dimensional space* (where *p* is the number of predictors, (Hengl et al. 2017). The RK procedure is mainly based on functions provided in the R package GSIF (Hengl 2016). RK needs 50 unique point locations at least to perform the internal cross-validation procedure as provided in the GSIF package.

3.2. Machine Learning modelling

Machine learning (ML), a subfield of artificial intelligence, is an application of artificial intelligence that provides systems with the ability to automatically learn and improve from experience. ML algorithms build a model based on sample data, known as "*training data*", to make predictions or decisions without being explicitly programmed to do so (learn for themselves). Typically, a random subset of the data is put aside for completely independent testing ("*validation dataset*"). ML is ideal for addressing those problems where our theoretical knowledge is still incomplete but for which a significant number of observations and other data are available. The process of learning begins with observations or data, such as examples, direct experience, or instruction, in order to look for patterns in data and make better decisions in the future based on the examples that are provided. Within ML, there are two basic approaches: *supervised learning* and

unsupervised learning. The difference between these two main classes is the existence of labels in the training data subset.

Supervised learning algorithms involve predetermined output attributes besides the use of input ones. The algorithm "learns" from the training dataset by iteratively making predictions on the data and adjusting for the correct answer. It is also important to point out the learning process stops when the algorithm achieves an acceptable level of performance. While supervised learning models tend to be more accurate than unsupervised learning models, they require upfront human intervention to label the data appropriately. The supervised learning algorithm can also compare its output with the correct, intended output and find errors in order to modify the model accordingly. In contrast, **unsupervised learnings** involve pattern recognition without the implication of a target attribute. All the variables used in the analysis are employed as inputs and because of the approach, the techniques are suitable for clustering and association mining techniques. That is, unsupervised clustering algorithms identify inherent groupings within the unlabeled data and subsequently assign a label to each data value. On the other hand, unsupervised association mining algorithms tend to identify rules that accurately represent relationships between attributes.

3.2.1. (Supervised) Learning problem formulation

Before the particular algorithms are examined, it is needful to pose a learning problem and present the matter more exhaustively, illustrating the landslide evaluation framework. The principal purpose is to exploit the possibility of automating the process of landslide susceptibility mapping, i.e. to make a plausible prediction of landslides spatial distribution by using ML techniques. The expected automated procedure assumes that after the initial acquisition of the necessary spatial data, an expert is presented with a (possibly small) representative region. Such a scenario supposes a supervised learning approach in which the expert performs mapping in the representative region. The algorithm subsequently uses that expert map for training, i.e. learning from instances of the expert map by linking his interpretation with a set of Predisposing Factors (PFs).

Ultimately, after learning the mapping rule proposed by the expert, the algorithm extrapolates the rule in the rest of the area and gives an automated prognosis of the spatial distribution of landslides. Initially, the input data should be presented as 2D rasters of pertinent PFs (geological, morphometric, environmental) and the appropriate Landslide Inventory map. The inventory is theoretically required only for the training area, but it is usually provided for the remaining area for the model evaluation. The input rasters are structured in the way that each grid element (pixel) represents a data instance at a certain point of the area. The suggested approach leads to a classification task. The task is to place each pixel into an appropriate landslide category using the

PF values associated with that pixel. The training area size choice is very delicate and requires specific strategies. On the one hand, an optimal approach is to build a sufficiently accurate model with a smaller number of training examples, thus leading to a reduced engagement of the expert. On the other hand, a practical value of a model in the landslide assessment framework lies in the model's prediction power, which implies a more meaningful training sampling strategy. Therefore, it is desirable to have a training area that is physically separated from the testing area.

Building an ML model is not just about feeding the data, there is a lot of deficiencies that affect the accuracy of any model. *Overfitting*, also referred to as random error or noise, in ML is one such deficiency that hinders the accuracy as well as the performance of the model. It is the issue of underperforming in the testing/validation set, while showing high performance in the training. In other words, it is a paradox of reduced performance while having increased complexity of the model or a bigger amount of data to build the model with. It might emerge when a machine has been taught to scan for specific data, but when the same process is applied to a new set of data, the results are incorrect. This is because of errors in the model that was built, as it likely shows low bias and high variance. The model may have had redundant or overlapping features, resulting in it becoming needlessly complicated and therefore ineffective. There are several techniques to avoid overfitting in ML, in this thesis, have been basically employed Cross-Validation and Ensembling (see paragraph 3.2.3).

One of the most powerful features, probably the most efficient, to avoid/prevent overfitting is *Cross-Validation*. The idea behind this is to use the initial training data to generate mini training-testing-splits, and then use these splits to tune the model. In a standard k-fold validation, where *k*, also referred to as folds, stands for the number of partitions of the training split and therefore also represents the number of iterations. In the first run, one partition is taken for validation, also known as holdout fold, while *k-1* partitions are merged for training. In every subsequent iteration, different splits take the validation role, while the remaining *k-1* splits take the training role until all *k* iterations are finished. If one seeks the optimal parameter combination, the Cross-Validation needs to be repeated for each parameter configuration.

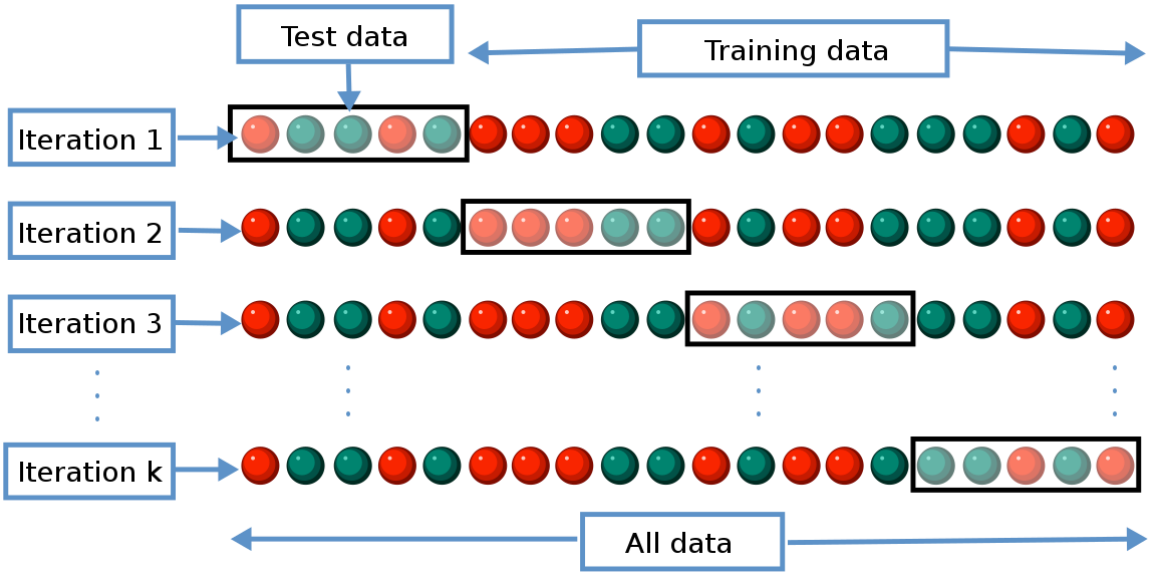

Figure 3.1 A k-fold Cross-Validation scheme. The black rectangles represent the testing data, wherein the remaining parts represent training one.

3.2.2. Spatial Distribution Model (SDM)

Spatial Distribution Models (SDMs) are widely used to predict and study occurrences distributions. Many different methods and associated algorithms are used and continue to emerge (Elith et al. 2020). SDMs aim is to estimate the similarity of the conditions at any site to the conditions at the locations of known occurrence of a phenomenon. In SDM, the following steps are usually taken: *i*) locations of occurrence of a phenomenon are compiled; *ii*) values of environmental predictor variables at these locations are extracted from spatial databases; *iii*) the environmental values are used to fit a model to estimate similarity to the sites of occurrence; *iv*) the model is used to predict the variable of interest across the study region. SDMs can be fitted to a range of data types, the application of Presence-Only (PO) and Presence-Background (P-Bg) models are very common, contrary Presence-Absence (PA) ones.

Nowadays, SDMs are widely used among statistical methods and ML algorithms (Yilmaz 2010; Lombardo et al. 2016; Di Napoli et al. 2020). Fit and evaluation of SDMs is often achieved through Cross-Validation; that is, using subsets of the data iteratively for either training and fitting the model or for evaluating (Hijmans 2012; Roberts et al. 2017). SDMs are sensitive to the quality of training data. Different training data may lead to significant changes in the derived landslide susceptibility maps (Arnone et al. 2016; Steger et al. 2016; Bordoni et al. 2020). When performing any PA predictive algorithm, one of the principal steps is represented by the selection of locations where instability and stability conditions are expressed (Conoscenti et al. 2016; Hong et al. 2019; Pourghasemi et al. 2020). The quality of landslide presence data is relatively more acceptable

because it is sampled based on the landslide inventory, which is often executed through the interpretation of aerial photographs with field checks (Zhu et al. 2018). The quality of landslide absence data is arguable. The landslide absence data is not available and has to be generated from landslide free areas that have no history of landslide events in the past. The landslide absence data are sampled either from the safe areas delineated by expert knowledge or from the areas beyond the buffer zones of the landslide sites (Conoscenti et al. 2016; Hong et al. 2019).

However, these sampling strategies have two critical shortcomings. Firstly, these sampling strategies have no uniform standard in partitioning the landslide free areas, making the sampling of landslide absence difficult to implement (Hirzel et al. 2002; Anderson et al. 2003; Guo et al. 2005; Yao et al. 2008; Zhu et al. 2018). Secondly, these landslide free areas could contain sites very susceptible to landslides but have not yet failed in the past simply because of the lack of triggering factors. Sampled based on these false landslide free areas, the quality of landslide absence data is decreased as well as the whole training data, resulting in many unconfirmed assumptions and false performance of models (Hirzel et al. 2001; Zaniewski et al. 2002). Hence, although PA data are desirable for evaluation (El-Gabbas and Dormann 2018) they are very often not available.

Due to the low availability of landslide absence data, some PO methods simply use landslide presence as training data to develop the relationships between landslide susceptibility and PFs (Wang et al. 2015; Steger and Glade 2017; Novellino et al. 2021). A problem with PO data is that they can be spatially biased with some areas sampled intensively and others not at all (Reddy and Dávalos 2003; Hortal et al. 2008; Amano and Sutherland 2013; Isaac and Pocock 2015) and thus, may not be representative of the distribution of the occurrence in the study area. When evaluating with PO or P-Bg data, such biases remain, thus wrongly emphasising the suitability of some environments and under-reporting the suitability of others. A model trained and evaluated with biased PO or P-Bg data may appear to perform well, although it does not produce meaningful predictions of the true distribution (El-Gabbas and Dormann 2018).

3.2.3. Ensemble modelling

The principle of "*the wisdom of the crowd*" shows that a large group of people with average knowledge on a topic can provide reliable answers. The aggregate results cancel out the noise and can often be superior to those of highly knowledgeable experts (Kittur 2007). The same rule can apply to ML techniques. Ensemble Methods (EMs) are algorithms that combine several ML techniques into one predictive model to decrease *variance* (i.e., the model is very sensitive to the provided inputs - *bagging*), *bias* (i.e., the model relies heavily on one or a few variables while making a prediction - *boosting*), or *improve predictions* (one model or one algorithm to fit the entire

training data might not be good enough to meet expectations - *stacking*). This approach allows the production of better predictive performance compared to a single model.

Ensemble methods fall into two broad categories, i.e., *sequential ensemble* techniques and *parallel ensemble* techniques. Sequential ensemble techniques generate base learners in a sequence, e.g., Gradient Boosting. The sequential generation of base learners promotes the dependence between the base learners. The performance of the model is then improved by assigning higher weights to previously misrepresented learners. In parallel ensemble techniques, base learners are generated in a parallel format, e.g., Random Forest. Parallel methods utilize the parallel generation of base learners to encourage independence between the base learners. The independence of base learners significantly reduces the error due to the application of averages. Most EMs use a single base learning algorithm to produce homogeneous base learners, i.e. learners of the same type, leading to homogeneous ensembles. Some methods use heterogeneous learners, i.e. learners of different types, leading to heterogeneous ensembles. For EMs to be more accurate than any of its members, the base learners have to be as accurate as possible and as diverse as possible.

Bagging stands for *bootstrap aggregation*. It increases the accuracy of models through the use of decision trees, which reduces variance to a large extent. The reduction of variance increases accuracy, hence eliminating overfitting, which is a challenge to many predictive models. Bootstrapping is a sampling technique where samples are derived from the whole dataset using the replacement sampling procedure, aiding the randomized selection procedure. Aggregation in bagging is done to incorporate all possible outcomes of the prediction. Without aggregation, predictions will not be accurate because all outcomes are not put into consideration. Bagging is advantageous since weak base learners are combined to form a single strong learner that is more stable than single learners. One limitation of bagging is that it is computationally expensive.

Boosting is an ensemble technique that learns from previous predictor mistakes to make better predictions in the future. The technique combines several weak base learners to form one strong learner, thus significantly improving the predictability of models. Boosting works by arranging weak learners in a sequence, such that weak learners understand from the next learner in the sequence to create better predictive models.

Stacked Generalization or **Stacking** is an ensemble learning technique that combines multiple classifications or regression models. Unlike bagging, in stacking, the models are typically different (e.g. not all decision trees) and fit on the same dataset (e.g. instead of samples of the training dataset). Unlike boosting, in stacking, a single model is used to learn how to best combine the predictions from the contributing models (e.g. instead of a sequence of models that correct the predictions of prior models). The architecture of a stacking model involves two or more base

models, often referred to as level-0 models, and a meta-model that combines the predictions of the base models referred to as a level-1 model. Level-0 Models (*Base-Models*) fit on the training data and whose predictions are compiled; while, Level-1 Model (*Meta-Model*) learns how to best combine the predictions of the base models. Hence, Stacking learns how to best combine the predictions from multiple well-performing ML models.

3.2.4. Algorithms

In the following sections, the different ML algorithms exploited in this dissertation were presented. All ML algorithms are included in the package "biomod2" implemented by Thuiller et al. (2009) and all statistical calculations have been developed in free statistical software R (R Core Team 2021). ML models can be split into two different algorithms classes: *generative* and *discriminative*. The **generative** model is considered a class of statistical models that can generate new data instances. This model is typically used to estimate probabilities, modelling data points and distinguish between classes based on these probabilities. As they often rely on the Bayes theorem, generative models can tackle a more complex task than analogous discriminative models. Generative modelling is used in unsupervised machine learning as a means to describe phenomena in data, enabling computers to understand the real world. On the other hand, a **discriminative** model refers to a class of models used in statistical classification, especially in supervised machine learning. Also known as conditional models, generative modelling learns the boundary between classes or labels in a dataset. Hence, generative models try to model how data is placed throughout the space, while discriminative models attempt to draw boundaries in the data space.

In this thesis, two different discriminative ML algorithms (i.e., Artificial Neural Network and Generalized Boosting Model) and one generative ML model (i.e., Maximum Entropy) have been adopted, all well-known for their good performance (Elith et al. 2006).

3.2.4.1. Artificial Neural Network

Artificial Neural Network (ANN) is an attempt to simulate the network of biological neurons that make up a human brain so that the computer will be able to learn things and process information (Zurada 1992; Chen et al. 2017). ANN algorithm uses different layers of mathematical processing to find relationships between response and predictor variables. Typically, a neural network has dozens of artificial neurons, called units, organized in sequences of layers. The input layer contains the predictor data. From the input, data go through one or more hidden layers containing several unit neurons. The hidden unit's job is to transform the input into something the output unit can use. On the other side of the network, there are the output units, i.e., the response

variable. Connections between nodes and hidden layers may be characterized by specific weights that can be randomly assigned at the beginning of the process (the higher the weight, the greater influence one unit has on another), and later updated for algorithm optimization employing back-propagation processes (Pijanowski et al. 2002). The neurons in each hidden layer represent different combinations of the environmental variables balanced by the weights' sum of the previous neurons (Peh et al. 2000) (Eq. 3.3):

$$c_j = \sum_{i=1}^{p} w_{ij} x_i \qquad 3.3$$

where w_{ij} is the weight from neuron *i* in the input layer to neuron *j* in the hidden layer, x_i is the *i-th* input element and *p* is the number of neurons in the input layer. This calculation is performed for each neuron in the hidden layer. At each neuron, if the weighted sums coming from the previous layer neurons is higher enough for a so-called "activation function", then that specific neuron, i.e. a specific combination of the input variables, is turned on and the signal passes to the following layer neurons up to the output layer. There are many different forms of activation functions and a commonly used one is the logistic function, which produces a sigmoid curve with an outcome between 0 and 1 (Peh et al. 2000) (Eq. 3.4):

$$o_j = \frac{1}{1+\exp(-c_j)} \qquad 3.4$$

where o_j is the output of the *j-th* node in the hidden layer. The outcome of the activation function is then passed to the output layer.

3.2.4.2. Maximum Entropy

MaxEnt stands for Maximum Entropy modelling. MaxEnt is a presence-only ML method (Phillips et al. 2006), and, because is one of the most efficient and powerful algorithms in predicting event's spatial distribution, currently it is one of the most popular algorithms for presence-only datasets. This algorithm relies on the assumption that the best model to represent the true distribution is the one maximising the system entropy. Maximising the entropy means that the best model is the one with the maximum uncertainty about event's probability of occurrence. This means that the model has no starting hypothesis and all the combinations of predictor variables can trigger the studied event. This strategy ensures to remove any bias from the predictions.

This algorithm compares the observed Probability Density Functions (PDFs) of environmental factors at the event's occurrence sites (i.e., landslides locations or *presence*) with the PDFs of the same variables of a remaining landscape's random sample (Elith et al. 2011). Generally, it is necessary a very large sample of the study area (at least 10000 point locations) and these points are called *background* samples. MaxEnt algorithm assesses the predicted (actual) PDFs of

environmental variables characterizing the events that approximate the PDFs on the landscape, i.e. by maximizing the entropy of information. This maximized entropy model produces information to predict the event occurrence probability at unsampled locations. MaxEnt then calculates the ratio between these two probability densities, which gives the relative "environmental suitability" for the presence of an event for each location in the study area (the landscape) (Elith et al. 2011, Eq. 3.5):

$$\Pr(y = 1|\, z) = f_1(z)\Pr(y = 1)\,/f(z) \qquad 3.5$$

Equation 5 shows that if the PDF of the environmental variables at the presence locations is known, f_1(z), along with the density of the same variables across the study area f(z), it then only needs knowledge of the prevalence (proportion of occupied sites) Pr(y = 1) to compute the event's occurrence probability at unknown locations.

The main theoretical MaxEnt principle is that at the sampling locations the event is more associated with particular combinations of the predictor variables than others, then the probability of the event to occur at unsampled locations is higher when those variables combinations that are most frequent at the sampling locations are found. The newly created distribution represents a set of probability values.

3.2.4.3. Generalized Boosting Model

Gradient Boosting Models (GBMs) are a family of tree-based algorithms characterized by very high predictive performance for continuous and categorical response variables. A GBM produces many decision trees which are combined to provide one ensemble (combination) model by means of an iterative (repeated) procedure. These algorithms can be finely tuned by using different kinds of parameters. The side effect of this high tuning opportunity is that the researcher has to master parameters' tuning operations. Given *X* as the matrix of some predictor variables and *Y* as the values of a response variable, a simple decision tree starts from its root to splitting dichotomously (nominal variable with only two modes, e.g. yes or not) the values of some randomly-chosen predictor variables into subsequent nested-smaller clusters. This splitting produces some branches, and it continues until identifying combinations of *X* values resembling those characterizing the observed *Y*. The *X* values are not to be split, until perfectly identifying the predictor values associated with the observed *Y* values, in order to avoid overfitting (i.e. a model standing too much on observations) and to create a model with predictive ability. A single decision tree is called "a weak learner" and a GBM algorithm is based on the idea that a combination of many "weak learners" has a higher predictive performance than a single "strong learner".

Indeed, a GMB algorithm starts by building a first decision tree relying on a random subset of *X* variables and then by measuring its performance in predicting the observed *Y* values. The algorithm

carries on new different subsequent decision trees and a new tree is added to the previous one only if improving the predictive performance of the ensemble model. To reduce the overfitting issue, the best trees' ensemble model is the one minimizing a "*loss function*", which is represented by a combination of the model's prediction errors and complexity (i.e. the number of trees) (Knoll et al. 2019). The *loss function* (*L*) can be represented as follows (Eq. 3.6):

$$L = \sum_i l(\acute{y}_i - y_i) + \sum_k \Omega(f_k) \quad 3.6$$

where the first term (namely, *training loss*) measures the difference between a predicted value achieved by the score at the terminal node ($\acute{y}_i$) and its corresponding observed value (y_i) in the training dataset; while, the second one (i.e., *regularization*) represents the complexity of the model. The algorithm self-calibrates in order to choose the model with the best predictive performance (low loss term) and the lowest overfitting (low regularization term). To do this, the algorithm runs "*n*" times (iterations) until the aforementioned conditions are achieved.

3.3. Runout Modeling

During the Ph.D. project, beyond the implementation of data-driven models to evaluate detachment landslide susceptibility, a geometrical approach was applied to estimate the landslide runout susceptibility. The first experiences on runout evaluation were made by Heim (1932) and Terzaghi (1950). Calculating the runout of mass movements and understanding their rapidity are basic elements of any landslide hazard or risk assessment (Hungr et al. 2005). In this thesis, the Landslide Runout Susceptibility (LRS) assessment was performed adopting the geometrical method of the "reach angle" (Hsu 1975), also known as "fahrböschung" (Heim 1932), which is one of the most used empirical approaches to evaluate landslide mobility. The main parameters used in this approach are shown in Figure 3.2. Runout distance (*L*) is defined as the horizontal projection of the line (straight line) that connects the highest point of the landslide source area with the landslide deposit toe; slope height (*H*) represents the difference in elevation between the landslide crown and the farthest edge of the displaced mass, while θ is the slope angle before the failure occurrence (Corominas 1996). The model assumes that the landslide will arrest at the intersection point of the straight line with the topography. The intersection of the straight line with the topographic surface provides both *H* and *L* (Corominas et al. 2003), from which the reach angle (α) can be determined. Corominas (1996) demonstrated that the reach angle depends on the landslide volume, the type of movement and topographic constraints along the path. Moreover, the runout behaviour of flow-like landslides can be controlled by several factors, such as land use, soil properties, local morphology and water content. Therefore, it is not easy to determine the runout path and the travel distance for future debris flows (Guinau et al. 2007).

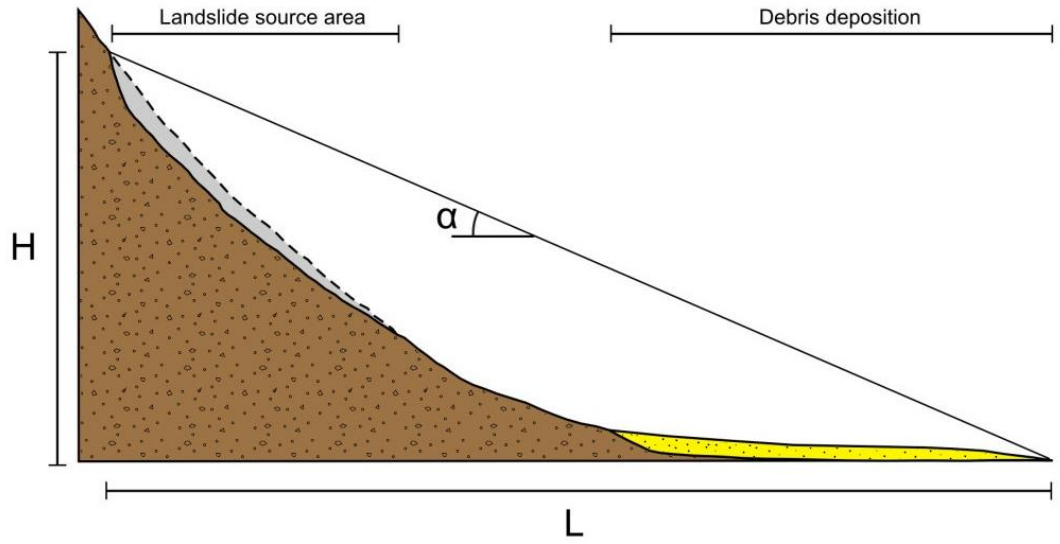

Figure 3.2 Graphical representation of the "reach angle" method (from *Sarno* Basin Authority, 2011), modified and redrawn): *α*: reach angle; *H*: height difference (m) between the landslide source area (i.e., landslide crown) and the farthest edge of the landslide deposit; *L*: travel distance (m).

3.4. Bayesian Computing

Following the application of data-driven algorithms and reach angle method, further analyses have been conducted. In particular, Bayesian algorithm was exploited to obtain the so-called landslide intensity (Lombardo et al., 2018), which corresponds to how many mass movements may occur per mapping unit. Moreover, recent studies have been demonstrated that the intensity is closely correlated to the planimetric extent of landslides per mapping unit (Lombardo et al., 2020). Considering these observations, the relation between landslide intensity and planimetric extent was applied to generate maps that predict the aggregated size of landslides per mapping unit and the portion they may affect (see section 5.3).

3.4.1. Spatial Point Process fundamentals

The occurrence locations of the landslide events represent the response variables that have to be modelled and predicted. Because they are unknown before the phenomena occur, they are treated as *random*. The natural distribution for representing a random points collection over continuous space is through *Spatial Point Processes*, whose realizations are point patterns. Even if occurrence locations are random they may be more or less limited in a specific region, showing clustering or repulsion properties at small scales. In the landslide framework, the modelling of clustering structures due to unobserved effects (in our case the precipitation trigger) is of great importance. The principal point process peculiarity is its intensity $\lambda(s) \geq 0$. The intensity may be interpreted as the expected number of points falling into an infinitesimal region around the location *s*. More

precisely, the count of events occurring in area *A* is a non-negative random variable $N(a) \geq 0$, whose expectation is given by the integral of the intensity function over A, i.e., $E(A) = \int_A \lambda(s)ds$.

The fundamental point process model is the *Poisson point process*, which is characterized by two probabilistic properties: *i*) the number of events *N(A)* occurring in a bounded area *A* follows the Poisson distribution; *ii*) if A_1 and A_2 denote two disjoint areas of space, then $N(A_1)$ and $N(A_2)$ are independent. In other words, the events are randomly scattered over space, yet according to the Poisson distribution defined in terms of a deterministic intensity λ(s) that may vary spatially. This probabilistic framework based on point processes is much richer than the dichotomous presence-absence setting for specific areal units, fixed a priori, either based on a fine-scale regular grid (at pixel resolution) or larger-scale administrative or geological areal units (such as slope units or catchments). In classical data-driven landslide modelling, estimation and prediction are tailored to the concept of susceptibility, whereby areal units hit by landslides are contrasted to a random selection of unaffected units. Through its capability to provide probabilities of the type for any area *A*, the modelling paradigm may be used to derive susceptibility maps in the traditional sense, but it also gives valuable additional information on the point intensity over space and probabilities and any areal unit *A*.

When allowing for such random components in the intensity functions λ, the resulting stochastic model for the observed point pattern is called a *Cox point process* (Cox 1965). In other words, conditional on $\Lambda(s) = \lambda(s)$, it is possible to achieve Poisson point process with intensity $\lambda(s)$. Through their stochastic construction, Cox point processes are natural models for capturing clustering of points, i.e., the fact that even after taking into account the effect of observed covariates in the Poisson intensity, there remain areas with relatively higher or lower point intensity. In such cases, the point pattern shows clustering structures that cannot be fully explained by the available covariates; however, this may be modelled by assuming that the intensity function is random and contains a latent spatial effect that governs the remaining variation of the intensity over space. The Gaussian process is the workhorse of spatial statistics, while the log-Gaussian Cox process has risen as its counterpart for modelling point patterns. More specifically, the Poisson intensity $\Lambda(s)$ is assumed to be a log-Gaussian process, allowing for the inclusion of fixed and random effects, obtaining *Log-Gaussian Cox Process* (double stochastic construction, Lombardo et al. 2018, and reference therein). More precisely, the log-intensity $\log\{\Lambda(s)\}$ is described as a Gaussian random field, in which fixed covariate effects and random effects are embedded through an additive structure (see paragraph 3.3.3).

Among the random effects one can include categorical covariates or properties represented by discrete classes each one independent from the others, and model them as *iid* (or *independent and*

identically distributed) effects. Additionally, one can model ordinal covariates or properties represented by discrete classes which retain an ordinal structure (hence from small to large corresponding values per class). Ordinal covariates can be modelled accounting for adjacent-class-dependence by using a *random walk* function of the first order (*rw1*) between class estimations (Bakka et al. 2018; Lombardo et al. 2018). Furthermore, one can model covariates expressed at a latent level, either in space, in time or both (Lombardo et al. 2020a). This concept in the geomorphological literature has been introduced by Lombardo et al. (2018). The idea behind it, and in the context of the present thesis, assumes that the covariates may not express the whole variability in the landslide distribution over space. In other words, there is virtually always an unexplained but still spatially structured component that is hardly accounted for in landslide susceptibility studies. This component or missed covariate or *Latent Spatial Effect* (*LSE*), can reflect the spatial signal of the trigger for event-specific inventories (Lombardo et al. 2019b) or any other unaccountable effects for which we do not have explicit data, in the case of geomorphological inventories.

The LSE can be computed by using a *Besag* model (Besag 1975; Blangiardo and Cameletti 2015). But, there is a large literature available on the calculations of latent covariates, both over space and time, offering valid alternatives such as *spde* models (Bakka et al. 2018). Irrespective of the specific model, when it comes to the estimation of latent covariates, the core idea is that any predictive model, be it physically- or statistically- based, produces a distribution of residuals between the prediction estimates and the observation. This concept is valid also for susceptibility models. In advanced spatial statistical applications, these residuals are evaluated over space, and whether they are non-randomly geographically distributed, their signal can be captured and reintegrated in the modelling procedure as a covariate acting at a latent level (Bakka et al. 2018). Simply computing the residuals and re-introducing them would inevitably lead to overfitting issues and misinterpretation of the results; for this reason, solutions have been proposed inspired by concepts such as *smoothed residuals* (Baddeley et al. 2005).

In this thesis, being the space partitioned into SUs, it is opted to implement a latent spatial effect that is driven as a function of neighbouring mapping units. In practice, a moving window through space returns the average residual per SU from all the adjacent SUs (which share a border in the corresponding shapefile) and adds for each SU a random error component (ε). In this way, one can retrieve the effect of unexplained covariates and drive modelling performance strength from its inclusion in the model itself. Moreover, a model without a spatial latent effect will tend to naturally "trust/rely" any effect or dependence carried by the chosen set of covariates. This inevitably leads to credible intervals which are narrower than they theoretically are. The estimation of the residual

spatial dependence in the data and its inclusion in the model via spatial latent effects also helps in avoiding this issue of biased credible intervals. In fact, as the model is informed of spatially structured dependencies, this information is taken away from the other covariates allowing for a more precise estimation of the uncertainty in their effects (Lombardo et al. 2020a).

3.4.2. Bayesian modelling

In this paragraph, the general idea of fully Bayesian modelling is recalled. The aim is to simultaneously estimate the latent intensity function and more specifically its components such as the coefficients of the fixed covariate effects and random effects, if present. Moreover, a relatively small number of so-called hyperparameters governing the smoothness and variance of the random effects is also calibrated automatically. Bayesian inference was summarised as the posterior probability of a hypothesis (probability of parameters given data - $\pi(\theta|data)$) being equal to the likelihood function (probability of data given parameters/hypothesis - $\pi(data|\theta)$) multiplied by the prior probability (prior belief in parameters - $\pi(\theta)$ all normalized/divided with the probability of the data ($\pi(data)$).

In general, prior distributions allow incorporating expert knowledge and can help stabilise estimated models when these have a very complex structure and/or when data are very noisy. Bayes' famous Theorem indicates how can construct posterior distributions (densities, expected values, etc.), i.e., parameter estimates and precise probabilistic uncertainty statements, by confronting prior information with observed data. Hence, the object of interest is the posterior distribution $\pi(\theta|data)$, which can be found using Bayes' Theorem as (Eq. 3.7):

$$\pi(\theta\,|data) = \frac{\pi(data\,|\theta)\pi(\theta)}{\pi(data)} \qquad 3.7$$

Therefore, the Bayesian algorithm is able to wander from the specification of "data distribution given the model parameters and their prior information" to the estimation target corresponding to the "distribution of model parameters given the data and prior information". The fitted posterior distribution $\pi(\theta|data)$ can then be exploited to make inference (e.g., on model parameters and their uncertainty), derive any model-based diagnostics, and draw practical conclusions.

Through the specification of priors, the Bayesian paradigm resolves potential parameter identifiability issues by naturally integrating constraints in the prior distributions. For example, if some covariates have a tendency towards collinearity (e.g., if they are strongly correlated, hence providing redundant information - a common issue in landslide susceptibility and hazard studies), then the prior structure can reduce numerical instabilities and keep the model and its parameters well identifiable from the data. Therefore, the specification of priors is crucial in models where the number of unknown parameters and/or latent random variables to infer is large compared to the

observed sample size. In particular, linear covariates have been standardised to have mean 0 and variance 1, such that the importance of estimated coefficients can be interpreted and compared more easily, and estimated coefficients will tend to be significant if they are at least moderately large in absolute value. Since only a relatively small number of such coefficients are estimated from a quite large number of observations, these coefficients are usually well estimated in the posterior model. Therefore, it makes sense to fix a moderately informative prior distribution with fixed prior variance for such coefficients, and the exact value of the fixed prior variance has little influence on the posterior model. For example, in implemented models, a moderately informative normal distribution with mean 0 and variance 1 independently for the global intercept and all covariate coefficients was specified.

Simpson et al. (2017) describe a novel and principled approach for the construction of priors suited for additive models defined by different components (e.g., latent effects). They propose priors that penalize departure from a base model and for this reason they are called *Penalized Complexity* (*PC*) priors, which reduce complex model components towards simpler reference models, making sure that they can be reliably estimated. PC priors are designed following a general principle resulting from the law of parsimony known as “Occam's razor” that avoid overly complex models. If the stochastic behaviour of such complex model components is not properly controlled by suitably chosen prior distributions, this can lead to overfitting and poor estimation and prediction performances. Even with principled approaches such as the PC priors, there is no general rule providing exactly the “best” choice for the prior distribution, such that some subjectivity remains. In general, if exist fairly large credible intervals of hyperparameters in the estimated model, or if numerical instabilities arise during the estimation of the model, it is recommended to study the sensitivity of estimated models to prior choices before taking the final choice of how to fix prior distributions.

3.4.3. Integrated Nested Laplace Approximation (INLA)

For many years, Bayesian inference has relied upon Markov Chain Monte Carlo methods (MCMC) to compute the joint posterior distribution of the model parameters. This is usually computationally very expensive as this distribution is often in a space of high dimension. To implement an approximate inference, certain restrictions and assumptions are introduced. Firstly, rather than being a solution applicable to any model (as is the MCMC case), approximate inference models comprehend a limited broad of techniques (called structured additive regression models). This specific, but very wide, family of models are generally Generalized Linear Models (GLM), Generalized Linear Mixed Models (GLMM), Generalized Additive Model (GAM), Generalized

Additive Mixed Model (GAMM). Secondly, if it assumes that probability distributions behave like standard distributions (such as the Gaussian distribution), then they can be approximated from a smaller set of properties (such as location and spread).

Rue et al. (2009) propose a novel approach that makes Bayesian inference faster developing a new approximation to the posterior marginal distributions of the model parameters based on Laplace approximation, i.e. the *Integrated Nested Laplace Approximation* (*INLA*). Nowadays, INLA becomes the most popular tool for Bayesian spatial modelling thanks to its implementation in R package R-INLA (Rue et al. 2017; http://www.r-inla.org/). INLA models are built on the following concepts:

- Latent Gaussian Models
- Gaussian Markov Random Fields
- Laplace Approximation

Latent Gaussian Models (***LGM***) are the class of Bayesian models amenable to INLA-based inference. An LGM consists of three elements: a likelihood model, a latent Gaussian Field and a vector of hyperparameters. In a structured additive regression model, the observation (or response) variable *y* is assumed to be distributed according to an exponential family (such as Gaussian, Poisson, Binomial, Negative Binomial, Gamma etc) and the expected value of the response (μ) is linked to structured linear predictor (η) via a link function (g(μ)=η). It is considered additive as the different structured components (associated with the covariates) are assumed to accrue to the linear predictor additively. Familiar formulations of a structured additive regression model include (Eq. 3.8):

$$\eta_i = g(\mu_i) = \beta_0 + \sum_{j=1}^{J} \beta_j z_j(s) + \sum_{k=1}^{K} W_{z_k}(s) + \varepsilon_i \qquad 3.8$$

where η_i is the linear predictor, $g(.)$ is the link function, μ_i are the expected values of the i observations, β_0 is the intercept, z_j are fixed (linear) covariate effects with coefficient β_j, $j = 1,\ldots..,J$, and W_{z_k} encodes additional (non-linear) random effects according to some functional form defined with respect to covariate set z_k, $k = 1,\ldots..,K$. These problems are commonly solved via Generalized Additive Mixed Models (Steger et al. 2021). GAM offers the possibility to model linear (or fixed) and non-linear (or random) effects representing the functional relation between a set of explanatory and dependent (presence/absence of landslides per mapping unit, separately) variables (e.g., Brenning, 2005). The LGM thus estimates a range of parameters $\theta = \{\eta, \beta_0, \beta_j, z_k\}$. If it assumes that each of the parameters are Gaussian, then the model is considered a *Latent Gaussian Model* and if jointly assumed to be drawn from a multivariate normal distribution, then it is considered a *Gaussian Latent Field*.

Secondly, they focus on models that can be expressed as latent ***Gaussian Markov Random Fields*** (***GMRF***). A process is considered to have Markov properties if the expected future state of a parameter depends only on the current state and not on the state prior to the current. That is the expected state depends only on the directly adjacent state. Hence, the future state is independently conditioned only on the immediately adjacent state (depend only on immediate neighbours). If it then extends this to multiple parameters (for example, multiple random effects), then it is said to be a *Markov Random Field*. For example, considering temporal autocorrelation, the dependency amongst times would be considered *Markov* if the expected value at a particular time was only dependent on the values immediately adjacent (*i.e.*, x_4 depends only on x_3 and x_5).

The ***Laplace Approximation*** is an essential component of INLA, allowing for fast computations across a wide range of likelihoods and link functions. A Laplace Approximation is used to estimate any probability density function with a normal distribution. Laplace approximation is a method that first locating the mode of the posterior, taking this as the mean of the normal approximation, and then calculating the variance of the normal by "looking at" the curvature of the posterior at the mode. For complex models resulting in multimodal posteriors, it will obviously not be a good approximation, but for simple models (such as GLMM or GAMM), it works pretty well. Notwithstanding, this approximation could be slightly misleading, but it is preferred to MCMC because Laplace Approximation only has to find the mode of the posterior, it does not have to explore the whole posterior distribution and therefore it can be really fast.

Essentially, the data are assumed to follow a "well-behaved" distribution function and to be conditionally independent given some latent (multivariate) Gaussian random effects. In this dissertation, landslide counts are modelled using the Poisson distribution, whose mean is expressed on the log scale in terms of various fixed effects and latent random effects that are correlated over space. Each of the covariate coefficients simply has a normal distribution prior, independent from the others. As for hyperparameters, the prior distributions are chosen more specifically depending on the role of the parameter. The key advantages of R-INLA relies on the systematic use of random effects with sparse precision (i.e., inverse covariance) matrices within this latent Gaussian modelling framework, coupled with astute analytical and numerical approximation schemes (Rue et al. 2009, 2017), which provide exceptional speed-up for fitting large and complex models compared to more traditional Markov Chain Monte Carlo (MCMC) methods.

CHAPTER 4: STUDY AREA

4.1. Geographical framework

Located in the easternmost part of the *Liguria* region, *Cinque Terre* is a 38 km^2 wide area that encompasses a narrow coastal zone and five small hamlets (i.e., *Monterosso al Mare, Vernazza, Corniglia, Manarola* and *Riomaggiore),* representing a significant national and international tourist attraction (Fig. 4.1). Despite its seaside location, this area exhibits the peculiar characteristics of mountain landscapes due to its rugged morphology, with very steep slopes, deeply cut valleys and small catchments with ephemeral streams (Cevasco 2007; Brandolini 2017). The restricted coastal zone of *Cinque Terre* is bounded to the northeast by a series of peaks ranging in altitude, from 400 to around 800 m a.s.l., following an approximately NW-SE trending alignment that runs parallel and very close to the shoreline and separate *Cinque Terre* from *Vara* valley. The *Monterosso*, *Vernazza*, *Manarola* and *Riomaggiore* villages are mainly located along the coast adjacent to rivers and partly on the top of the sea cliff; only the *Corniglia* hamlet is wholly placed on an ancient marine terrace at an elevation of 100 m. Based on their environmental, scenic and historical significance, *Cinque Terre* has been recognised since 1997 as a "World Heritage List" by UNESCO and since 1999 has been included within the National Park of *Cinque Terre* (hereafter, CTNP), for its environmental and naturalistic relevance. Due to the morphological characteristic of this area, the landscape is characterized by terraces, supported by dry-stone walls, for the cultivation of vineyards (Terranova 1984, 1987, 1989).

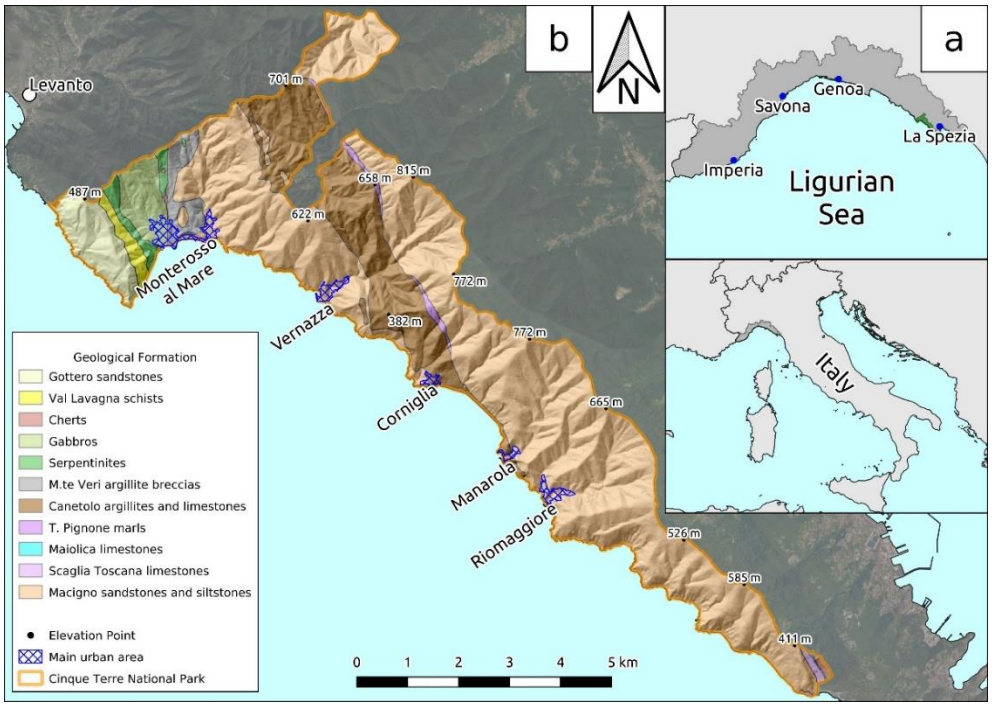

Figure 4.1 (a) Geographic location of the study area; (b) *Cinque Terre* National Park geological map (modified after Raso et al. 2019a); blue areas show the location of the historic coastal hamlets of *Cinque Terre*.

4.2. Geological and geomorphological setting

CTNP territory is characterized by the presence of five overlapping tectonics units belonging to the Tuscan, Sub-Ligurian and Ligurian domains (Giammarino et al. 2002). These units belong to an NW-SE oriented segment of the chain, which during the orogenic phases of the Tertiary age, were arranged in a large SW-verging antiform fold (Giammarino and Giglia 1990). The aforementioned succession comprises, from top to bottom, the following units: *Gottero* Unit, *Ottone* Unit, *Canetolo* Unit, *Marra* Unit, and Tuscan Nappe (Abbate et al. 2005).

The most widespread rock formation is flysch which primarily comprises thick sandstone-claystone turbidites, locally known as *Macigno* Fm. (upper Oligocene), and secondly by limestones, only observable nearness of the easternmost border of the CTNP. This formation belongs to the Tuscan Nappe (**Tuscan Domain**) which diffusely is cropping out both along the coast, between *Monterosso* and *Monesteroli* promontory, and inland.

Regarding the **Sub-Ligurian Domain**, claystones with limestones and silty sandstone turbidites (*Canetolo shales and limestones*, Paleocene), marly limestones with thin claystone interbeds and calcarenitic turbidites (*Groppo del Vescovo limestones*, early-middle Eocene) and fine-grained sandstone turbidites (*Ponte Bratica sandstones*, upper Oligocene) belonging to the *Canetolo Unit* outcrops in the central part of *Cinque Terre*, in particular along the coast between *Corniglia* and *Manarola*. Moreover, a few outcroppings, belonging to the *Marra Unit*, of silty marls and siltstones (*Torrente Pignone marls*, Oligocene), chiefly are found into the *Vernazza* catchment boundaries.

The **Ligurian Domain** is partitioned into two different domains, namely *external* and *internal* ones. *Mt. Veri complex* (upper Cretaceous) belongs to the external domain and it is part of the *Ottone* tectonic unit. The *Mt. Veri complex* is distinguished by the presence of claystones and limestones with olistolites of ophiolitic and granitic breccia and it is present in the westernmost sector of the CTNP between the *Mesco* promontory and *Monterosso*. Lastly, concerning the internal Ligurian Domain formations (*Gottero* Unit, upper Cretaceous), quartz-feldspar sandstones in thick beds with thin claystone interbeddings (*Mt. Gottero sandstones*, Campanian/Paleocene); banded shales typically consist of shales alternating with thin beds of laminated, sometimes marly, siltstones (*Lavagna shales*, upper Cretaceous); grey shales with intercalations of dark grey calcilutites and rare siltstones (*Palombino shales*, upper Cretaceous); gabbros (middle jurassic) and serpentinites (Jurassic) crop out in the westernmost part of the Park.

From a geomorphological point of view, the study area is distinguished by tiny catchments with steep and very steep slopes (roughly 57% of the area shows a slope gradient higher than 30°) (Raso et al. 2020b). These slopes are mantled by thin covers of eluvial-colluvial deposits, extensively reworked by human activities over the past centuries (Cevasco et al. 2013a; Scopesi et al. 2020).

The geomorphological landscape of *Cinque Terre* is dominated by gravity and running water processes. These terrestrial processes interact with marine erosion along the coast, resulting in the presence of several large coastal landslides and an almost continuous rocky sea cliff. The catchments, very small in extent (from less than 1 km^2 up to approximately 6 km^2), are drained by short and steep fluvial stems, whose mouths are often inhabited by the main hamlets (Brandolini 2017). The most common landscape feature of the study area is represented by agricultural terraces, here sustained by dry-stone walls, and mainly built by local inhabitants since the 1^{st} – 12^{th} century for agricultural purposes (Terranova 1984, 1989; Terranova et al. 2002).

Considering the intense rainfall that regularly affects the *Cinque Terre* area and the high steepness of the slopes, which are typically characterised by eluvial-colluvial covers of only 1–2 m in thickness, shallow landslides are widespread throughout *Cinque Terre*. The principal phenomena that occur in the CTNP are debris slides (~23%) and debris rock/avalanches (~21%). However, debris slides, during heavy rainfall, can rapidly evolve into flow-like landslides (~11%), with a failure surface represented by the contact between debris cover and bedrock, have particularly affected mostly abandoned or non-maintained terraced slopes in the CTNP (Cevasco et al. 2013a, 2014; Pepe et al. 2019; Raso et al., 2019a). Almost the entire littoral zone of *Cinque Terre* is characterised by a spectacular rocky coast, cut by the action of prevailing sea storms from the SW (*Libeccio*) and SE (*Scirocco*). Most of these sea cliffs are active and have an edge of scarp typically ranging between 5 and 30 m, but reaching 100 m just along from the *Corniglia* promontory. In fact, the interaction between the rock mass geo-structural features and the sea action determines the occurrences of rockfalls (~18%), which are widespread in the CTNP.

Beaches in the region are few and small and are associated with the main rivers (*Fegina* and *Vernazza*) or occur at the foot of some coastal slopes affected by active gravitational processes (*Guvano*, *Campi* and *Monesteroli*). Several artificial beaches (*Corniglia, Vernazza* and *Monterosso*), currently in retreat, were created in 1870 and 1970 by nourishment with materials derived from the construction of tunnels on the *Genova-La Spezia* railway line (Brandolini 2017).

4.3. Agricultural Terraces

Agricultural terraces are one of the most common features in cultivated hilly and mountainous landscapes. During the last millennium, due to rugged morphology and by a lack of wide flat areas suitable for cultivation, the geomorphological landscape of CTNP has been almost totally modified by human activity through the construction of agricultural terraces, from sea level up to 400 - 500 m, producing an unusual man-made coastal landscape (Fig. 4.2).

Early farmers reworked and retained the shallow colluvial covers by constructing dry stone walls, selecting the most suitable bedrock for cultivation. Not coincidentally, the borders of the terraced areas line up almost exactly with the geological contacts of the different formations which crop out in the area. In fact, vineyards and olive groves in CTNP are found only on terraces built on sandstones and clayey siltstones (Tuscan Unit), claystones with limestones and silty sandstone turbidites (*Canetolo* Unit), clayey shales with siliceous micritic limestones (*Gottero* Unit) and claystones and limestones with olistolites (*Ottone* Unit). Significantly, no terraces have been built on quartzose and micaceous-feldspatic sandstones (*Gottero* Unit) (Brandolini 2017). Terraced slopes cover an area of about 15 km^2, corresponding to about 41% of the entire CTNP area; however, approximately 67% of the terraced areas have been abandoned (Raso et al. 2020b). Considering that the width of terraces ranges from 2 to 4 m, the maximum linear extent of dry stone walls can be estimated to total around 6000 km. Furthermore, considering that wall height normally ranges between 1.5 and 2.5 m, depending on slope steepness and terrace width, the total volume of reworked dry stone is likely to exceed 8000000 m^3 (Terranova 1984).

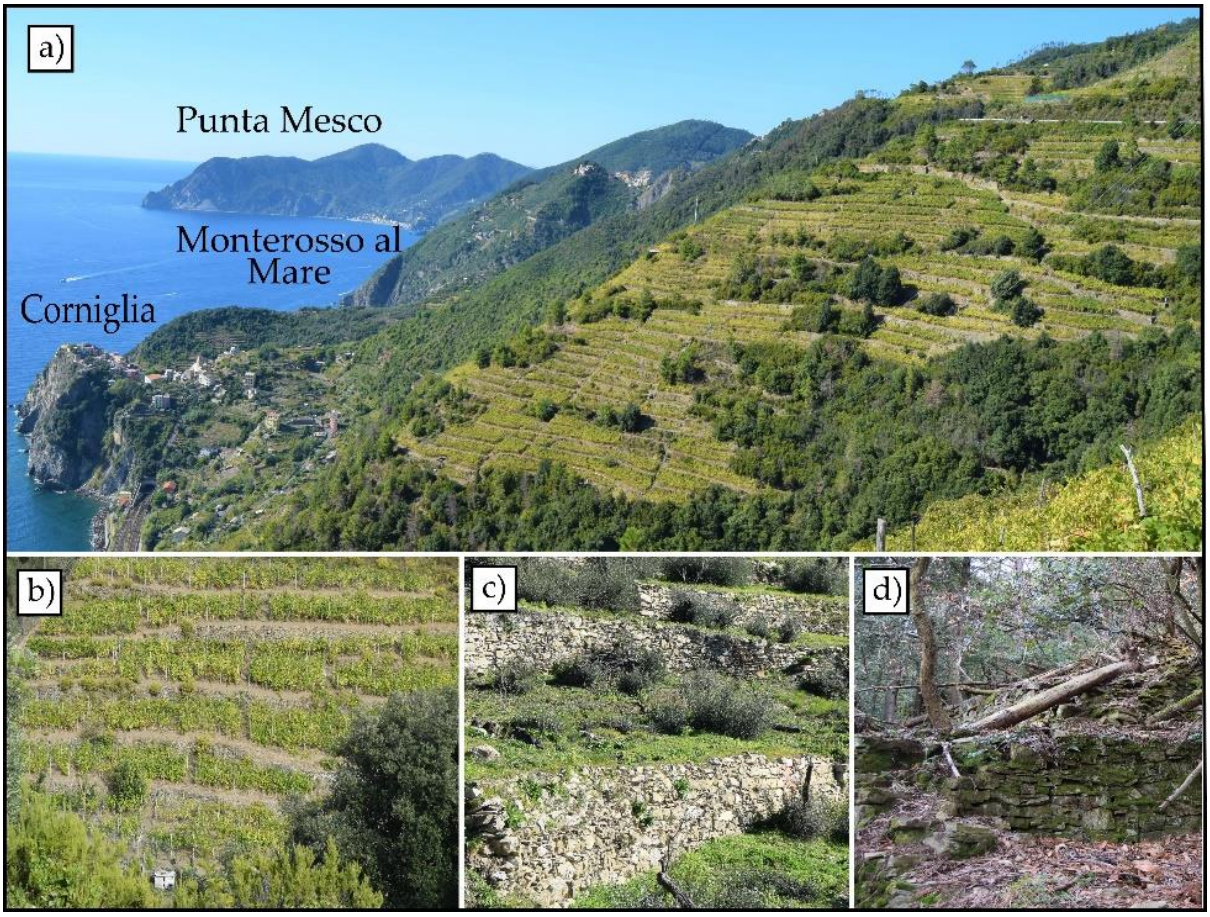

Figure 4.2 (a) Overview of the agricultural terraced landscape typical of the *Cinque Terre* National Park (Di Napoli et al. 2021). In the lower-left corner, the *Corniglia* hamlet, while in the background the *Punta Mesco* headland and the *Monterosso al Mare* village are shown; (b) well-maintained terraced slope cultivated with vineyards; (c) abandoned terraces with poor cover (the growth of shrubs is visible); (d) abandoned terraces with dense cover (tree species are visible).

Among the indirect human-related land use modifications, the abandonment of farming areas can be considered by far one of the most relevant (Poyatos et al. 2003; García-Ruiz 2010; Del Monte et al. 2015; Lasanta et al. 2015). Agricultural terraces can be distinguished into four different land use and land cover classes: *i*) cultivated terraced area, *ii*) terraced area covered by shrubs, *iii*) terraced area covered by forest tree species and *iv*) unterraced area, including mainly and minimally urban area. Currently, about 33% of terraced areas results cultivated, 48% is affected by shrub covers whereas about 19% presents dense forest covers. Cultivated terraced areas are characterized by vineyards, olive and citrus groves and they are widespread near urban centres and along S-SW exposed slopes. Terraced areas covered by shrubs can be assumed as recently abandoned while terraced lands presenting dense forest covers as abandoned for decades or centuries. Abandoned terraced slopes are common in areas not easily accessible by agricultural vehicles and in the most fragmented farming properties (Pepe et al. 2019).

In Europe, due to the significant social and economic changes which occurred at the end of the 1800s and accelerated after the Second World War (MacDonald et al. 2000), many hilly and mountainous regions have experienced severe and accelerated slope degradation issues led by farmland abandonment (Koulouri and Giourga 2007; Agnoletti 2007; Arnaez et al. 2011; Brandolini et al. 2018b). Slope degradation in conjunction with extreme rainfall can produce significant growth in susceptibility to erosion and landslide phenomena (Cevasco et al. 2015; Piacentini et al. 2018; Pepe et al. 2019). Moreover, abandoned slopes may become a source of risk scenarios when located in the proximity of urban areas (Cevasco et al. 2014, 2015; Galve et al. 2016).

The negative effect of farmland abandonment on slope stability can be especially important in terraced landscapes. It is widely known from technical literature that agricultural terraces, if properly maintained, have a positive role in soil conservation and slope stability by reducing the overall slope gradient and by regulating water infiltration and runoff (Gallart et al. 2002; Cammeraat et al. 2005; Morgan 2009; Stanchi et al. 2012). On the other hand, a lot of studies demonstrated that when these traditional systems are abandoned, land degradation issues (i.e., gully erosion, terrace failure, mass movement, piping, hydrological connectivity) arise (Tarolli et al. 2014; Arnáez et al. 2015; Moreno-de-las-Heras et al. 2019). The dry-stone walls and complementary drainage structures are no longer adequately maintained and managed, causing the efficiency of the hydrological and retaining functions to decrease. Accordingly, agricultural terraces become more vulnerable and therefore highly susceptible to collapses and failures (Camera et al. 2012; Tarolli et al. 2014; Brunori et al. 2018). Many studies addressed that the degree of abandonment and lack of maintenance of dry stone walls are crucial factors in regulating the susceptibility of terraced slopes to be affected by rainfall-induced landslides (Glade 2003; Lasanta-

Martínez et al. 2005; Lesschen et al. 2008; Cevasco et al. 2014; Brandolini et al. 2018a; Moreno-de-las-Heras et al. 2019).

Numerous studies have shown that to prevent water erosion processes and to improve slope stability, terraces require constant maintenance (Gallart et al. 1994). A lack of wall maintenance has resulted in crumbling of many spectacular areas of terraced slopes, which are now widely affected by soil erosion and landsliding (Fig. 4.3). In only a few decades, the upper parts of the abandoned terraces became overgrown with pine trees, and the middle-lower slopes by Mediterranean scrub (Brandolini 2017). Furthermore, recent studies have shown that in Mediterranean areas, because of climate changes, a modifying distribution of precipitation with an increase in extreme events or multiday events is occurring (Piccarreta et al. 2013; Cevasco et al. 2015). The effects of terrace abandonment may even result in increased risk conditions when slopes are located in proximity to urbanized areas.

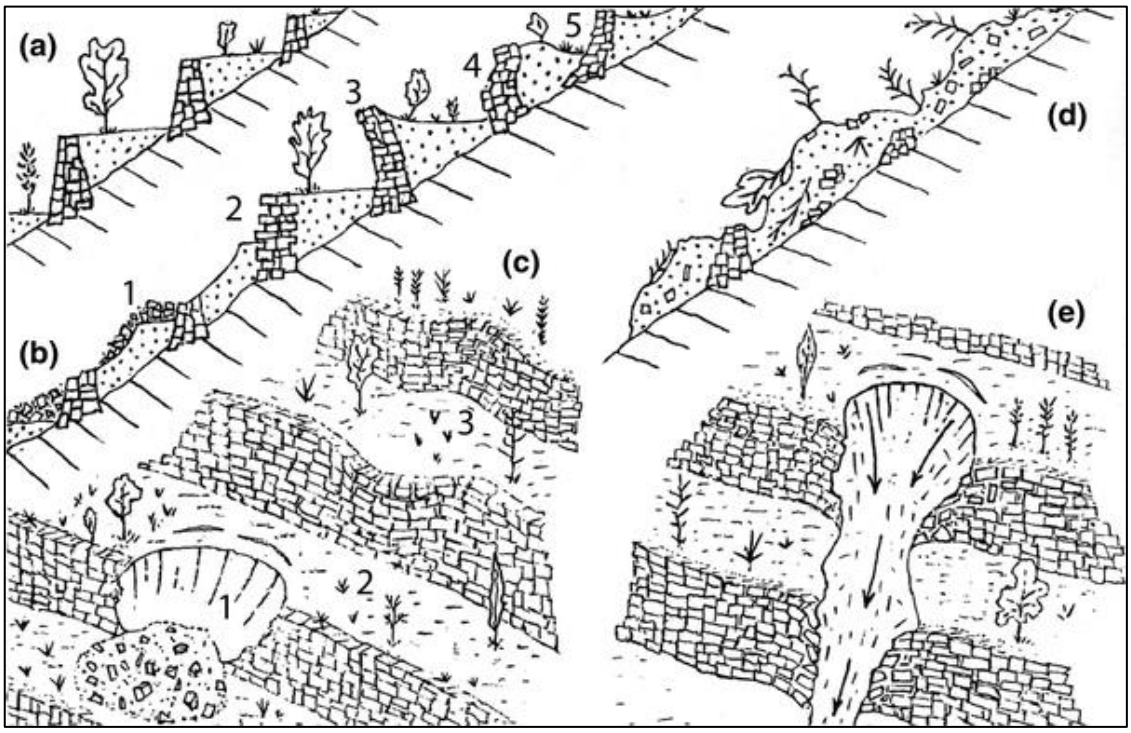

Figure 4.3 Evolution of slope terracing after farming abandonment: a, cultivated terraces in good state of conservation; b, different types of dry stone walls crumbling: fall (1), sliding (2), topple (3), bulging and sliding (4, 5); c, terrace collapse along a concave surface (1), dry stone walls deformations (2, 3); d, drystone walls completely destroyed; e, terraced slope affected by shallow landsliding (modified after Terranova 2005).

In the study area, abandoned terraced slopes are particularly susceptible to shallow landsliding, especially due to intense rainfall (Cevasco et al. 2014). During high-intensity rainfall, materials mobilized by mass transport and landslide phenomena have a considerable impact on the solid discharge, flow and energy of streams. These dynamics, which are quite common in the entire *Liguria* region, often cause flow-like movements, debris floods and flash floods, which are increasingly affecting, in particular, the coastal settlements (Guzzetti et al. 2004). Within the CTNP,

these phenomena represent a serious threat to human settlements, inhabitants and trail users, as dramatically observed after the intense rainstorm that hit the *Monterosso* and *Vernazza* areas on 25th October 2011 (Cevasco et al. 2015; Giordan et al. 2020). Lack of maintenance of dry stone walls plays an important role in making terraced slopes susceptible to instability, but it is not the only factor that has to be considered (Crosta et al. 2003).

4.4. Climatic features

The physiographical features of the CTNP deeply control the local climate setting. Southerly exposition, the orientation of the main basin parallel and very close (approximately 3 km) to the sea acting as a barrier, which produces a topographic effect that locally protects the coast from continental influxes and enhances the features of the peculiar Mediterranean climate, characterised by warm, dry summers and mild winters. Moreover, the humidifying action of the sea on the air masses coming from the southern quadrants and the effect of the Alpine-Apennine chains, which frequently divert Atlantic perturbations towards the Gulf of Genoa, produces relatively abundant rainfalls (Cevasco et al. 2015).

The average annual temperature ranges between 14.5 and 15.5 °C, reaching a mean peak of 22 – 24.5 °C in July and August and a low of 7 – 8 °C in January. The annual rainfall value ranges between 900 and 1100, with maximum rainfall typically occurring in December; a mean value of 224 mm has been recorded for this month at the Levanto gauge station for the period 1932 – 2011. A sudden increase of the mean annual precipitation with altitude was observed, with values reaching approximately 1500 - 1600 mm in the immediate and higher inland *Vara*/*Magra* valleys. The rainiest period commonly comprised between October and November, when intense rainstorms often can occur (Cevasco et al. 2015). Heavy rainfall events of short duration are very recurrent in the area, with intensities greater than 150 mm/3h and 200 mm/6h as recorded during the period 1951 – 2011. Extraordinary rainfall events are also very frequent due to the geomorphological setting, especially in the ongoing climate change context (Galanti et al. 2018).

One of the most significant rainfall events occurred on 25 October 2011. Its exceptional nature was confirmed by an analysis of historical climate series between 1932 and 2011 conducted using data from the coastal rain gauge at *Levanto* (Cevasco et al. 2015). During these 80 years, the mean annual precipitation was 1042 mm with a minimum of 668 mm (1989) and a maximum of 1541 mm (1979). The rainiest month was December, with a mean precipitation of 224 mm. The analysis of high-intensity rainfall for the period 1951 - 2011, for which data are available, indicates that 2 events with intensities greater than 150 mm/3 h, 2 events with intensities greater than 200 mm/6 h, and only one event with an intensity greater than 250 mm/12 h were recorded. The rainfall

intensities recorded at *Monterosso* during the 25 October 2011 event exceeded any recorded in the *Cinque Terre* area during the period 1951 - 2011. In addition, the cumulative rainfall of the 25 October 2011 event recorded at *Monterosso* (382 mm) was much higher than the mean rainfall of the rainiest month in this area (224 mm). The analysis of the maximum precipitation intensity at 12h may be further evidence of the uniqueness of the event. A review of historical archives showed that the *Vernazza* hamlet was affected by extensive damage caused by floods only in 1857 and 1859 (Rollando 2003).

4.5. The 25th October 2011 event (from Cevasco et al. 2015)

On October 25th 2011, after a long dry period, a rainfall event hit a wide area between eastern *Liguria* and north-western Tuscany (Fig. 4.4a). After a few hours of low-intensity rainfall, a violent storm system with a"self-healing" structure originated in the *Cinque Terre* area, in a very short time interval. Huge amounts of rainfall fell between 9:00 and 15:00 (Universal Time Coordinated, UTC) on the coastal area of the *Cinque Terre* and the *Vara* valley and, subsequently, on *Lunigiana*. Rainfall was recorded by several rain gauges located in eastern Liguria (ARPAL-CFMI-PC 2012) and northern Tuscany (CFRT, 2011).

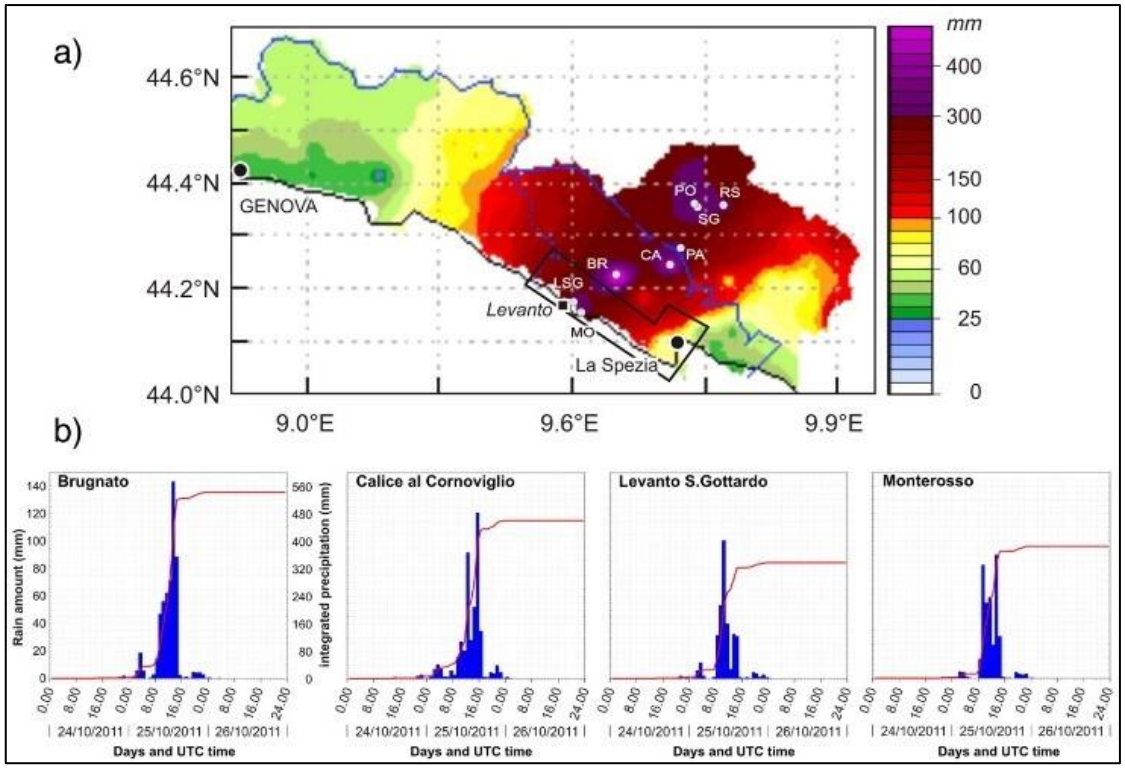

Figure 4.4 Characteristics of the October 25th , 2011 event (from Cevasco et al. 2015). a) Spatial pattern of cumulated rainfall around and across the study area (bounded in black) of October 25th 2011 (after ARPAL-CFMI-PC 2012), modified). The grey points mark the rain gauges cited in the text. LSG: *Levanto San Gottardo*; MO: *Monterosso*; BR: *Brugnato*; CA: *Calice al Cornoviglio*; PA: *Parana*; SG: *Santa Giustina*; PO: *Pontremoli*; RS: *Rocca Sigillina*. b) Hyetographs (blue bars) and cumulative rainfall plots (red lines) of the *Brugnato*, *Calice al Cornoviglio*, *Levanto San Gottardo* and *Monterosso* rain gauges (data from the *Liguria* Region - ARPAL, 2011, http://www.arpal.gov.it).

As shown in Table 4.1, in eastern *Liguria*, very high cumulative rainfall amounts were recorded in the inland *Vara* valley at the *Brugnato* and *Calice al Cornoviglio* rain gauges and, along the coast, at the *Levanto San Gottardo* and *Monterosso* rain gauges with 539 mm, 454 mm, 333 mm and 382 mm, respectively. Hourly intensity rainfall peaks recorded at *Brugnato*, *Calice al Cornoviglio*, *Levanto San Gottardo* and *Monterosso*, were 153 mm/h, 129 mm/h, 111 mm/h and 92 mm/h, respectively (Fig. 4.4b). Rainfall intensities at 3, 6 and 12 h were also extremely high. The higher values (e.g. 472 mm/6 h) were recorded at the *Brugnato* rain gauge. Moreover, in *Lunigiana* (northwestern Tuscany) rainfall amounts reached their maximum at the *S. Giustina* rain gauge, with 376 mm; lower, but significant values of cumulative rainfall were also recorded at *Rocca Sigillina* (318 mm), *Pontremoli* (366 mm) and *Parana* (315 mm).

Table 4.1 Cumulated rainfall on 25th October 2011 and maximum rainfall intensity in 1, 3, 6, 12, 24h recorded by some rain gauges of eastern *Liguria* and northern Tuscany (elaborated by Cevasco et al. 2015) from data from the *Liguria* Region, 2012 and CFRT, 2011). The bold type indicates rain gauges and data regarding the study area.

Rain gauge	Cumulated rainfall Oct. 25, 2011 (mm)	Maximum rainfall intensity (mm)				
		1 h	3 h	6 h	12 h	24 h
Brugnato	538.2	153.4	328.4	472.0	511.0	538.8
Calice al Cornovoglio	452.8	129.2	228.4	365.4	404.0	453.8
Levanto San Gottardo	**333.0**	**111.0**	**204.0**	**282.4**	**312.0**	**333.4**
Monterosso	**381.8**	**91.8**	**197.0**	**348.8**	**362.0**	**382.2**
Parana	315.2	88.0	164.8	230.4	265.6	315.2
Santa Giustina	374.4	72.8	177.2	260.8	323.0	376.2
Rocca Sigillina	315.4	68.8	163.2	239.6	279.2	318.4
Pontremoli	365.8	67.0	164.8	251.4	319.8	366.0

The highest hourly intensity was recorded at the *Parana* rain gauge (88 mm). Rainfall intensities at 6 and 12 h were lower than those recorded in eastern *Liguria* but nevertheless were significant (Table 4.1).

The intense rainfall triggered hundreds of shallow landslides and floods affecting the Tyrrhenian basins between *Bonassola* and *Manarola* and the *Magra* river basin (Cevasco et al. 2012; D'Amato Avanzi et al. 2013). The event caused 4 casualties, severe damage to villages and infrastructures (the collapse of bridges, interruption of provincial and municipal roads, and stretches of highways and railways, and the temporary interruption of essential services such as gas, water, telephone and sewerage). In the study area, the *Vernazza*, *Monterosso*, *Levanto* and *Bonassola* catchments suffered considerable damage. This damage was particularly severe in the inhabited historic centres of *Vernazza* and *Monterosso* (Fig. 4.5), where enormous amounts of material were mobilized on the

slopes by shallow landslides and accelerated erosional processes and subsequently charged by torrents downhill, originating hyperconcentrated flows and mud/debris floods.

Three casualties occurred in *Vernazza*, one in *Monterosso*. These two villages are typical examples of anthropic transformations, which mainly occurred in the past century, leading to flood risk increase; in fact, in both cases, the main urban street was built by covering the final tract of the valley floor along which the stream originally flowed. In both cases, the covered tract of the stream beds was filled by debris and the above urban streets suddenly turned into raging torrents. As a result, the central streets of *Vernazza* and *Monterosso* were buried by mud and debris up to 4 and 3 m thick, respectively. Recent detailed studies on the relationships between slope processes induced by the intense rainfall of October 25th 2011 on the *Vernazza* basin and land-use (Cevasco et al. 2013a, b, 2014) highlighted that the rainfall event triggered more than 500 shallow landslides on an area of approximately 5.8 km^2 (about 1.5% of the basin area); additionally, 1.65% of the basin area was affected by very intense accelerated erosion.

These studies pointed out the extreme vulnerability of terraced slopes which, due to the lack of maintenance of dry stone masonries, currently represent the main areas prone to landsliding and accelerated erosion. An even more recent study (Cevasco and Brandolini 2015) has shown that the anthropic modifications which occurred in the *Vernazza* basin during the 1970s (e.g. roads construction), played a negative role, especially in increasing the effects of the October 25th 2011 debris flows and debris flood.

Figure 4.5 Some damage suffered in the *Vernazza* and *Monterosso* catchments due to the October 25th 2011 precipitation (from Cevasco et al. 2015). a) Destruction of roads (*Vernazza* basin); b) accelerated erosion on cultivated terraces (*Vernazza* basin); c-d) the main street of *Vernazza* buried by mud and debris immediately after the rainfall (photo cfromhttp://www.youreporter.it, integrated) and after the removal of the debris flood deposits; e) destruction of a part of the covered tract of the *Canale Pastanelli* at *Monterosso*; f) the main street of *Monterosso* during the works for removing the debris flood deposits.

CHAPTER 5: APPLICATIONS

The following sections include all the applications that have been developed during the three-year doctoral experience. The different methodologies were applied to areas of vaying size located within the *Cinque Terre* National Park (CTNP) using different algorithms and different input data resolutions. Firstly, a test area (5.4 km^2 wide) was chosen to apply ML methods and, subsequently, the same approach was adopted to the whole CTNP (38 km^2 wide) but considering also the runout analysis. Lastly, the Bayesian method was applied to a portion of the CTNP (18 km^2 wide), including the *Monterosso al Mare* and *Vernazza* catchments.

5.1 Landslide Detachment Susceptibility – Monterosso al Mare case study

All the information described below is taken from the Di Napoli et al. 2020 paper entitled "*Machine Learning ensemble modelling as a tool to improve landslide susceptibility mapping reliability*" published in the international journal *Landslides* (Volume: 17, Issue: 8), https://doi.org/10.1007/s10346-020-01392-9.

5.1.1. Research objectives

Many authors have proposed methods to minimize uncertainty, which relies on combining the prediction yielded by multiple algorithms, as testified by the work of Umar et al. (2014), Chen et al. (2017), Kim et al. (2018) and Bueechi et al. (2019). The investigation of new EMs for LSM is therefore highly necessary, as also highlighted by Chen et al. (2018a). Anyhow, EM provides a solid contribution to minimize uncertainty and to refine and improve the prediction accuracy, which is always the key parameter to take into account when working with landslide susceptibility.

In this application, three different ML algorithms were ensembled to determine landslide susceptibility within some small coastal basins located near *Monterosso al Mare* (western portion of CTNP, Fig. 5.1). Specifically, each susceptibility model was implemented with 100 different landslide data combinations, every time splitting the landslide database in 80% as data training and 20% as data testing. The study area is highly susceptible to rapid shallow landslides, as testified by the rainfall-induced ground effects produced by the severe rainfall that occurred on October 25th, 2011 (see paragraph 4.5). In particular, more than 260 shallow landslides were triggered in this area (Schilirò et al. 2018).

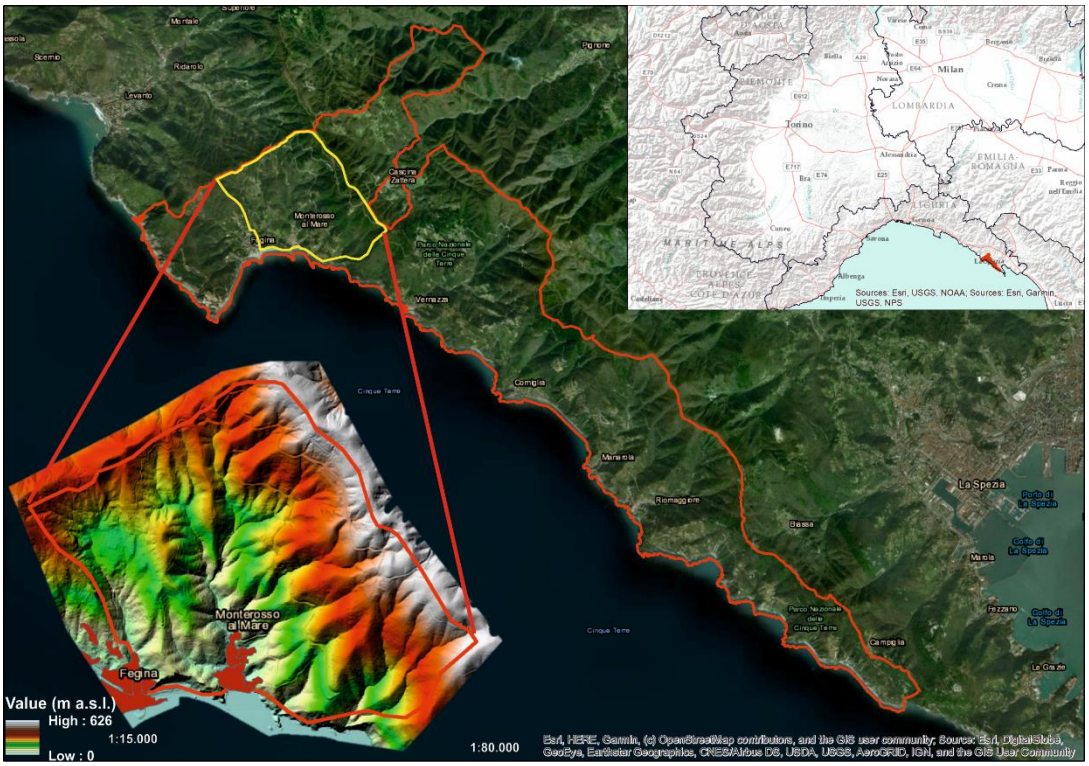

Figure 5.1 Setting of the study area. In the top-right inset, the location of the *Cinque Terre* National Park in northern Italy is represented. In the main map, the *Cinque Terre* National Park boundary is shown in red and the study area is outlined in yellow. In the bottom left, the elevation map of the study area along with urban areas and drainage network are shown (from Di Napoli et al. 2020).

Hence, the main objective of this work was to exploit, for the first time, advanced statistical techniques in a peculiar geological, geomorphological and environmental setting. The produced outcomes have been processed to understand if they could be useful to decision-makers, highlighting regions most prone to instability. With this purpose, these tools could represent potentially a fundamental tool for the safety of people and for many travellers that every year visit this outstanding landscape.

5.1.2. Landslide inventory

The landslide inventory used in this study was prepared by A. Cevasco in the aftermath of the October 25th, 2011 event (Schilirò et al. 2018; Fig. 5.2). This inventory was compiled through analysis of high-resolution aerial ortophotogrammetry and field survey, allowing to map both landslides and erosion processes. The air photo analysis was carried out on digital geo-referenced orthophotos, provided by *Liguria* Regional Administration, taken on 11 November 2011 by the Air Service of Remote Sensing and Monitoring of Civil Protection of *Friuli Venezia Giulia* Regional Administration (ground resolution from 3 to 50 cm, according to the altitude; Schilirò et al. 2018). A total of 260 shallow landslides were mapped within *Monterosso* hamlet, whereas, about 500 phenomena were triggered in the *Vernazza* basin (Cevasco et al., 2013). The shallow landslides

triggered during the event initiated as debris slides (Cruden and Varnes 1996) and in most cases evolved into debris avalanches or, in a few cases, into debris flows (Hungr et al. 2014). Shallow earth and debris covers (from 0.5 m to about 2.5 m thick) and, sometimes, portions of the weathered and fractured bedrock were involved.

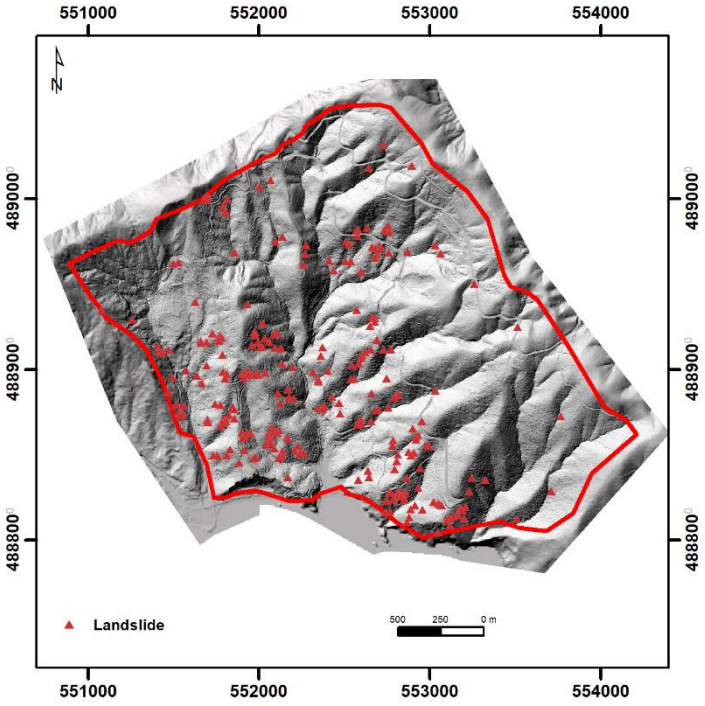

Figure 5.2 Landslide inventory map of the studied area.

Landslide areal extent ranged between a few tens of square metres up to a few thousand square metres. Earth and debris mobilized on slopes or along channels by shallow landslides increased the sediment transport along the drainage network and also the erosive energy of streams. The inability to dispose of flowing water/sediment mixtures of the final culvert of the *Canale Pastanelli*, played a fundamental role in originating the mud/debris flood that affected the Monterosso village. Concerning the *Vernazza* basin, the huge mass of water, earth, and stones flowing quickly downhill in torrents was channelled at the valley bottom just a few kilometres upstream from the inhabited area, originating a debris flood. The obstruction by solids of the final artificial tract of the *Vernazza* stream caused mud and debris to flood the centre of the village, following the original path of the stream. Bottlenecks along the central thoroughfare in *Vernazza* caused mud and debris to accumulate to heights of up to 4 m in the centre of the village and up to 5–6 m locally (Cevasco et al. 2014). In addition, some houses, bridges, roads and cars were swept away by the flood as it moved towards the villages.

Furthermore, having available the surveyed landslides as polygons, only one of the highest points, characterized by the highest altitude in the detachment area, has been selected. This

operation has been conducted to make possible the different models' execution requiring points as input data.

5.1.3. Predisposing factors

The set of potential environmental factors selected to predict unstable areas was defined based on the most representative local morphological and spatial features. This operation allowed the selection of 13 PFs (Fig. 5.3). PFs include slope angle, aspect angle, planform curvature, profile curvature, distance to roads, distance to streams, Topographic Wetness Index, Topographic Position Index, Stream Power Index, agricultural terraces state of activity, land-use, geo-lithology and soil thickness (for further detail, see paragraph 3.1). The analysis is focused on environmental variables since it does not take into consideration the triggering factors (e.g. intense rainfall or earthquakes). For this case study, environmental variables were set to 5 × 5 m grid cells resolution.

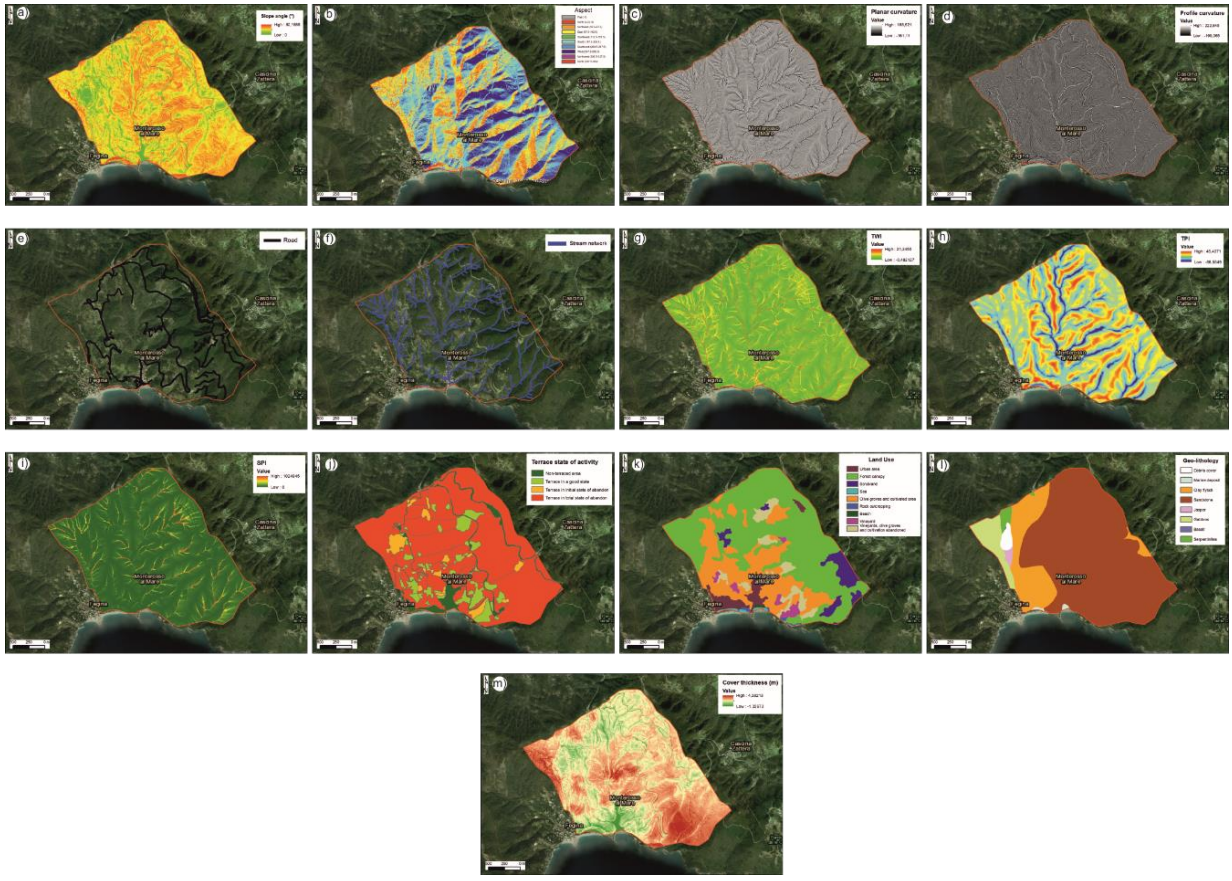

Figure 5.3 Maps of the PFs employed for the susceptibility models. *a*) Slope angle, *b*) slope aspect, *c*) planar curvature, *d*) profile curvature, *e*) distance to roads, *f*) distance to rivers, *g*) Topographic Wetness Index, *h*) Topographic Position Index, *i*) Stream Power Index, *j*) terrace state of activity, *k*) land-use, *l*) geo-lithological map and *m*) soil thickness.

5.1.4. Model building and validation strategy

In susceptibility modelling studies, the investigated area has to be partitioned into mapping units, the functional areas for which the modelling procedure is then able to predict the stability conditions. A large set of mapping units is proposed in the literature (Guzzetti et al. 1999), in this study the mapping unit adopted was the 5 m side cell of the DTM. The spatial probability of landslides in the study area was estimated considering three ML techniques (namely, ANN, GBM and MaxEnt). Models were calibrated and evaluated through a k-fold cross-validation procedure. This methodology consists of randomly dividing the original dataset into *k* portions and by using *k-1* portions of data (training data, 80%) for models' calibration, whereas the remaining set (testing data, 20%) is used as an independent record to measure model's predictive performance. The whole approach is then repeated several times for a single model and the average predictive accuracy is finally reported (Araújo et al. 2005; Thuiller et al. 2009). Once trained all stand-alone ML models the EM approach has been exploited. This procedure has been adopted for the first time by Burnham and Anderson (2002), who performed a simple average of several regression models. EMs approach, which produces a predictions integration of every stand-alone model, provides a solid contribution to minimize uncertainty and to improve the prediction accuracy (key parameter indispensable when working with susceptibility). Such EMs often result in better classification than individual ones (Pourghasemi et al. 2017). EMs help to minimize these issues as long as single algorithms are different and independent. The complete modelling procedure is visible in Figure 5.4 and can be subdivided into different steps.

The first one allows recognizing landslide occurrence data as the response variable and the predisposing factors as predictors. In the second step, to evaluate the possible correlations among each predictor, the VIF was measured. There is no well-defined and accepted threshold in the literature, the general rule of thumb is that VIFs exceeding 4 need more analysis, while VIFs exceeding 5 or 10 denotes a serious multicollinearity issue, requiring revision (Hair et al. 2010). In detail, two different VIF strategies were chosen: Vif_{cor} (*cor* stands for correlation) finds a pair of variables that has the maximum linear correlation and excludes the one having the largest VIF and Vif_{step} calculates the VIF for all variables, excludes the one with the highest VIF (greater than the threshold) and repeats the procedure until there are variables with VIF greater than the remainder (Guisan et al. 2017). In the next step, the third, the above-mentioned algorithms were performed to model susceptibility over the study area. Furthermore, during this phase, the contribution of each environmental variable has been evaluated by applying the "variable importance" tool included in the "biomod2" package (Thuiller et al. 2016). The principle of this tool is to shuffle a single variable and make a model with this "shuffled" variable. Then a simple correlation (Pearson's

coefficient) is performed between a reference model (simulated by using unmodified variables) and the "shuffled" one. The importance index is calculated as 1 minus Pearson's correlation coefficient, returning values between 0 and 1. The higher the value, the more influent the variable is on the model. This procedure is performed for each environmental variable (Lomba et al. 2010; Thuiller et al. 2016). As regards the measures of the models' predictive performance, Area Under the Curve (AUC) has been engaged (Hanley and McNeil 1982). AUC is the measure of the area under the curve of sensitivity (i.e. the proportion of accurately predicted true presences) plotted against 1-specificity (the proportion of accurately predicted true absences) for the range of all the possible thresholds to discretise the probability values assigned to either predicted presences and absences and hence it is "threshold independent" (Raes and Aguirre Gutierrez 2018).

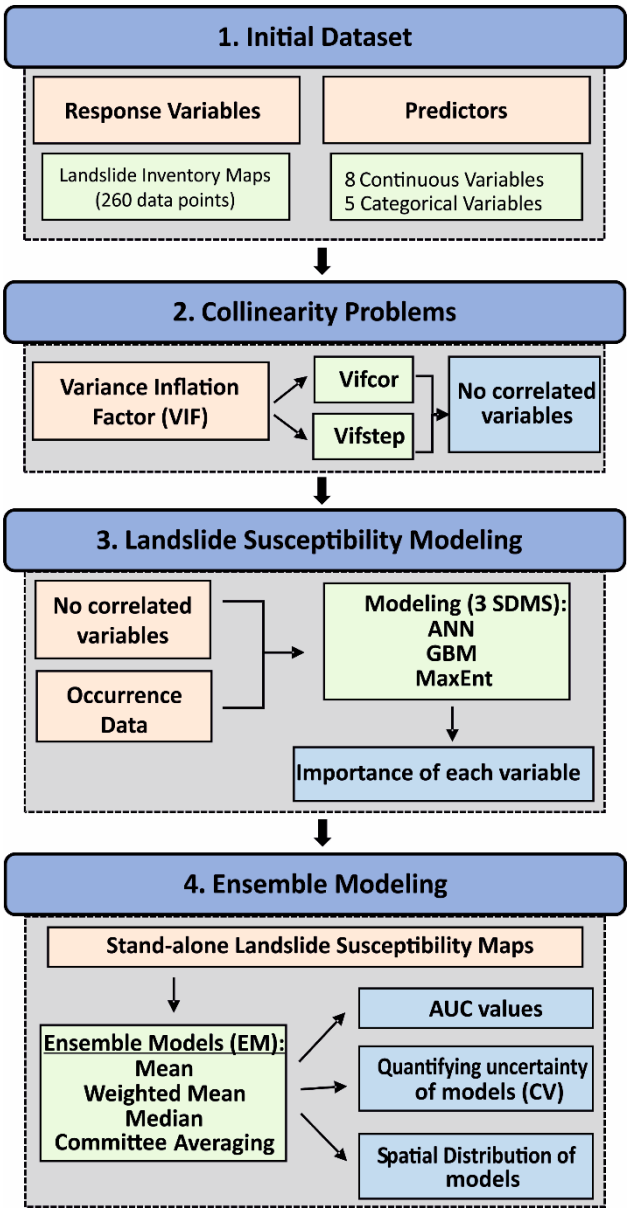

Figure 5.4 Scheme of the proposed approach for landslide susceptibility modelling.

One of the main advantages of the AUC is its ability to be insensitive to prevalence (i.e. the proportion of observed sites in which the species were recorded as present; McPherson et al. 2004; Somodi et al. 2017). AUC values range from 0 to 1, where values < 0.6 indicates weak modelling accuracy, 0.6 – 0.7 shows moderate accuracy, 0.7 – 0.8 exhibits good accuracy, and > 0.8 indicates very good accuracy (Swets 1988; Peterson et al. 2008; Corsini and Mulas 2017). The applied ensemble models are Mean of Probabilities (PM), Weighted Mean of Probabilities (PMW), Median of Probabilities (PME) and Committee Averaging (CA). The first three models correspond to the mean, weighted mean and median probabilities over each selected model respectively, while the CA needs more explanation. This ensemble forecasting method (CA) is based on the binary classification of occurrence probability maps. The CA method transforms any probability map coming from stand-alone models into binary maps using a threshold (the one maximizing both sensitivity and specificity). These binary maps are, then, overlayed and a cell-wise scores sum is performed. The final CA map is the one in which any single map's cell score is divided by the number of the original models. The interesting feature of this measure is that it gives both a prediction and a measure of the prediction's variation (Gallien et al. 2012). When the prediction is close to 0 or 1, it means that all models agree to predict 0 and 1, respectively. If the prediction is around 0.5, it means that half the models predict 1 and the other half 0 (Thuiller et al. 2016).

Given the huge amount of data produced, to compare the obtained outcomes and to evaluate their uncertainty, the Coefficient of Variation (CV) has been computed. CV (i.e., standard deviation/mean of each pixel) is a measure of uncertainty of the ensemble models and it assumes relevant importance when there is a great availability of data. If the CV exhibits a high evaluation score, the uncertainty of a given data is high, while the lower the score, the better are the models' outputs. In this study, a matrix-based approach was used to analyse the relationship between the ensemble models and the uncertainty map, to generate a "confidence" map (Kim et al. 2018). In this way, the ensemble models reliability has been assessed. The susceptibility values derived from EM were subdivided into five groups (1–5), while the CV map was categorized into six classes (1–6); in both maps, the Natural Breaks method was applied (Jenks 1967). Natural Breaks aims at defining the best data distribution in significant classes, taking advantage of the intervals naturally present in the data distribution and attempting to reduce the variance within each class and maximizing that between the classes themselves. A further comparison between the ensemble susceptibility maps was produced in terms of the spatial distribution of the susceptibility values. As previously mentioned, the ensemble maps have been divided into five classes. Subsequently, an intersection operation between the different maps has been performed. It should be stated that the CA map was

not considered in the intersection because the map binary transformation could have a strong influence on the result.

5.1.5. Landslide detachment susceptibility results

Different landslide susceptibility maps have been generated by applying 100 different combinations between training (80%) and testing (20%) datasets, attempting to generate the best predicting models (Fig. 5.5). Every susceptibility map generated in this phase is characterized by small variations and with different values of errors and evaluation scores, subsequently reduced in the EM phase. Such discrepancy helps to understand how the stand-alone models diverge from each other and how the EMs are needed to achieve outcomes more reliable and accurate. The average AUC score of the 100 iterations for each model is resumed in Table 5.1, where it is evident that the best result is obtained by GBM and MaxEnt (0.84 and 0.83, respectively), while ANN result is slightly lower (0.74).

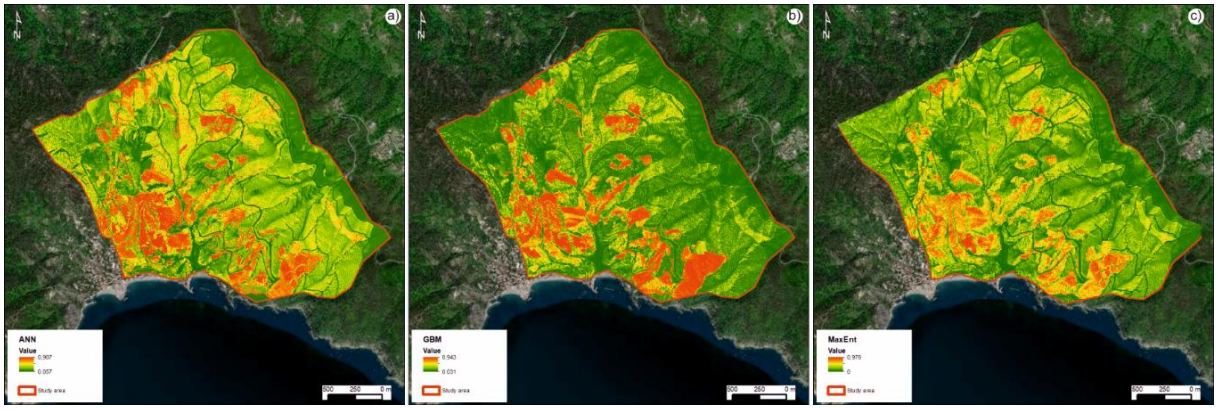

Figure 5.5 Stand-alone susceptibility maps examples. a) ANN, b) GBM and c) MaxEnt.

Table 5.1 AUC scores for the stand-alone ML algorithm used, on the top, and for EM on the bottom.

Stand-alone models	**AUC**
Generalized Boosting Model	0.84
Artificial Neural Network	0.74
Maximum entropy	0.83
Ensemble models	**AUC**
Mean	0.91
Median	0.90
Committee Averaging	0.89
Weighted Mean	0.91

Therefore, EM was performed by using four different Ensemble techniques (PM, PME, PMW, CA; Fig. 5.6). It is worth underlining that in all maps, susceptibility was shown using continuous data, without any division in classes, as often adopted in Italy in the framework of landslide risk

management. The most prone areas have been identified in the central and north-easting sectors. The EMs have improved the stand-alones' prediction reliability, as testified by the increase in the AUC values. The aforementioned stand-alone models' variability is confirmed by the CA ensemble model (Fig. 5.6c), in which areas characterized by dark green and dark red (i.e., 0 and 1) colours represent sectors where all stand-alone models predict similar outcomes. In contrast, the extreme models' variability is highlighted in the sectors with light green, yellow, orange and light red colours. The landslide distribution within the range of susceptibility value is reported in Table 5.2: the highest concentration of landslide can be found between the values 0.8 and 0.9. Moreover, the landslide distribution is characterized by an increasing trend when going from the lowest to the highest value of susceptibility. Conversely, the areal distribution of the susceptibility values shows a decreasing trend, with large parts of the territory characterized by low values of susceptibility and a limited extent for those characterized by higher values.

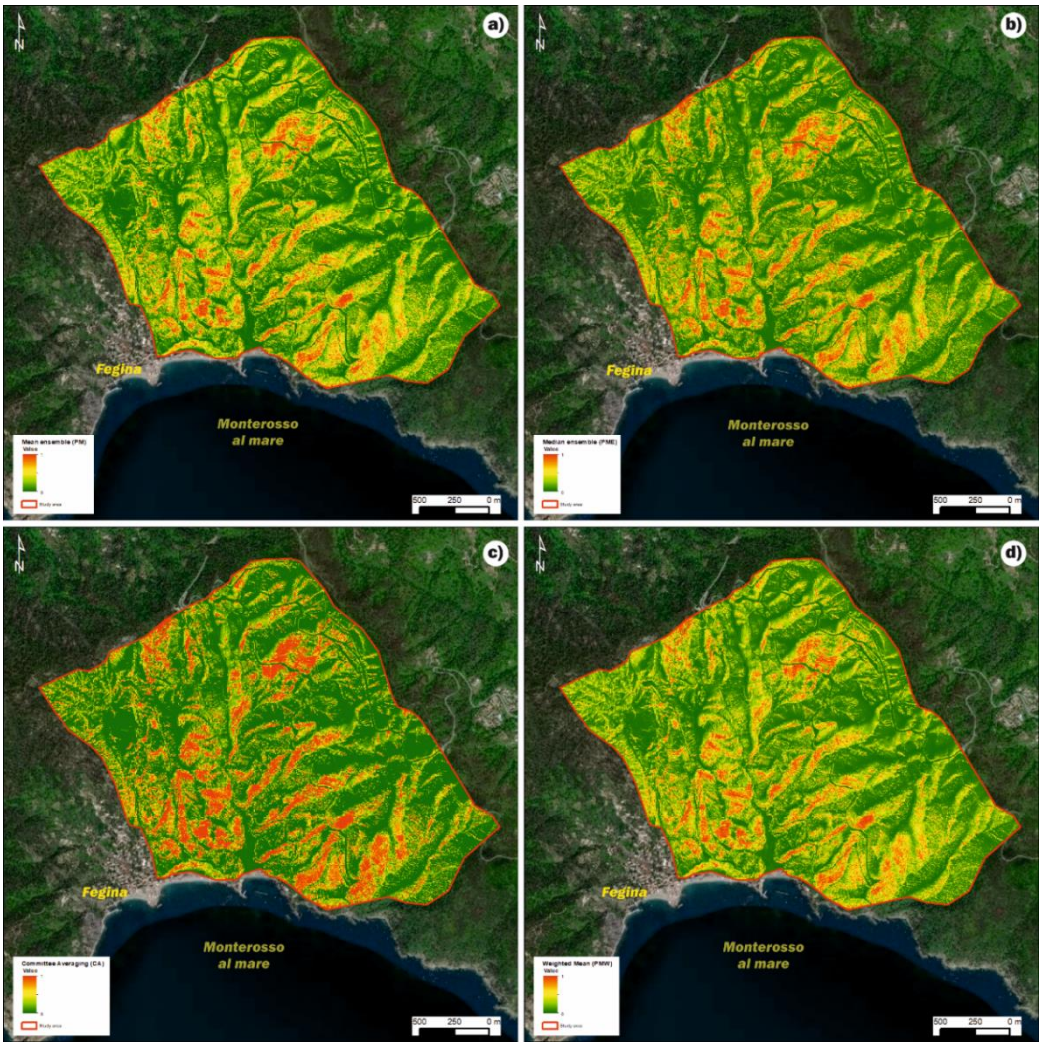

Figure 5.6 Ensemble susceptibility maps. a) Mean ensemble susceptibility map, b) median ensemble susceptibility map, c) committee averaging and d) weighted mean susceptibility map.

Table 5.2 Distribution of landslides according to the probability of occurrence value for each Ensemble model.

	PM	PME	CA	PMW
0 – 0.1	1	1	9	1
0.1 – 0.2	8	10	2	8
0.2 – 0.3	10	15	7	10
0.3 – 0.4	17	13	9	17
0.4 – 0.5	22	21	4	23
0.5 – 0.6	34	18	10	34
0.6 – 0.7	41	40	10	43
0.7 – 0.8	57	63	15	56
0.8 – 0.9	66	61	31	64
0.9 – 1	4	18	163	4

It is always hard to compare predictions from different models as they do not rely on the same algorithms, techniques and assumptions about the expected relationship between the input data and the environmental variables. In the "biomod2" package, it has been possible to examine the importance of the variables in the models. Table 5.3 shows every variable's importance for each applied algorithm, expressed in values ranging from 0 to 1 (no influence and maximum influence, respectively). Aspect and slope variables exhibited higher scores concerning stand-alone models. The other PFs showed moderate levels of importance, such as land use and terraces state of activity. In the case of EMs, five PFs (i.e., slope angle, slope aspect, planar curvature, terraces and land use) show significant values.

Table 5.3 Variable score for the stand-alone ML and Ensemble models.

Variables	GBM	ANN	MAXENT	PM	PME	CA	PMW
Slope aspect	0.40	0.52	0.29	0.38	0.39	0.43	0.38
Planar curvature	0.08	0.37	0.11	0.12	0.11	0.15	0.12
Profile curvature	0.08	0.34	0.10	0.10	0.10	0.13	0.09
Slope angle	0.17	0.36	0.17	0.18	0.17	0.22	0.18
Geo-lithology	0.01	0.18	0.03	0.03	0.03	0.05	0.03
TPI	0.05	0.05	0.11	0.05	0.06	0.07	0.05
TWI	0.06	0.03	0.09	0.04	0.06	0.06	0.05
Cover thickness	0.02	0.01	0.03	0.01	0.01	0.02	0.01
SPI	0.01	0.02	0.01	0.01	0.01	0.01	0.01
Terraces state activity	0.10	0.06	0.09	0.08	0.09	0.10	0.08
Land use	0.12	0.06	0.12	0.07	0.08	0.09	0.07
River	0.01	0.01	0.06	0.01	0.02	0.02	0.01
Roads	0.01	0.01	0.04	0.01	0.01	0.01	0.01

Consequently, CV has been computed to assess EMs uncertainty. Combining the information of landslide susceptibility and CV map a matrix was developed (Fig. 5.7). Such a matrix-based approach allowed to generate a "confidence" map (Kim et al. 2018), evaluating the EMs reliability (Fig. 5.8). In detail, the value of 51 in the matrix table highlights pixels characterized by high landslide likelihood with low variability. Conversely, a value of 16 means that a pixel has a high uncertainty with a low proneness to collapse. As can be seen from Figure 5.8, the central and north-eastern sectors of *Monterosso al Mare* catchments showed lower CV values (light areas), while the other portions of the basins showed high CV values (dark areas). This is an expected pattern, taking into account that the ensemble models highlighted analogous values of susceptibility in the central and north-eastern study areas. However, areas with high CV values can be identified where mainly low susceptibility values are located. In general, the CV map gives a more powerful basis to estimate landslide-susceptible areas of the study area along with ensemble maps. However, the CV map could not take into account uncertainty coming from predisposing factors; thus, uncertainties from variables were reduced by using the same input variables for each SDM.

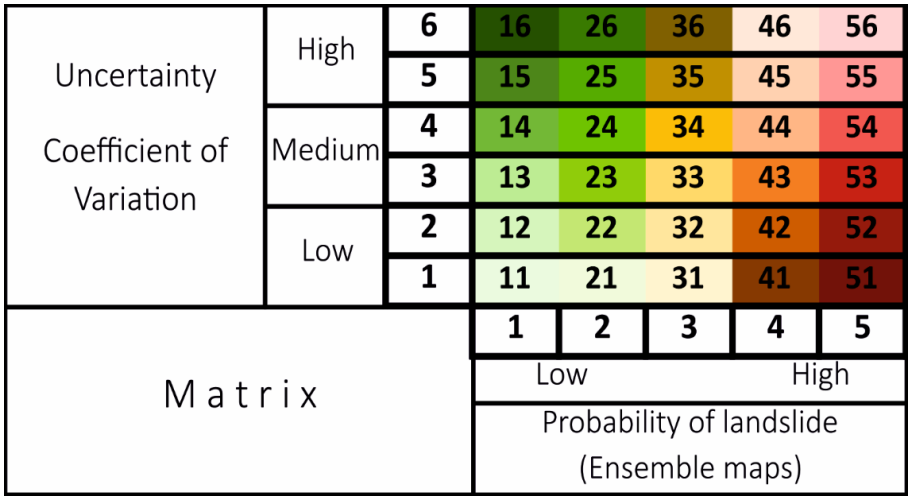

Figure 5.7 Matrix resulting from all possible interactions between the coefficient of variation and landslide susceptibility.

The maps in Figure 5.8 (i.e., "confidence map") presents areas with two different typologies, namely, zones with a high probability of landslide occurrence and low uncertainty (i.e., 41, 51) and areas with pixels with low susceptibility and low uncertainty (i.e. 12, 22). Areas with high landslide susceptibility and high uncertainty (56, 55) were hard to recognize. However, small areas with low probabilities and high uncertainty (i.e., 15, 16) can also be identified. The graphs represented in Figure 5.9 confirmed the statistical analyses performed on these maps. As can be observed from the graph in Figure 5.9a, most of the landslides (about 75%), in all ensemble models, fall into classes 51 and 41 (i.e., high susceptibility and low uncertainty), confirming how EM correctly identified potential triggering areas, with a low uncertainty value. In addition, landslides falling into low-

susceptibility classes are about 3%. The second graph (Fig. 5.9b) confirms that the largest areas are those with low susceptibility, although the degree of uncertainty varies from low to moderate (classes 13, 14, 15). Nevertheless, pixels with higher susceptibility values are mainly distributed (about 90%) in correspondence of classes 41 and 51. Therefore, highly susceptible areas are not particularly extended, contrary to those with low susceptibility, and assume low values of uncertainty.

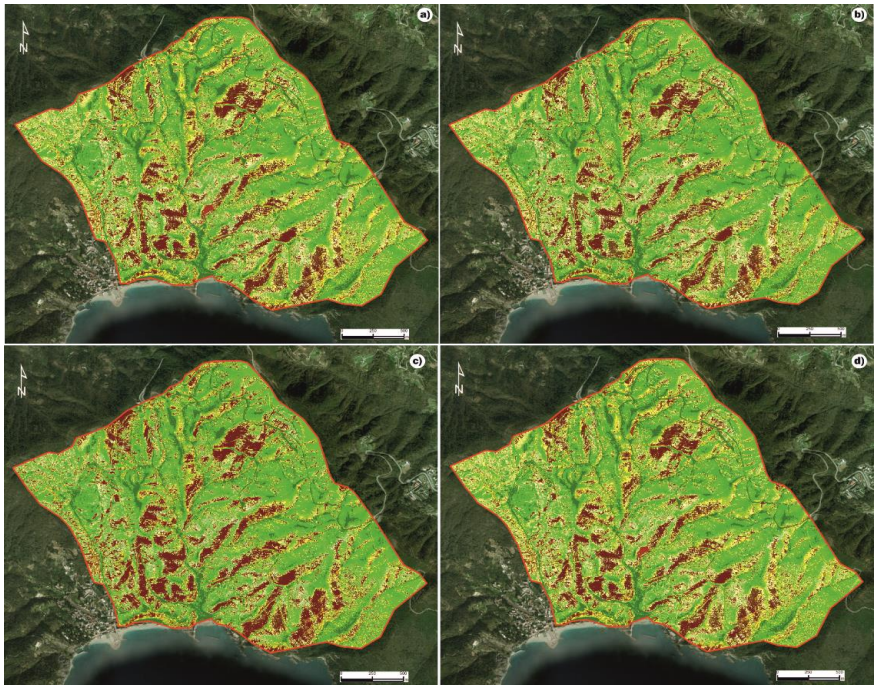

Figure 5.8 "Confidence map" resulting from the intersection between the coefficient of variation and landslide susceptibility. a) Mean (PM), b) Median (PME), c) Committee averaging (CA), d) Weighted mean (PMW). For the colour legend, refer to the matrix of Fig. 5.7.

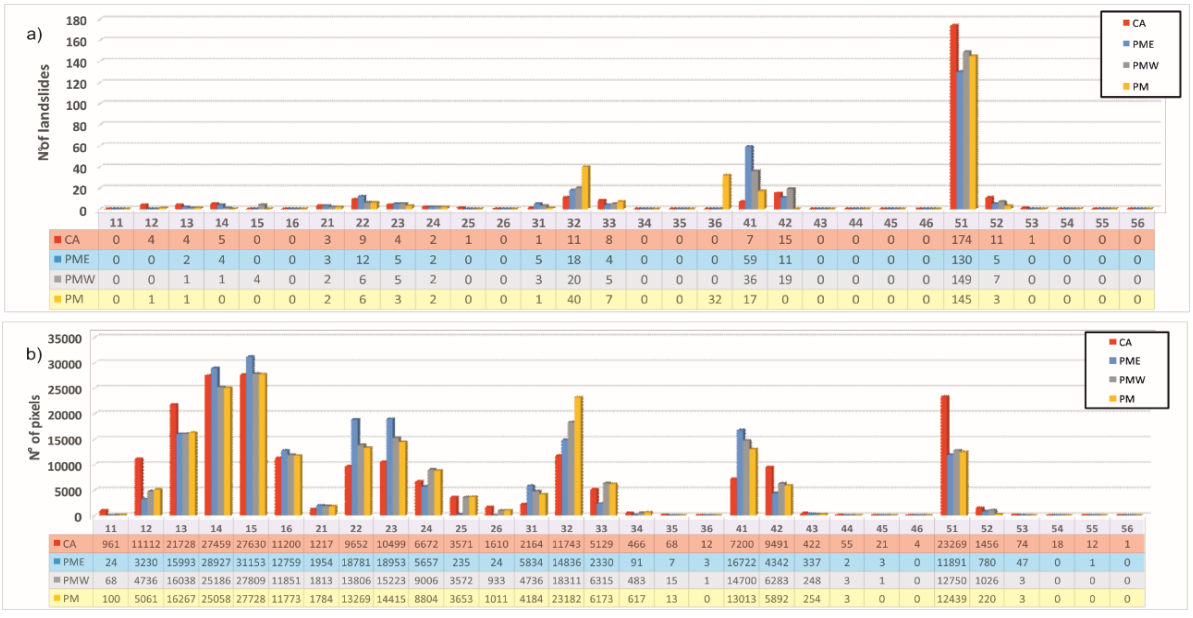

	11	12	13	14	15	16	21	22	23	24	25	26	31	32	33	34	35	36	41	42	43	44	45	46	51	52	53	54	55	56
CA	0	4	4	5	0	0	3	9	4	2	1	0	1	11	8	0	0	0	7	15	0	0	0	0	174	11	1	0	0	0
PME	0	0	2	4	0	0	3	12	5	2	0	0	5	18	4	0	0	0	59	11	0	0	0	0	130	5	0	0	0	0
PMW	0	0	1	1	4	0	2	6	5	2	0	0	3	20	5	0	0	0	36	19	0	0	0	0	149	7	0	0	0	0
PM	0	1	1	0	0	0	2	6	3	2	0	0	1	40	7	0	0	32	17	0	0	0	0	0	145	3	0	0	0	0

	11	12	13	14	15	16	21	22	23	24	25	26	31	32	33	34	35	36	41	42	43	44	45	46	51	52	53	54	55	56
CA	961	11112	21728	27459	27630	11200	1217	9652	10499	6672	3571	1610	2164	11743	5129	466	68	12	7200	9491	422	55	21	4	23269	1456	74	18	12	1
PME	24	3230	15993	28927	31153	12759	1954	18781	18953	5657	235	24	5834	14836	2330	91	7	3	16722	4342	337	2	3	0	11891	780	47	0	1	0
PMW	68	4736	16038	25186	27809	11851	1813	13806	15223	9006	3572	933	4736	18311	6315	483	15	1	14700	6283	248	3	1	0	12750	1026	3	0	0	0
PM	100	5061	16267	25058	27728	11773	1784	13269	14415	8804	3653	1011	4184	23182	6173	617	13	0	13013	5892	254	3	0	0	12439	220	3	0	0	0

Figure 5.9 a) Graph resuming the results of the cross-comparison between landslides and each class of the confidence map; b) graph resuming the results of the cross-comparison between the number of pixels and each class of the confidence map.

Lastly, the spatial distribution of the susceptibility values has been evaluated (i.e., the spatial similarity between the different models was analysed; Fig. 5.10). The ensemble maps have been divided into five classes (1–5) and, subsequently, an intersection operation between the different maps has been performed. Each pixel of the intersection map represents the different combinations that the individual models can assume. Thus, values labelled as 111 represented pixels in which all models have low susceptibility. Similarly, the pixels labelled as 555 represented areas where all models have high susceptibility. During this operation, intermediate combinations have been also obtained as output (e.g., 121), in which the first and third models have a low susceptibility while the second one has a higher susceptibility. An intersection analysis between the landslides and the output map was performed. Figure 5.11a represents the obtained areal extension for each class. "Coherent" classes represent 83% of the total study area, where the main part (42%) is characterized by the lowest susceptibility level (class 111), while about 15% is represented by the "non-coherent" classes. In Figure 5.11b, the number of landslides in each specific class and the relative percentages are represented. About 84% of the total landslides fall within "coherent" susceptibility values (e.g. 555, 444, etc.), while the remaining 16% are in "non-coherent" classes (Fig. 5.11c). Furthermore, 55% of the total landslides fall into the 555 class, in which all the models are characterized by very high susceptibility. Lastly, about 80% of the landslides fall into the classes with moderate to very high susceptibility.

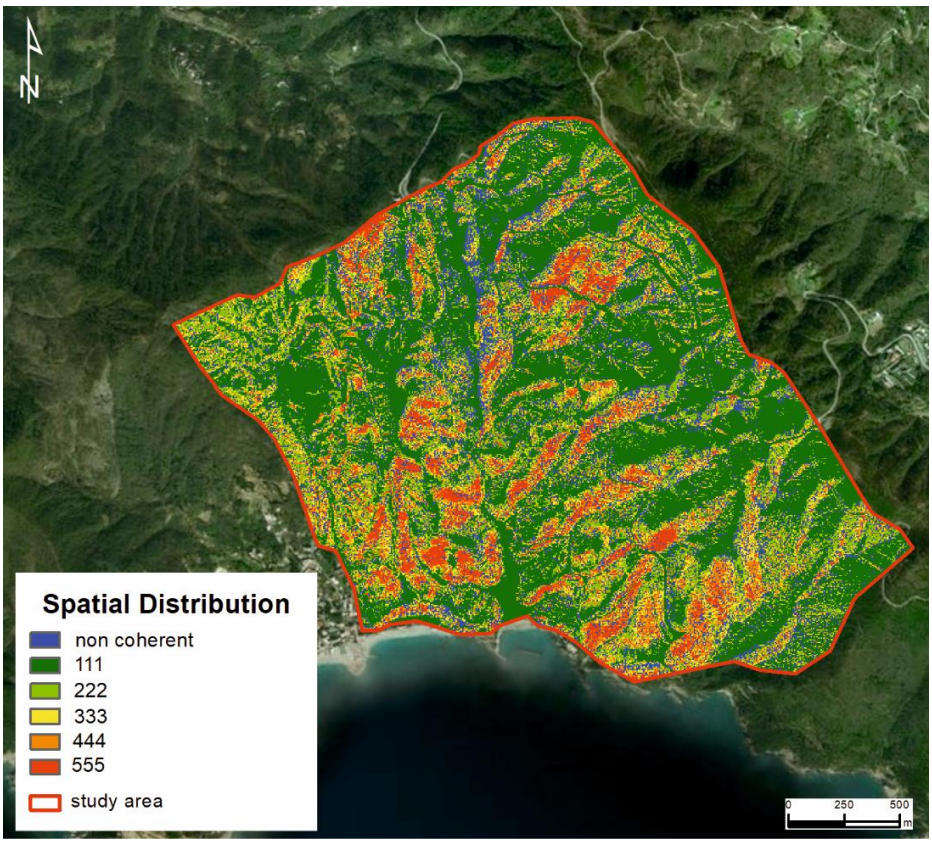

Figure 5.10 Spatial distribution of susceptibility classes for each coherent susceptibility level.

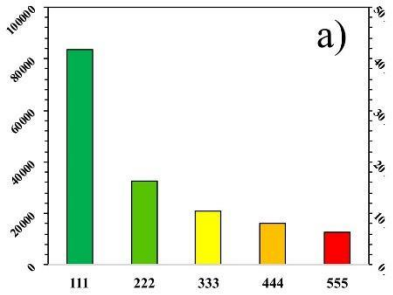

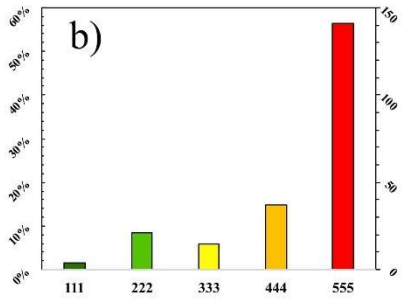

c)

Classes	N° Landslides	%	
111	4	2%	
222	21	8%	218
333	15	6%	83.85
444	37	14%	
555	141	54%	
122	2	1%	
123	1	0%	
133	1	0%	
211	2	1%	
233	8	3%	42
234	1	0%	16.15
255	1	0%	
323	1	0%	
344	7	3%	
455	11	4%	
544	7	3%	
	260	100%	

Figure 5.11 a) Distribution of landslides for each coherent susceptibility level, b) distribution of pixels for each coherent susceptibility level, c) distribution of landslides for each susceptibility level, "coherent" (dark green, light green, yellow, orange and red) and "incoherent" (purple).

5.1.6. Discussion and conclusion

Landslide susceptibility mapping represents an essential tool in terms of landslide risk mitigation, especially if carried out rigorously and supported by an accurate dataset. In this contribution, a strategy to develop susceptibility maps that are focused on the detachment phase was processed. EM modelling has been carried out 100 times, every time with a different combination of training and testing datasets, for each of the three stand-alone methods. Ensemble results seem to be encouraging and improved concerning stand-alone methods, showing AUC values higher than 0.9, hence excellent according to the various classifications available in the literature (Swets 1988). As to confirm, landslide distribution in the study area is mainly concentrated in the areas characterized by high susceptibility. A further refinement of EM reliability has been achieved by comparing the ensemble susceptibility maps with the uncertainty value, computed through the CV. Susceptible areas with low uncertainty value provide high-quality outputs, which may be especially useful for decision-makers, willing to obtain trustworthy information. Likewise, non-susceptible areas with low uncertainty value may represent areas where new social and economic activities may potentially be addressed. Moreover, the spatial comparison done through the intersection of the different outcomes of each EM shows a general consistency, with a very high coincidence (about 84%) of susceptible areas computed in different ways, and a general presence of inventoried landslides almost exclusively in high susceptible coherent areas.

By analysing the score derived from the stand-alone and ensemble susceptibility computation, it is possible to observe that geomorphological variables, such as slope and aspect, are very significant and influences the debris cover deposition, the hydrological circulation, evapotranspiration processes and thus erosion, land use and slope dynamics. Among the other variables, an important role is played by those strongly influenced by human activities, such as the presence of terraces and their state of activity and land use. The influence of these factors has been already highlighted in

previous works (Cevasco et al. 2013a, 2014; Brandolini et al. 2018a, b; Pepe et al. 2019), revealing that the recently abandoned terraces showed the highest landslide susceptibility. Moreover, slope failures affecting cultivated zones were characterized by a lower magnitude than those occurring on abandoned terraced slopes. Furthermore, the role of vegetation may also be positive, both increasing the evapotranspiration potential and controlling the erosional processes. Besides, the constant maintenance of dry-stone walls, and thus terraces conservation, is a key aspect to preserve the function of dissipating the pore water pressure excess generated behind the wall and subsequently protect and conserve a unique man-made landscape (Camera et al. 2012, 2014).

Therefore, these findings can be used by the administrators and decision-makers for planning any measures in this vulnerable region. By considering this novel approach, the impact of landslides and associated losses can be minimized. This last aspect should not be underestimated, especially considering the high-risk condition affecting this area.

5.2. Landslide Detachment, Transit and Runout Susceptibility – Cinque Terre National Park case study

The following material is published in the international journal *Water* (Volume: 13, Issue: 4) in the Di Napoli et al. 2021 work entitled "*Rainfall-Induced Shallow Landslide Detachment, Transit and Runout Susceptibility Mapping by Integrating Machine Learning Techniques and GIS-Based Approaches*".

5.2.1. Research objectives

The integration of landslide detachment and runout dynamics has been accepted by many authors as an appropriate and complete methodology for landslide susceptibility assessment (Hungr 1995; Corominas et al. 2003; van Westen et al. 2006; Mergili et al. 2019). Regrettably, most of the current landslide zoning maps only consider susceptibility to landslide detachment, neglecting landslide transit and invasion (Melo et al. 2019). Nowadays, only a limited number of studies include both Landslide Detachment Susceptibility (LDS) assessment and Landslide Runout Susceptibility (LRS) assessment. Most of these studies focused on either landslide susceptibility mapping or mobility assessment by considering them separately. The coupled prediction of the potential for landslide detachment and runout remains a challenge for researchers (Pradhan et al. 2017). In Italy, the well-known landslide disasters of *Sarno* (*Campania* Region, southern Italy; Calcaterra et al. 2000; Guadagno et al. 2005; Revellino et al. 2008) and *Giampilieri* (*Sicilia* Region, southern Italy; Aronica et al. 2012; Lombardo et al. 2016), which occurred in 1998 and 2009, respectively, are impressive examples of loss of lives and damage experienced by urbanized areas and infrastructure due to long-distance flow-like movement propagation (up to some km from detachment). As regards the *Liguria* region, the recent cases of *Cinque Terre* in 2011 (Cevasco et al. 2013a, 2014) and of *Leivi* (central-eastern *Liguria*) in 2014 (Cevasco et al. 2017) are still impressed on local people's memory since both caused fatalities and severe damage.

In this contribution, a combined methodology to assess simultaneously the susceptibility of shallow landslide failure and runout has been developed. Such a procedure is based on the integration between LDS and LRS assessment using, respectively, ML statistical models and GIS-based tools. In this application, the methodology has been applied to the whole CTNP. ML techniques and GIS-based tools were adopted based on their reliable predictive performance and capability to perform large-scale analysis, respectively. Moreover, GIS-based tools are easy to use in any GIS software achieving high performance. This kind of susceptibility map can represent an important tool for urban planning administrations and policymakers. Furthermore, a complete analysis of these geological hazards is fundamental in risk assessment and management, since the landslide runout mainly considers the areas located in the lowland zones. In the detachment

susceptibility analyses, these areas are always underestimated and classified with low to extremely low landslide susceptibility.

5.2.2. Landslide inventory

CTNP has been historically affected by recurrent landslide events, mostly due to intense rainfalls (Cevasco et al. 2015; Zingaro et al. 2019). LIM are basic elements of both landslide zoning and land-use planning (Fell et al. 2008) and they represent powerful and easily understandable tools for researchers and stakeholders involved in landslide risk management (Guzzetti et al. 2012; Raspini et al. 2017). A landslide inventory map of CTNP was recently compiled by (Raso et al. 2019b). The authors conducted a recognition and partial reworking/revision/update of the pre-existing national landslide inventory such as *I.F.F.I.* (*Inventario dei Fenomeni Franosi in Italia* - Landslide Inventory in Italy) and *A.V.I.* (*Aree Vulnerate Italiane* - areas affected by landslides or floods in Italy) and of previous researches (Cevasco 2007; Raso et al. 2019a). These analyses were performed through the visual interpretation of satellite images and aerial photos integrated by field validations and observations.

Geomorphological field surveys were carried out on topographical maps at 1:5000 scale whereas remote sensing activities were carried out on Landsat™ and Google™ satellite images, digital georeferenced orthophotos taken from both *Friuli-Venezia-Giulia* Regional Administration and *Regione Liguria* Administration and through the use of data obtained from a GNSS (Global Navigation Satellite Systems) monitoring which started in 2015. Data collected from the field and remote sensing activities were then georeferenced and digitized as polygons within a GIS environment. Based on the scale adopted in mapping activity, this map was produced at 1:45000 scale and it includes landslides with size greater than 25 m^2. This inventory consists of more than 450 landslides classified according to Cruden and Varnes (1996) and Hungr et al. (2014), and, in this implementation, a total of 281 rainfall-induced shallow landslides, mostly debris slides, debris avalanches and debris flows were selected (Fig. 5.12). In addition, the inset in Figure 5.12 represents the area distribution of the landslide inventory used for this case study. The area distribution of a landslide event quantifies the number of landslides that occur at different sizes. This curve does not reflect a uniform distribution because most of the landslide are centred around small dimensions (i.e., ~1000 m^2), and their frequency decreases as the landslide sizes increases.

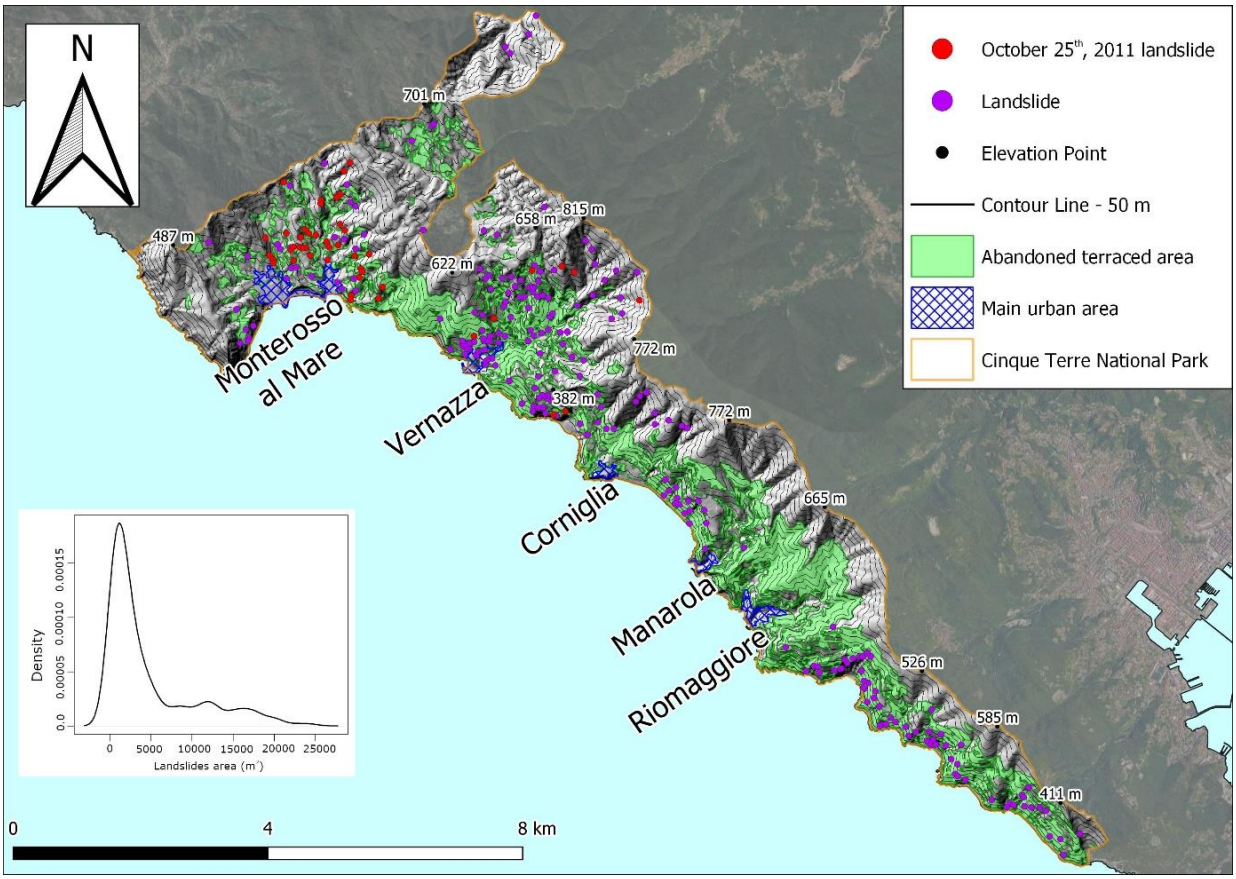

Figure 5.12 Shallow landslide inventory map used in this study. Landslides are represented by points (data source modified from Raso et al. 2019a). The inset on the bottom-left of figure represents the area distribution of the *Cinque Terre* landslide inventory redacted by Raso et al., 2019a in meter square.

To perform the LDS analysis, as the algorithm works with punctual features, the selected landslides were represented by points. The highest elevation point of each landslide was chosen as representative, according to the approach adopted by the Italian *I.F.F.I.* project, where each landslide could be statistically identified by mean of its *P.I.F.F.* (*Punto Identificativo del Fenomeno Franoso* - Landslide Phenomenon Identification Point). By convention, *P.I.F.F.*s correspond to the highest elevation points on the landslide crown (Trigila et al. 2007); hence, they can be regarded as landslides source points.

5.2.3. Datasets

Based on the previous knowledge of the study area, the independent variables dataset used in the modelling consist of 9 geo-environmental attributes: *i*) slope angle, *ii*) slope aspect, *iii*) planform curvature, *iv*) profile curvature, *v*) distance from roads, *vi*) distance to streams, *vii*) degree of abandonment of agricultural terraces, *viii*) land-use and *ix*) geo-lithological features. In this application, being the largest study area, all morphometric variables were derived from a DTM with 10 m cell size released by the *Liguria* Region Administration in 2017 (https://geoportal.regione.liguria.it/). As in the first case study, this analysis has been focused only

on environmental variables, without taking into consideration triggering factors (e.g., intense rainfalls).

All PFs were widely described in paragraph 3.1 but, in this implementation, further information has to give concerning the agricultural terraces. In this study, special care has been paid to the recognition and mapping of both agricultural terraces and non-terraced areas. In particular, using data from previous studies (Cevasco et al. 2013a; Di Napoli et al. 2020), four classes were distinguished: *1*. cultivated terraced areas; *2*. abandoned terraces with poor vegetation cover (initial state of abandonment); *3*. abandoned terraces with dense vegetation cover (advanced state of abandonment); *4*. non-terraced areas (including either urban areas, outcropping rocks and woods).

5.2.4. Procedure implementation and validation

To achieve the objective of this study a three-step methodology was applied (Fig 5.13). The first step consisted of modelling and mapping the landslide detachment susceptibility. To assess the detachment susceptibility for shallow landslides, ML approaches were implemented. The whole employed procedure to estimate the slope instabilities is the same procedure applied in the first case study. Achieving reliable models and good models performance, it was decided to employ this procedure at the park scale. Therefore, EM techniques were exploited to reduce the generalization error of prediction. Multicollinearity issues were detected by adopting the VIF method and also calculating the environmental predictors' contribution to the model outputs (i.e., variable importance). The predictive performance was evaluated with spatial cross-validation estimates of the AUC, which is one of the most common statistics to assess model performance (Beguería 2006). Differently from the first application, to identify the potential landslide source areas and to obtain an outcome compared with the existing landslide hazard zoning maps provided by the local authorities, the continuous LDS map was classified into six susceptibility classes, precisely from “very low” to “very high” susceptibility, using Natural Breaks classification methods (Jenks 1967). Anyway, the complete and detailed procedure description can be consulted in paragraph 5.1.4.

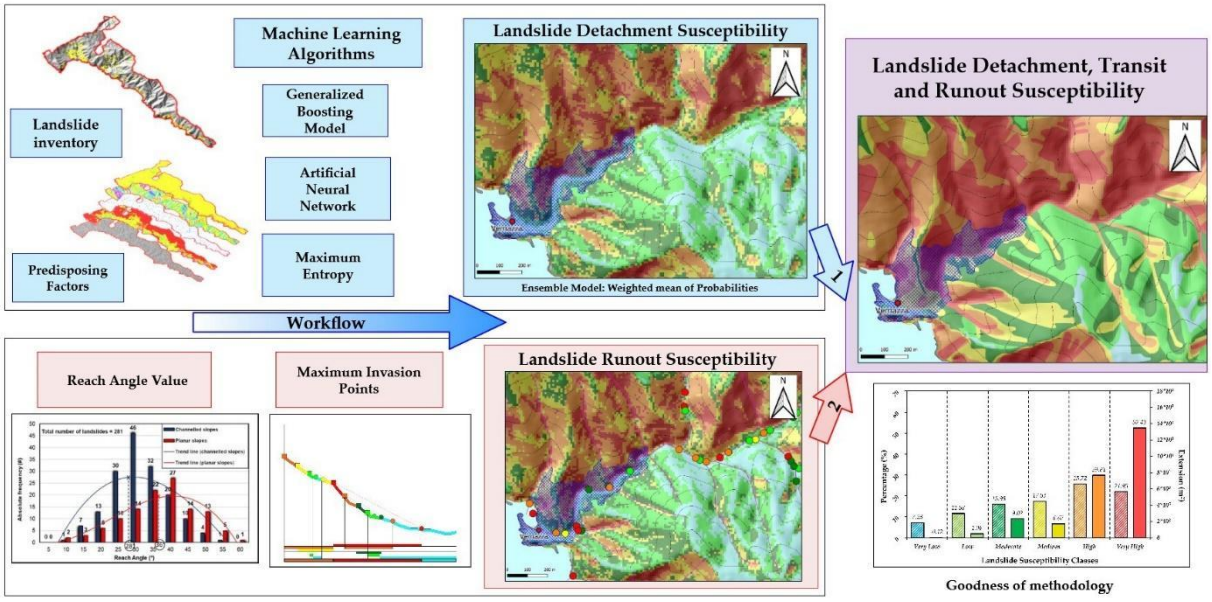

Figure 5.13 Schematic flowchart showing the steps followed to produce the Landslide Detachment, Transit and Runout Susceptibility map.

The second step was aimed at modelling Landslide Runout Susceptibility (LRS). The main objective of these studies was to understand the characteristics of landslides that occurred in the past to predict the possible future invasion areas, therefore preventing economic losses and fatalities (Hungr et al. 2005). Calculating the runout of mass movements and understanding their rapidity are basic elements of any landslide hazard or risk assessment. In this case study, LRS assessment was performed adopting the geometrical method of the "reach angle" (Hsu 1975), which is one of the most used empirical approaches to evaluate landslide mobility (further detail in paragraph 3.3 – Runout Modeling).

In the first phase of LRS assessment, values of *H* and *L* were carefully measured, in an open-source GIS environment. This was carried out both for landslides triggered along or upstream of channels and for failures on open/planar slopes. Subsequently, the reach angle was calculated through the following formula (5.1):

$$\alpha = arctan\frac{H}{L} \qquad 5.1$$

The reference values of the reach angle for the two different slope types (i.e., channelled and open/planar) were obtained through the definition of the modal values. During the second phase, using the LDS map as a base map, different topographic sections were drawn. These sections identify the hypothetical/potential path that a detached landslide could travel. The sections were drawn along the main creeks, in case of channelled slopes, and along the maximum slope line, in case of open/planar ones. Topographic sections were automatically obtained using the Profile tool plug-in (Jurgiel et al. 2020) in open-source QGIS. In the third phase, Maximum Invasion (MI) points were identified for different potential detachment points positioned in the upper part of the

slope (Fig. 5.14a). The straight-line equation was used to define the MI point corresponding to a certain potential detachment point. Such a straight-line is described by the following equation (5.2):

$$y = x\ tg\alpha + c \qquad 5.2$$

where:

α = reach angle;

x = progressive distance;

c = highest detachment point altitude.

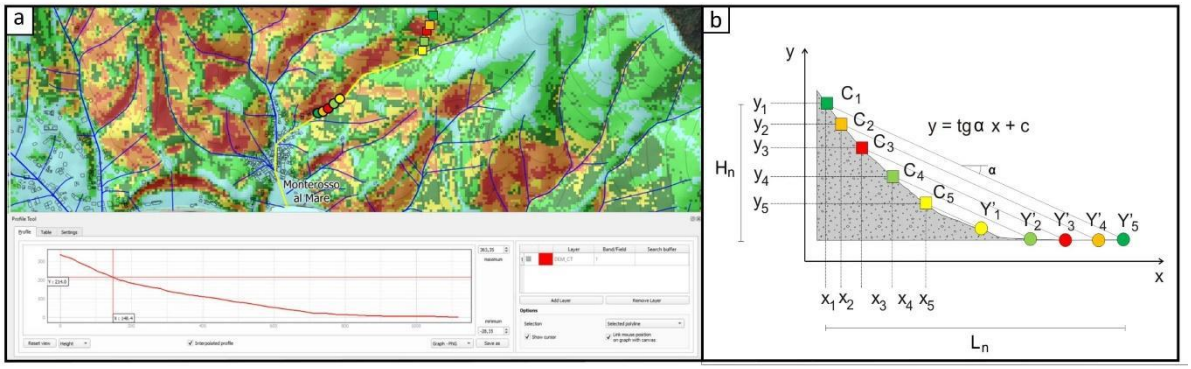

Figure 5.14 a) Example of an LDS map showing the topographic sections on channelled slopes (blue lines represent the streams) used to identify the MI points and their susceptibility. Squares and circles represent the detachment and the MI points, respectively, of potential landslides detached at different points in the upper part of the slope along a selected topographic profile (yellow line); b) geometric sketch of MI point identification; x_n and y_n are the co-ordinates of the selected detachment points; Y'_n are the respective MI points. Different colours of squares and circles refer to the LDS and LRS classes, respectively.

Starting from the highest elevations, different detachment points (C_n) were considered along the topographic profile. Each point was positioned within a certain susceptibility class derived by the LDS modelling. Subsequently, every point of the straight line was iteratively compared with the local topography obtained through the DTM. In this way, the MI point (Y'_n) is identified by the intersection between the straight line and the local topographic profile (Fig. 5.14b). The susceptibility assigned to the MI point is the same as its potential detachment point.

Lastly, as a third step, to produce the Landslide Detachment, Transit and Runout Susceptibility (LDTRS) map, information coming from the previous analyses (namely, LDS and LRS information) were used. Specifically, the implementation of the LDTRS map was carried out through areas enveloping procedure aimed at *i*) harmonizing areas with different LDS and *ii*) including information derived from the LRS assessment (i.e., areas showing the same susceptibility degree to both detachment and runout were enclosed in a single area). To ensure higher safety conditions, a *conservative* approach was adopted during the areas enveloping procedure. Hence, priority was always given to the highest susceptibility classes (Fig. 5.15). In this way, the areas located downstream of a portion with a higher susceptibility are included in these ones, even if they are characterized by a lower susceptibility.

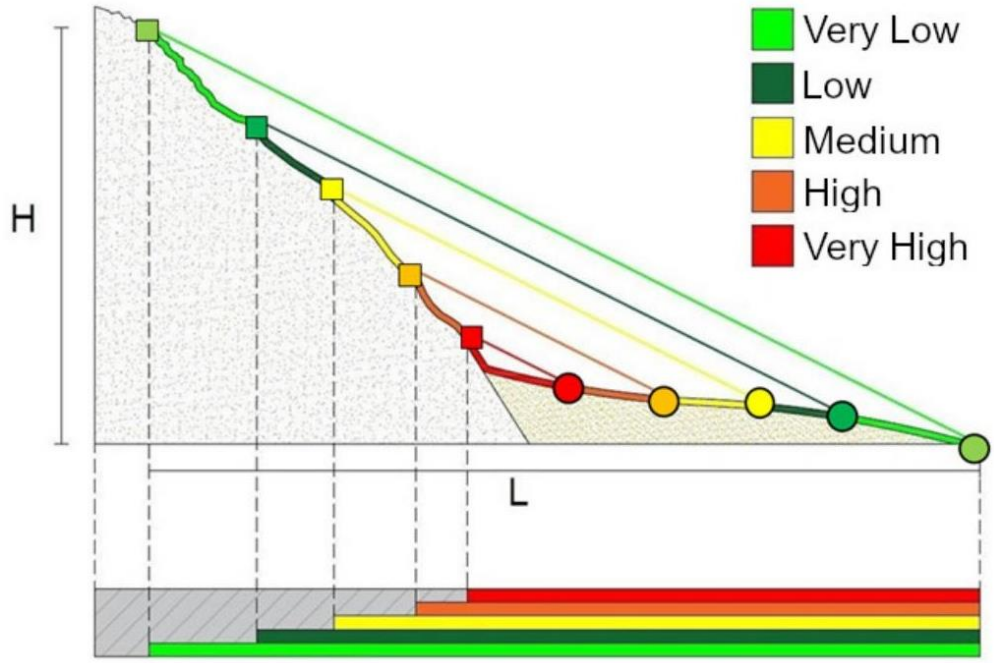

Figure 5.15 Schematic representation of the procedure used for assigning the LDTRS class to a stretch of the topographical profile during the areas enveloping procedure. Coloured slope sections are the LDS class; coloured lines are the different calculated straight lines; squares identify the potential detachment points and their related susceptibility class; circles represent MI points and their related susceptibility class. The lower part of the figure shows a simplified representation of the conservative approach applied, which gives priority to higher susceptibility classes.

Figure 5.16 summarizes the different operations executed during the area enveloping procedure. LDTRS sectors were drawn in order of decreasing susceptibility class (Fig. 5.16b-f). Furthermore, an attempt was made to obtain an indication of the goodness and effectiveness of the LDTRS model. The test area of the *Vernazza* catchment, where data from the catastrophic event of 25th October 2011, were available (Cevasco et al. 2013), was selected. The adopted testing methodology consists of a quantitative comparison of the deposition areas of shallow landslides (mostly debris slides and debris avalanches), detected through field surveys and aerial imagery analysis, with the respective degree of susceptibility resulting from the output LDS and LDTRS maps. As debris flows propagated into the drainage network, they were not included in this analysis. In fact, in this case, the deposits were swept away along the channels and uncertainties occurred in identifying the boundary between debris flows and debris flood deposits (Bordoni et al. 2020).

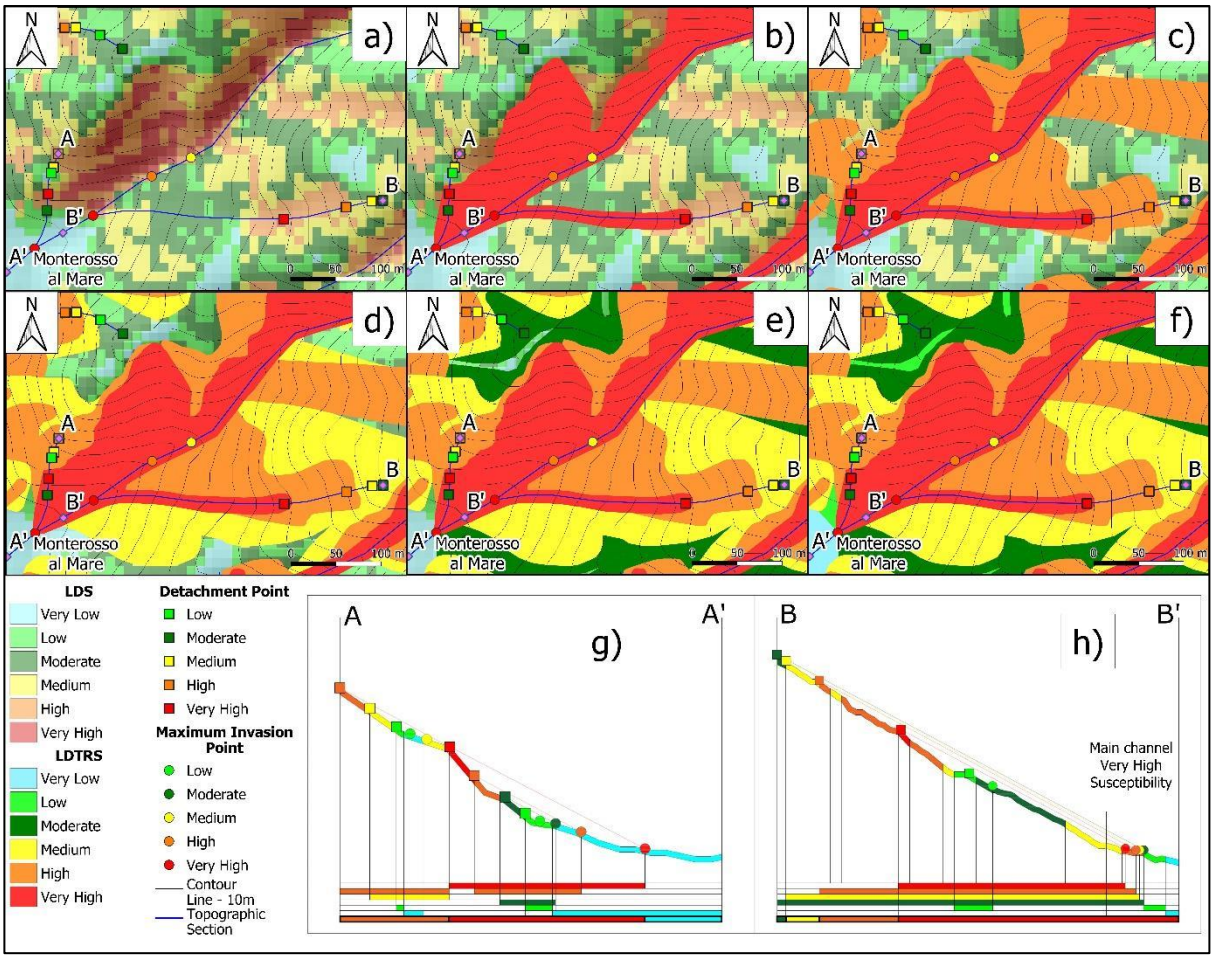

Figure 5.16 Representative steps followed to obtain the LDTRS map. The selected area is located close to *Monterosso* (western sector of the *Cinque Terre* National Park). a) Details of the LDS map with topographic profiles (blue lines) and MI points (circles); b) envelope procedure for areas with "very high" LDS degree including information derived from the LRS assessment; c-f) harmonization of areas with "high", "medium", "low" and "very low" LDS degree, respectively; g) and h) examples of real topographic profiles that outline the conservative approach applied during the areas enveloping procedure; the susceptibility values along each profile refer to sub-figure (a); the final susceptibility value is shown in the bar at the bottom of each picture and refers to sub-figure (f).

5.2.5. Landslide "detachment, transit and runout" susceptibility outcomes

In landslide susceptibility modelling, the predictive capability of the predisposing factors should be considered and factors with non-predictive value should not be included in the models, improving the performance of the prediction. In this study, VIF was examined to estimate the possible correlations between each variable. In this study, VIF values of each predisposing factor are smaller than 4, values greater than 5 or 10 denotes multicollinearity issues (Hair et al., 2010). The highest VIF is 1.94, corresponding to slope angle, while the smallest one is 1.02, which is associated with slope aspect. No multicollinearity problems were found among the predisposing variables considered in the analyses and the outcomes have been summarized in Table 5.4.

Table 5.4 Multicollinearity diagnosis indices for the selected variables and their importance for the Weighted mean (Wmean) ensemble model.

Predisposing Factors	Variance Inflation Factor	Variable importance (Wmean)
Slope angle	1.94	0.22
Slope aspect	1.02	0.24
Profile curvature	1.35	0.04
Planform curvature	1.54	0.12
Degree of abandonment terraces	1.39	0.38
Distance to road	1.18	0.02
Distance to river	1.28	0.01
Geology	1.36	0.04
Land use	1.14	0.06

Another meaningful outcome, which allowed to understand the contribution of PFs to the model outputs, is related to the significance of the selected variables. The results of the analysis show that slope angle, slope aspect and the degree of abandonment of agricultural terraces are the most important factors affecting landslide models (Table 5.4). The most important PFs for LDS assessment are related to agricultural terraced slopes that were abandoned and covered by Mediterranean scrub, unlike the areas where agricultural terraces are still cultivated or have been recovered in recent years (Table 5.4). The LDS map that resulted from the calculation of the weighted mean probability of the different models was reclassified into six classes describing the different susceptibility to landslide detachment (Figure 5.17a).

As can be seen from Figure 5.18, the distribution of landslides is characterized by an increasing trend, with the highest number of landslides placed in the high and very high susceptibility classes (ca. 63%). On the contrary, the areal distribution shows a decreasing trend, with the majority of areas characterized by low and very low susceptibility values (ca. 58%) and a small area characterized by higher values (ca. 14%). The opposite direction of the two trends reveals that most of the landslides fall within the highest susceptibility classes, although the range recognized as susceptible has a limited extension.

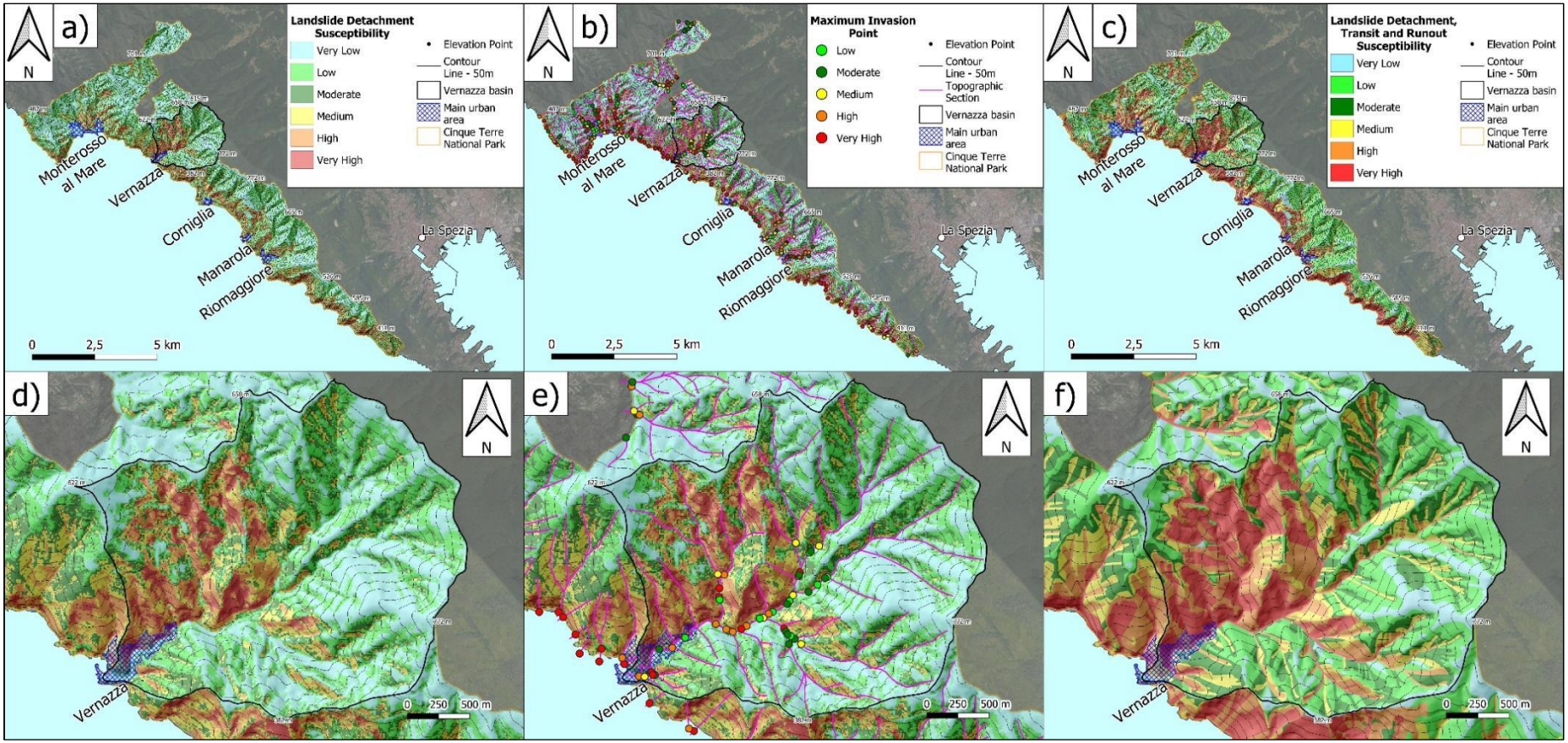

Figure 5.17 a) LDS map of the *Cinque Terre* National Park obtained by using Machine Learning techniques; b) LRS map showing both the topographic sections and the related MI points; c) LDTRS map of the whole study area; (d–f) detail of the LDS, LRS and LDTRS maps of the *Vernazza* catchment (western sector of the *Cinque Terre* National Park, black bold line).

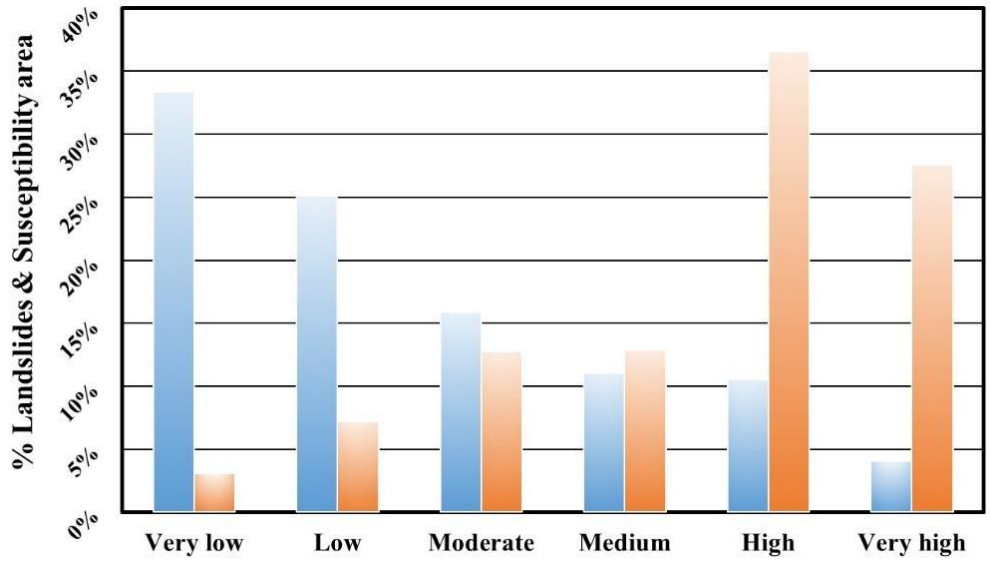

Figure 5.18 Results of the statistical analysis carried out through the Ensemble Wmean method. Orange bars represent the number of landslides falling in each LDS class, while the blue bars indicate the areal extension of the different LDS classes.

The first step of LRS assessment was to determine the reach angle of the inventoried landslides. As reported in Figure 5.19, reach angle values calculated for channelled landslides were generally lower than those related to landslides that occurred on open/planar slopes. In particular, the most frequent reach angle values for channelled and open/planar slopes landslides are in the range 26° - 30° and 36° - 40°, respectively. The choice of the reference values was made through the definition of the modal value, namely the higher frequency identified in the two respective classes, adopting a *conservative* approach. Therefore, values equal to 28° and 36° for landslides potentially occurring on channelled and open/planar slopes were chosen, respectively.

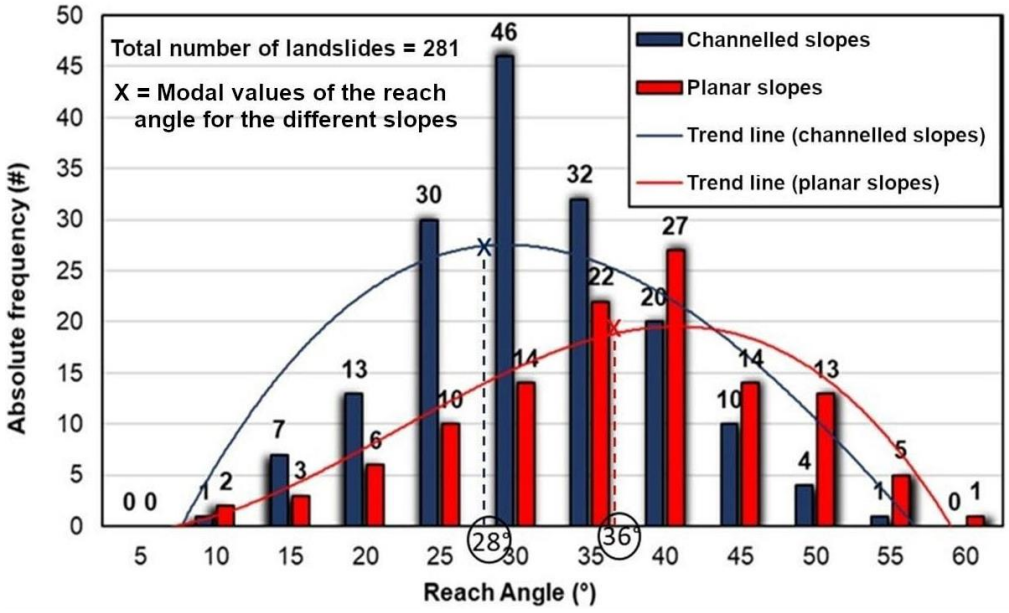

Figure 5.19 Frequency distribution of reach angle values for landslides that occurred on channelled and open/planar slopes.

Topographical sections were drawn as explained previously. In this way, 453 topographic sections were drawn (Figure 5.18b). This procedure allowed to identify 1853 MI points; subsequently, an LRS class has been assigned to each of them. The number of identified MI points is higher than the topographic sections drawn since along each section it was possible to identify up to five MI points.

The final product is a detailed LDTRS map resulting from the integration of the procedures used for LDS and LRS assessment (Figure 5.17a,b). In this way, besides susceptibility to shallow landslides detachment, both transit and runout susceptibility were taken into account (Figure 5.17c,f). The LDTRS map analysis (Figure 5.17c) highlights differences in the spatial distribution of susceptibility. Generally, terraced coastal slopes show high and very high susceptibility. Regarding the inland portions of the territory, high susceptibility values can be observed within the *Vernazza* catchment and in the areas behind the *Monterosso al Mare* hamlet. Interestingly, in the *Vernazza* catchment, there is a marked difference in susceptibility values between the western and the eastern side of the basin. In this case, the greatest landslide occurrence and susceptibility values were found on the right side of the catchment. On the other hand, the lowest landslide susceptibility classes are located at a higher altitude. Furthermore, most of the stream channels show high susceptibility values, highlighting their crucial role during debris flows runout.

Eventually, indication on the goodness of the LDTRS model was obtained for the test area of *Vernazza* through the comparison between deposition areas of shallow landslides that occurred on 25th October 2011, and respective degrees of susceptibility in the LDS and LDTRS maps. The obtained results are summarized in Figure 5.20. It can be noticed that the percentage of deposits falling in areas with high and very high susceptibility increases from about 48% for LDS to about 82% for LDTRS. At the same time, the percentage of deposits falling in areas with very low to medium susceptibility decreases from about 52% for LDS to about 18% for LDTRS.

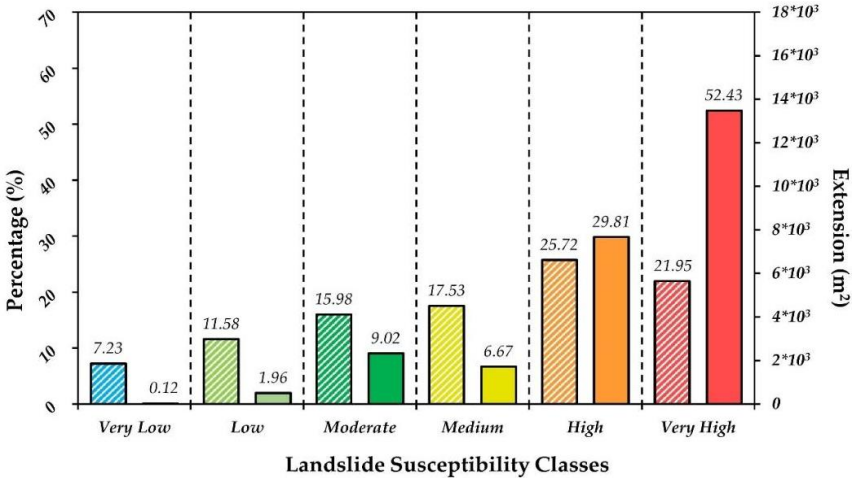

Figure 5.20 Percentage and size of shallow landslide deposition areas (25th October 2011, rainstorm event) falling into different LDS (oblique line fill) and LDTRS (continuous fill) classes.

5.2.6. Discussion

In this application, a combined approach was used to obtain a thematic map considering both aspects. Outcomes of the first part of this work have been focused on the LDS assessment. Such results revealed that the main causes of slope instability are: *i*) abandonment of agricultural terraces (Wmean parameters importance = 0.38), *ii*) slope aspect (0.24) and *iii*) slope angle (0.22). The high LDS of terraced areas can be chiefly interpreted as the outcomes of two conditions. Firstly, the flat portion of agricultural terraces hampers runoff avoiding soil losses, and, secondly, it increases water infiltration (Arnaez et al. 2011). During rainfall, the combination of these two hydrological functions leads to the formation of a groundwater table at the interface between layers (i.e., slope deposit and underlying bedrock) characterized by different permeability. The aforementioned conditions strongly influence slope stability (Tarolli et al. 2014). The lack of maintenance of agricultural terraces and artificial drainage networks caused by the progressive abandonment of agricultural practices becomes one of the main factors in increasing LDS (Cevasco et al. 2014; Brandolini et al. 2018a). Generally, the highest amount of rainfall-induced slope instabilities occurred on abandoned agricultural lands, while a small portion of them affected cultivated terraced slopes. Moreover, slope failures affecting cultivated zones were characterized by a lower magnitude than those occurring on abandoned ones (Brandolini et al. 2018a). Furthermore, Cevasco et al. (2014) reported that terraces abandoned for a short time showed the highest landslide susceptibility.

Slope angle is notoriously one of the most important predisposing factors, as gravity is the engine of landslide movements. Namely, the steeper the ground surface, the greater the magnitude of driving forces and the expected velocity of landslide movements. Indeed, more than 70% of the CTNP presents slope angles greater than 21°. Slope aspect plays a fundamental role in controlling soil moisture through solar radiation and rainfalls; in fact, the highest number of landslides are located on slopes facing SE-SW quadrants (72.3%). This could be explained by the presence of highly humid winds coming from the sea. Such winds increase humidity in south-faced slopes and, when heavy/intense rainfall occurs, the difference in water content of south-facing soil covers can play an important role in influencing triggering landslides (Dehnavi et al. 2015; Turan et al. 2020). Furthermore, north-facing slopes suffer from more severe weathering, since in the Northern Hemisphere these slopes preserve higher moisture than south-facing slopes. Therefore, it is expected that north-facing slopes have higher landslides occurrence compared to south-facing slopes. However, it should be noted that south-facing slopes may be subjected to greater landslide activity due to more frequent wetting–drying cycles compared to north-facing slopes (Sidle and Ochiai 2006).

Despite the complex geological and geomorphological setting of the study area, ML methods implemented in this work provided LDS maps of good quality, especially after the implementation of the EM that boosted the performance of LDS assessment (AUROC = 0.9). This statistical approach allowed to consider a great amount of available input data. In particular, the easy implementation of a great number of predisposing factors over a large area made ML techniques a more reliable solution for LDS mapping. During the subsequent phase of this study, reach angle identification was performed. The obtained results showed different modal values of the reach angle for channelled and open/planar slopes (28° and 36°, respectively). This difference, which is in agreement with several works reported in the literature (Corominas 1996; Calcaterra et al. 2003a), confirms that, on average, channelled landslides travel longer distances than landslides occurring on open/planar slopes. Moreover, it is worth noting that the obtained modal reach angle values are higher than those obtained in other areas (Corominas et al. 2003). This could be related to the fact that the reach angle depends on different factors (e.g., landslide volume, type of movement, land use, soil properties, water content, topographic constraints) that may differ from one setting to another. Given the high number of landslides selected in this study, it was not possible to identify with accuracy, among these factors, those responsible.

Using the LDS map as a basis, the application of the geometric method of the "reach angle" allowed mapping of MI points and their susceptibility. Through the combination of the procedures used for LDS and LRS assessment, the LDTRS map was obtained. The comparison between LDS and LDTRS maps highlights how certain portions of the study area show an opposite degree of susceptibility. This especially occurs in flat areas located at the base of slopes that, despite a low LDS, could be affected by the flow-like landslides runout (Fig. 5.16). Information in this sense were obtained comparing the propagation areas of shallow landslides occurred on 25th October 2011, at *Vernazza* with the degree of susceptibility resulting from the LDS and LDTRS maps (Fig. 5.21). The outcomes of this comparison were very encouraging, indicating a higher performance of LDTRS map concerning LDS map (percentages of landslide deposits falling in areas with high and very high susceptibility of 82% and 48%, respectively). The availability of future events data could provide further information about the reliability and effectiveness of the LDTRS map obtained in this study.

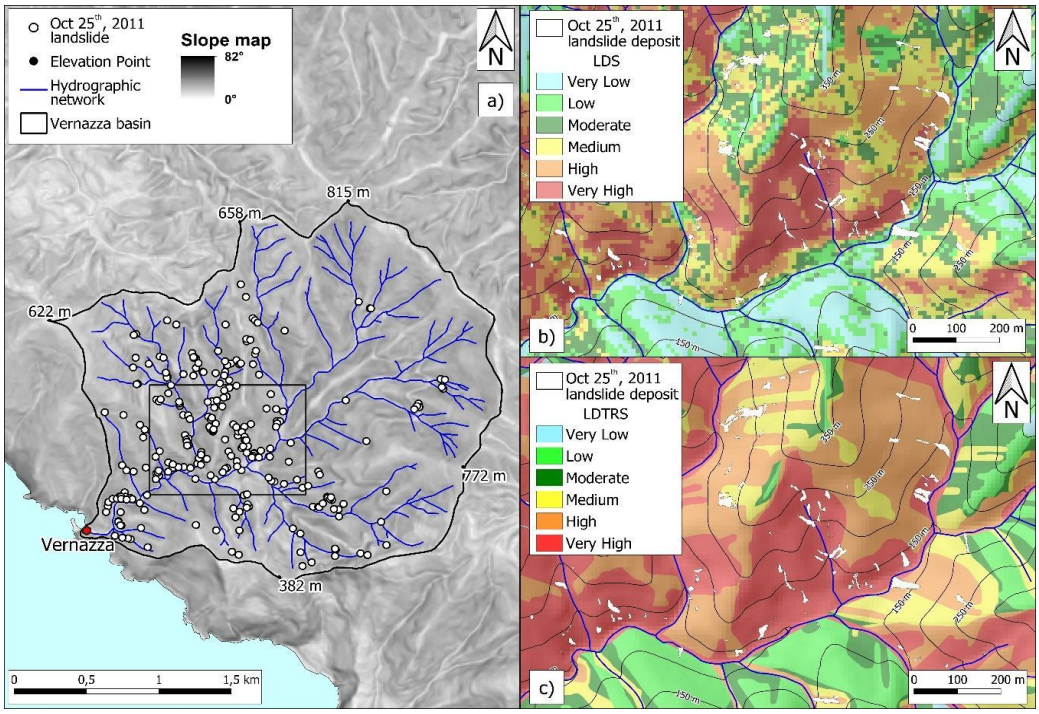

Figure 5.21 a) Slope map of the *Vernazza* catchment; the black frame represents the area shown in detail; b) and c) detail of the LDS and LDTRS maps, respectively, with superimposition of deposits of a shallow landslide triggered on 25th October 2011.

5.2.7. Conclusions

In mountainous and hilly areas, rainfall-induced shallow landslides have always been important worldwide threats for settlements located at the base of steep slopes. During detachment phases, such landslides are often shallow, but subsequently, they can evolve in higher-magnitude, dangerous mass flows with strong impacts on the social fabric. In this study, a methodology aimed at producing a shallow landslide susceptibility map taking into account both detachment and runout was presented. The proposed methodology was applied to the CTNP, which is an area characterized by increasing shallow landslide risk. The novelty of this work consists of a processing chain that considers both the detachment and runout susceptibility assessment. Moreover, the use of input data simply derived from DEMs allows for achieving a good level of accuracy at such a scale of analysis and predictive efficiency also in case of a lack of exhaustive information. The results obtained in this work indicate that the susceptibility map taking into account both detachment and runout performs better than a simple detachment susceptibility map. Therefore, the proposed methodology may be particularly useful for areas where rainfall-induced shallow landslides constitute a threat to human lives, buildings and infrastructures. In particular, the obtained map will be helpful for urban and land planning, as well as for decision-makers and stakeholders, to predict areas where rainfall-induced shallow landslides are likely to occur and travel in the future and to identify areas where hazard mitigation measures are required. Hence, this tool represents a step forward for more proper territorial planning.

5.3. Introduction to landslide intensity – a case study from Monterosso and Vernazza

In the previous two applications, models were implemented by using ML algorithms. In this last step of the study, the modelling approach deviates from the previously implemented fitted models that are based on binary presence/absence data. Specifically, a Bayesian hierarchical Cox point process model that describes landslide counts has been exploited (Lombardo et al. 2020). Precisely, Log-Gaussian Cox Process (LGCP), have rarely and only recently been employed in landslide applications (Lombardo et al. 2018), by assessing the landslide *intensity* rather than *susceptibility*. Landslide intensity represents an alternative measure, which includes landslide susceptibility. In fact, the latter only estimates where landslides may occur whereas the intensity probabilistically assesses where and how many landslides are likely to occur in any given terrain mapping unit. Below, this concept will be further detailed.

5.3.1. Research objectives

Maps that attempt to predict landslide occurrences have essentially stayed the same since (Brabb et al. 1972), even if models and algorithms have undoubtedly changed in fifty years. However, the current literature almost unanimously presents spatial models that evaluate whether a given mapping unit is expected to be stable or unstable (Reichenbach et al. 2018). This principle corresponds to landslide *susceptibility*, a paradigm that completely ignores how many landslides may trigger within a given slope, how large these landslides may be and what portion of the given slope they may interfere with. This way to evaluate landslide susceptibility presents a binary presence-absence set-up, which when probabilistically addressed essentially boils down to the implementation of a model that explains landslide occurrences according to a Bernoulli probability distribution. Conversely, Lombardo et al. (2018) have recently proposed an alternative procedure to estimate how many landslides may occur per mapping unit via the landslide *intensity* concept. Predicting landslide intensity, an alternative measure complementary to landslide susceptibility, provides more detailed and complete information as compared to the classical susceptibility mapping approach based on relative probabilities. The intensity can be estimated by assuming that the distribution of landslide counts per mapping unit behaves according to a Poisson probability distribution. Therefore, the choice of Poisson distribution rather than a Bernoulli case, brings a paradigm shift in the probabilistic models implemented so far extending the common binary situation, modelling counts instead of presence-absence data. A major benefit is an access to richer spatial information on landslide characteristics, which can be used to better plan mitigation measures for landslide hazard and ultimately risk. In fact, the number of landslides per mapping unit has been shown to closely follow the expected size of landslides for the same units, thus bringing the model one step closer to the standard definition of hazard.

In addition to the expectation of landslide occurrences across a given geographic space and/or time, the size of the landslides are considered to be equally important (Bellugi et al. 2021). The landslide area is in fact the only spatially reliable measure currently available over large geographic areas. Another alternative measure and probably even more suitable for landslide hazard is the kinetic energy associated with a moving mass. However, this measure is barely measurable in the field for single landslides, let alone for hundreds or thousands. This, in turn, makes the area the most suitable candidate to assess the landslide hazard when the scope of the analyses covers catchment to regional and even larger spatial contexts. Unfortunately, recent works, besides neglecting the potential number of landslides within a given mapping unit, have also ignored the information of the expected planimetric area or volume associated with landslides. At best, the geomorphological community has dealt with landslide sizes as part of the landslide event magnitude estimation albeit this parameter in itself can be associated with thousands of landslides, thus neglecting the spatial nature of the problem at hand (Malamud et al. 2004). Recently, Lombardo et al. (2021) have proposed an innovative approach to build statistical models capable of predicting the planimetric area of event-triggered landslides (Malamud et al. 2004; Guzzetti et al. 2012). In addition, Lombardo et al. (2020) have demonstrated that intensity is also closely correlated to the cumulated landslide area per mapping unit.

Therefore, in this study inspiration was taken from both of the above-mentioned contributions. Specifically, the spatial realization of landslide areas as information of crucial importance was considered. But, because (Lombardo et al. 2021) model this quantity on a logarithmic scale, an alternative way to keep the target in a metric scale was explored, which is much more intuitive to model, interpret and make decisions upon. What was attempted to do to achieve this task is to look back at the relation landslide intensity vs landslide area, demonstrated in (Lombardo et al. 2020a). There, the authors showed that these two quantities are closely related, almost in a linear relation to one another.

Therefore, instead of modelling directly landslide areas in a Log-Gaussian framework, it was opted to initially model the landslide intensity, estimate the dependence that exists concerning the landslide area and transform the intensity to area in a post-processing step. This operation ensures that the estimated landslide areas per mapping unit are expressed in squared meters. This further allows one to divide this quantity by the size of the mapping unit itself and generate landslide areal density models, a suitable candidate to express the hazard at any given location.

5.3.2. Materials and methods

This section briefly introduces to the study area characteristics and the landslide inventory employed for the simulations. Subsequently, the spatial partition and the environmental factors are described, together with the model selected.

5.3.3. Study area and landslide inventory

The study area where landslide intensity estimation was conducted is a portion of the CTNP (18 km^2 wide), including *Monterosso al Mare* and *Vernazza* catchments. This area was selected because of the severe rainfalls they experienced in October 2011, which, in turn, produced a rich landslide inventory (Cevasco et al., 2013; Schilirò et al., 2018). The peculiarities of the landslide inventory used were already discussed in section 5.1.2.

Figure 5.22 shows an overview of the study area and the landslides triggered by the extreme rainfall event. For this study, a total number of 695 landslides was considered.

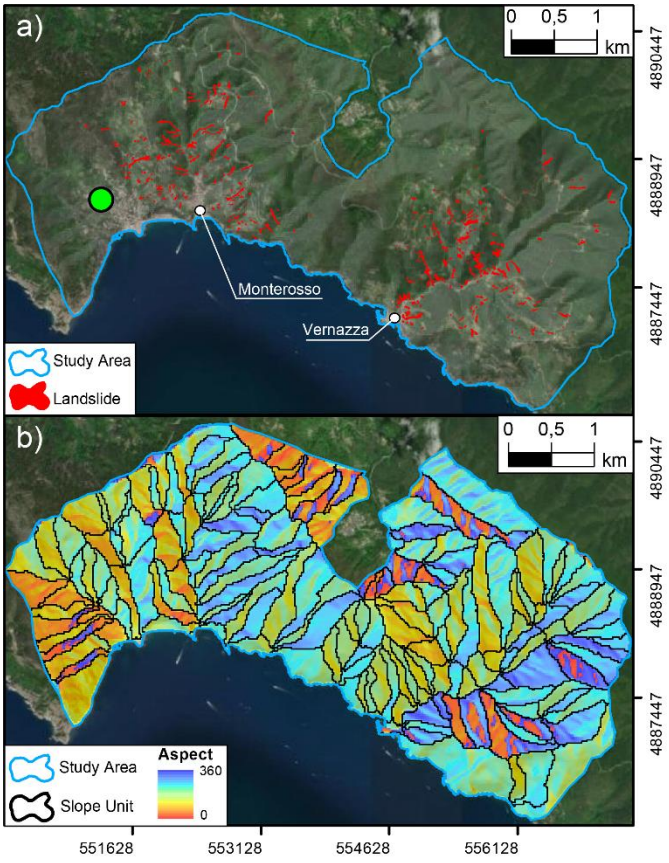

Figure 5.22 a) Overview of the landslide inventory and boundary of the study area; b) Slope Unit partition superimposed to the slope aspect. The green point corresponds to the location of the *Monterosso* weather station.

Also in this case study, an area distribution graph is shown (Fig. 5.23a). This inventory is more detailed than the inventory used in the second case study. For this reason, Figure 5.23a highlights a further shift to the left in the frequency of landslides with more limited extensions. Moreover, as discussed hereafter in sections 5.3.5 and 5.3.6, the estimated landslide intensity is used to determine

the expected landslide area aggregated by SU. For this reason, Figure 5.23b shows that the relationship between observed landslide (observed count) and the landslides areal extent (observed landslide area) is following a trend where at increasing count the aggregated landslide area also increases (Lombardo et al., 2020). The geomorphological validity of this relation could not hold in cases where a single or very few landslides combined would return an aggregated landslide area greater than many landslides together within a given mapping unit. The plot below suggests that not such case is applicable to our study area, and the only exception to the rule consists of the outliers (black dots) shown for limited counts along the x axis. condition.

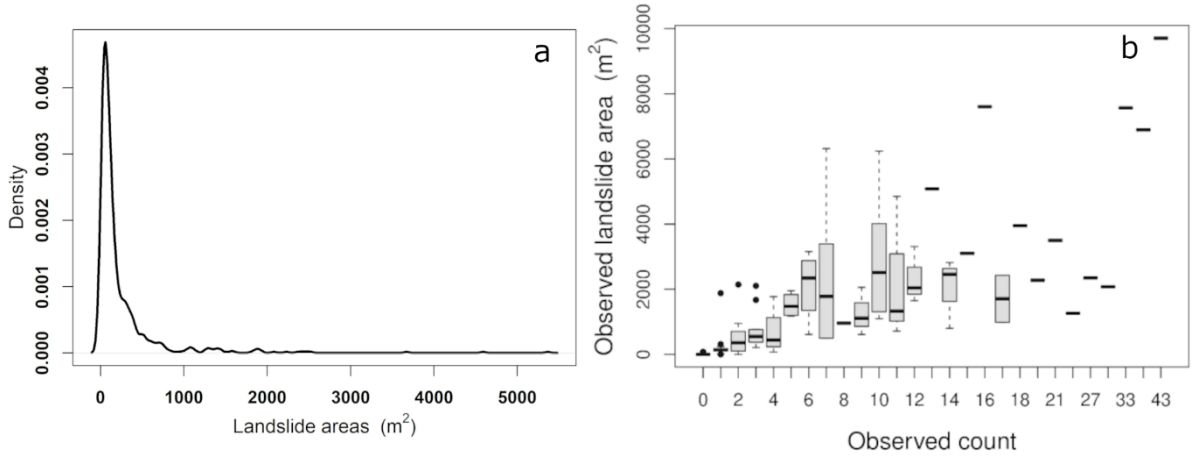

Figura 5.23 a) Area distribution of the *Cinque Terre* landslide inventory redacted by Cevasco et al., 2013; b) association between landslide counts and areas observation.

5.3.4. Mapping units and covariate set

To model landslide intensity a hierarchical structure was adopted. The hierarchy here is driven by a dual-use of mapping unit, expressing different spatial characteristics of the intensity model. Specifically, high-resolution Grid-Cells (GCs; Reichenbach et al. 2018) are used to construct the skeleton of the model in the form of the target variable and associated covariates. These units are then combined with a coarser resolution mapping unit such as Slope Units (SUs, Carrara et al. 1995), at which level the Latent Spatial Effect was computed. The combination of these two elements contributes to the estimation of the landslide intensity, which at the scale of the single GC is hardly distinguishable from the traditional susceptibility but as one aggregate to coarser spatial partitions, it begins to provide much richer information on how many landslides one can expect at certain locations (for more details, see Lombardo et al. 2019). More specifically, a 20 m resolution GC partition was selected whereas the SUs were computed by using the *r.slopeunits*, an open software for GRASS GIS (GRASS GIS Development Team 2020) developed by Alvioli et al. (2016), for the automatic partitioning of a landscape into SUs. *r.slopeunits* was parameterized by using a circular variance of 0.4, a minimum SU area of 12500 m^2 and a flow accumulation threshold of 100000 m^2, returning 171 SUs (Fig. 5.22 b). SUs are geomorphological and

hydrological terrain subdivisions bounded by drainage and divide lines (Carrara 1988; Alvioli et al. 2016) and they represent a good geometric description of natural slopes, where most landslides occur. Their strength, in the specific context of landslide modelling (irrespective of the susceptibility or intensity framework), resides in their ability to express the morphodynamic response of a slope to a given failure, independently from the neighbouring units.

The morphometric covariates selected to build the intensity model have been derived from a 5 m DEM accessed from the geoportal of the Ligurian region (https://geoportal.regione.liguria.it). This DEM has been later resampled at 20 m resolution to match the squared lattice which was defined. This 20 m reticular structure was chosen to generate counts beyond the mere 0/1 binary situation and to keep the covariate hyperspace to a size that could be more easily handled (to keep the computing costs in a reasonable size). The Euclidean distance was also computed from each GC to the nearest road or trail. As result, the following covariates set were selected: *i*) Elevation; *ii*) Slope Steepness; *iii*) Eastness; *iv*) Northness; *v*) Planar and *vi*) Profile Curvatures; *vii*) Relative Slope Position; *viii*) Topographic Wetness Index; *ix*) Distance to road or trail; *x*) Distance to stream; *xi*) Land Use; *xii*) Terrace status; *xiii*) Geology (further detail in section 3.1). Table 5.5 resumes the codes used for the categorical environmental variables.

5.3.5. Landslide "intensity" modelling

The inventory database is composed of 695 rainfall-induced shallow landslides. By counting their distribution per mapping unit, the resulting data as a Point Process can be modelled. More specifically, a Poisson Point Process can be defined as equation 5.3:

$$N(A) \sim Poisson \int_A \lambda(s)\, ds \qquad 5.3$$

where $N(A)$ is the number of the expected landslides within the study area, λ is the intensity assumed to be ≥ 0, and s is each of the GC within the park. This framework can be extended towards a doubly stochastic structure where the original stochasticity brought by a Poisson model is combined with the stochasticity of a Gaussian model. The latter being particularly useful to implement any sort of covariate effects. Such a task can be achieved by conveniently expressing the intensity on a logarithmic scale and modelling the latter via a Gaussian probability distribution. This procedure gives rise to Log-Gaussian Cox Process, and in this study can be expressed as follow (equation 5.4):

$$\log\{\lambda(s)\} \sim Gaussian\ Process$$

$$= \beta_0 + \sum_{J=1}^{J} \beta_j x_j(s) + f_{Geology} + f_{Land\ Use} + f_{Terraces} + f_{LSE} \qquad 5.4$$

where β_0 is the global intercept, β_j are the fixed effects used to model continuous covariates and $f_{geology}$, $f_{Land\ Use}$ and $f_{Terraces}$ are the random effects for categorical properties, whereas f_{LSE} is the random effect for the LSE.

Table 5.5 Codes classification of the categorical environmental covariates.

Covariate	Code	Description
Terrace Status	**T1**	Abandoned terraces with dense vegetation cover
	T2	Cultivated terraced areas
	T3	Abandoned terraces with poor vegetation cover
	T4	Non-terraced areas
Geology	**G1**	Macigno Sandstones
	G2	Groppo del Vescovo Limestones
	G3	T. Pignone Marls
	G4	Gabbros
	G5	M.te Veri Argillites and Limestones
	G6	Serpentinites
	G7	Gottero Sandstones
	G8	Val Lavagna Schists
	G9	Basalts
	G10	Cherts
Land use	**LU1**	Complex Cultivation Patterns
	LU2	Mixed Forest
	LU3	Urban and Industrial Area
	LU4	Olive Groves
	LU5	Moors and Scrubs
	LU6	Abandoned Olive Groves
	LU7	Vineyards
	LU8	Abandoned Vineyards
	LU9	Sclerophyllous Vegetation
	LU10	Beaches, Dunes, Sands and Bare rocks

LSE is used to capture the signal of unobserved covariates, such as the trigger, defined over SUs (see section 3.4.1). These problems are commonly solved via Generalized Additive Mixed Models (GAMM; Steger et al. 2021), which, in this application, it is implemented in the Bayesian formulation via INLA (Rue et al. 2009).

Two important properties of the landslide intensity should be recalled. The intensity can always be converted into the most common susceptibility being the latter binary case a simpler realization

of the count framework (Lombardo et al. 2019b). This can be achieved via the following formulation (equation 5.5):

$$Susceptibility = 1 - e^{-\lambda_A} \quad 5.5$$

Also, handling the intensity information over space is much easier than doing the same in the susceptibility case. In fact, the susceptibility is mapping-unit dependent whereas the intensity benefits from the aggregation property across any spatial units. In this work, this moving from the GC partition to the SU one, by summing all the λ values estimated within a given SU. Furthermore, landslides areas falling within each different SUs were quantified by measuring the size of each landslide as the planimetric area of the polygon encompassing it, namely landslide size. This information was then aggregated per SU by summing up the contribution of the distinct landslides area, obtaining the total planimetric area of mass movements per SU.

Being the model hierarchical in nature, the performance at the level of the two mapping units were evaluated. At GC scale, where the data is almost binary, AUC evaluation has been used (Arabameri et al. 2020). At the SU level, the agreement between the observed landslide counts and aggregated intensities were checked. In addition, the predictive performance of a fitted model has been evaluated using the Leave-One-Out-Cross-Validation (L1O) method (Tanyas et al. 2019; Lombardo et al. 2020a). The idea of the cross-validation is to perform several splitting of the data into the training sample used for fitting the model, and into the validation sample (remaining data) used for evaluating the predictive accuracy (see section 3.2.1). In the L1O procedure, each data object (in this case SU) is left out from the sample and used for validation. This means that different models are fitted (namely, 171), each one calibrates on 170 SU and alternatively predicted on the remaining one. It is important to note that this CV scheme was chosen to perturb the spatial dependence contained in the distribution of landslides. In fact, if single GC were removed at random, the spatial scale at which these units act, would have not weakened the spatial structure captured via the LSE. Conversely, removing all the GC contained in each of the 171 SU partitioning the study area would have caused any residual spatial dependence to be weakened enough to test the model as a predictive tool rather than a simpler exploratory tool.

Moreover, to go back to the initial research question, it was tested whether the estimated intensity (both the fitted and the CV one) per SU correlated with respect to the aggregated landslide area. This hypothesis was tested through visual interpretation (plotting one measure against the second) and also by computing the Pearson correlation coefficient between the two. For the visual part, a model with a reasonable performance should produce values aligned with the main diagonal (i.e., the 45° line), whereas Pearson correlation coefficients close to 1, imply a close association between counts and areas per SU. Lastly, analyses on linear and random effects were conducted to

verify the contribution of each covariate to the fitted model. This procedure values the exploratory component of our modelling protocol whereas the spatial cross-validation scheme provides a measure of how accurate the implemented model is in predicting unknown data.

5.3.6. Additional details: from landslide intensity to hazard and density

The landslide intensity has been shown to correlate with the total planimetric extent of landslides for each main unit (Lombardo et al. 2020). In the above-mentioned work, Lombardo and co-authors recognized this characteristic and stated that because of it, their model was the first unified hazard model, as per the current definition. However, Lombardo and co-authors stopped at this observation and missed an important implication. If intensity and landslide sizes can be expressed one as the function of the other, this also means that one can convert landslide intensity maps into expected landslide size-related maps.

In this work, this possibility by estimating the intensity per SU and then fitting a simple linear regression to predict the landslide extent for each SU was explored. The simple linear regression where the dependent variable is the sum of all landslide planimetric areas (for the positive part) per SU and the independent variable is the corresponding landslide intensity were employed to estimate the landslide area by means of the following equation (5.6):

$$Y = a + bX \tag{5.6}$$

where Y is the dependent variable (i.e., landslides areas aggregated per SU), a is the intercept, b is the angular coefficient and x is the explanatory variable, namely estimated landslide intensity. Furthermore, additionally, the analysis consists in dividing the estimated landslide areas for the corresponding SU size, thus estimating the landslide density.

5.3.7. Landslide "intensity" outcomes and discussion

At the scale of a fine GC, the data is usually near-binary in nature. In other words, no large landslide counts are contained. For this reason, two levels of performance assessments were implemented. At the GC level, Receiver Operating Characteristic curves (ROC) and their Area Under (AUC) the Curve were computed. At the scale of the SU, the agreement between observed and estimated landslides counts were checked. The corresponding results are shown in Figure 5.24 where the whole procedure appears to be very stable, irrespective of the considered mapping unit.

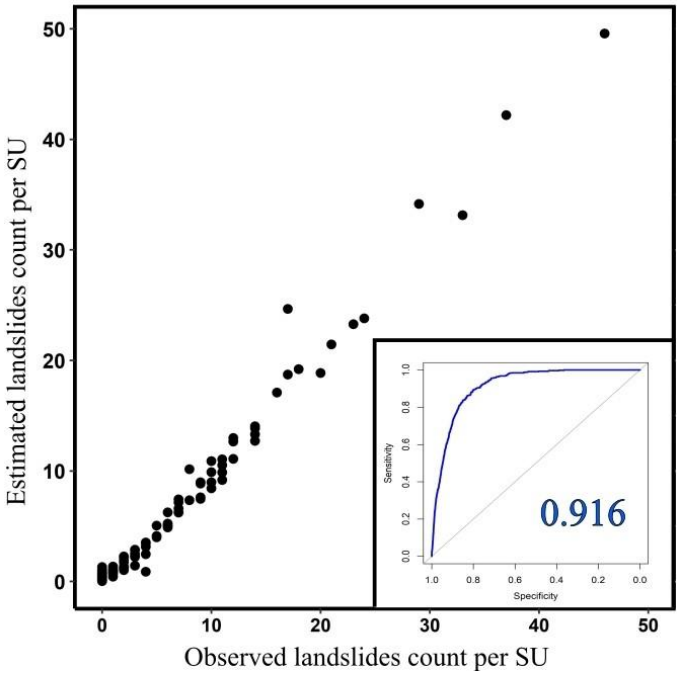

Figure 5.24 The bottom-right inset highlights the AUC value obtained for fitted models at GC level, whereas, the main graph shows the relationship between observed vs. estimated landslides aggregated for SU.

The performance of implemented model appears to be satisfactory. Indeed, visually and intuitively the graph highlights how the observed and predicted landslides pattern, aggregated per SU, match. Furthermore, to provide a numerical overview of the model's performance, the AUC was computed. Considering the classification proposed by Swets (1988) where values lower than 0.5 are considered random, values between 0.5 and 0.7 are accepted as poor, fair in the range 0.7 - 0.9 and, lastly, excellent for values greater than 0.9; the obtained AUC is diagnostic of outstanding performance (i.e., 0.916).

Inspected the model reliability and the positive relationship that exists between the observed and predicted landslides, cross-validation (i.e., L1O) was carried out in order to test the model as a predictive tool. With L1O, it is possible to verify whether the model can correctly estimate unknown landslide counts. Figure 5.25 shows the performance obtained for both the fit and the L1O. An LGCP model with the landslides surveyed after the October 2011 event was implemented. To adjust and verify if any covariates were missing in the model, or better, if any residual spatial coherence still existed aside from the one captured by the explicit covariates, a Latent Spatial Effect was also estimated by using a Besag model. A Besag model essentially computes the residual between a reference intensity model and the observed counts per SU. Then, it averages out these residuals per SU with respect to the neighbouring SUs, plus a random component. This operation captures residual spatial structures in the data and informs the model about them. A grid-search was implemented to find the optimal hyperparameter for the Latent Spatial Effect, after which, the Fit

and L1O produced an agreement between observed and estimated landslide counts as shown in Figure 5.25.

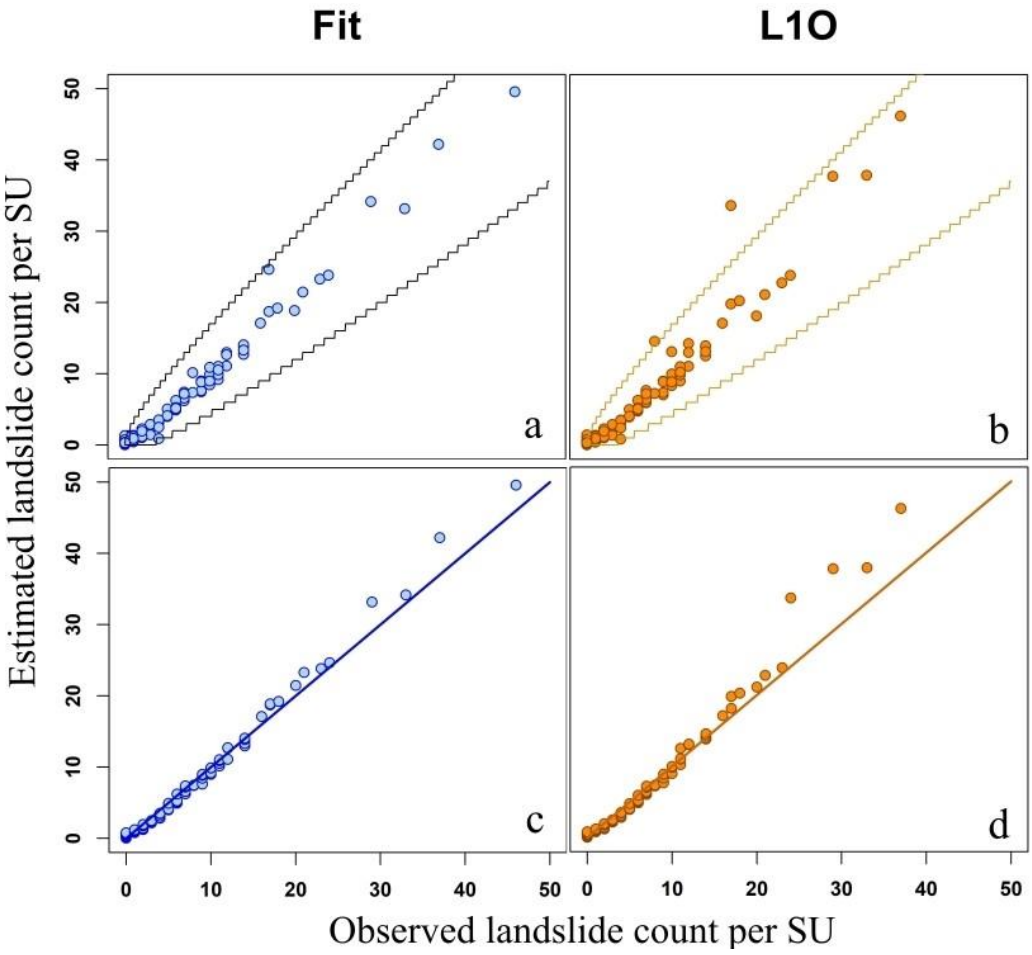

Figure 5.25 Performance obtained for both the fit and the L1O, c-d) q-qplot.

Let's recall here that the use of the fit ensured a benchmark against which we could compare the potential drop in performance when our model would have had to estimate unknown data. And, it also provided the base to interpret the covariate effects via a model that has all the available information within the study area. As for the L1O, the choice of this predictive framework ensured the assessment of the implemented model as a predictive tool. Once the model performance in its two forms was demonstrated to be suitable, it was checked the agreement of the intensity with respect to the landslide sizes. Figure 5.26 shows that this relationship exists almost equally for the fit and the L1O. Thereby, it was possible to model the landslide area, aggregated per SU, considering the obtained estimated intensity.

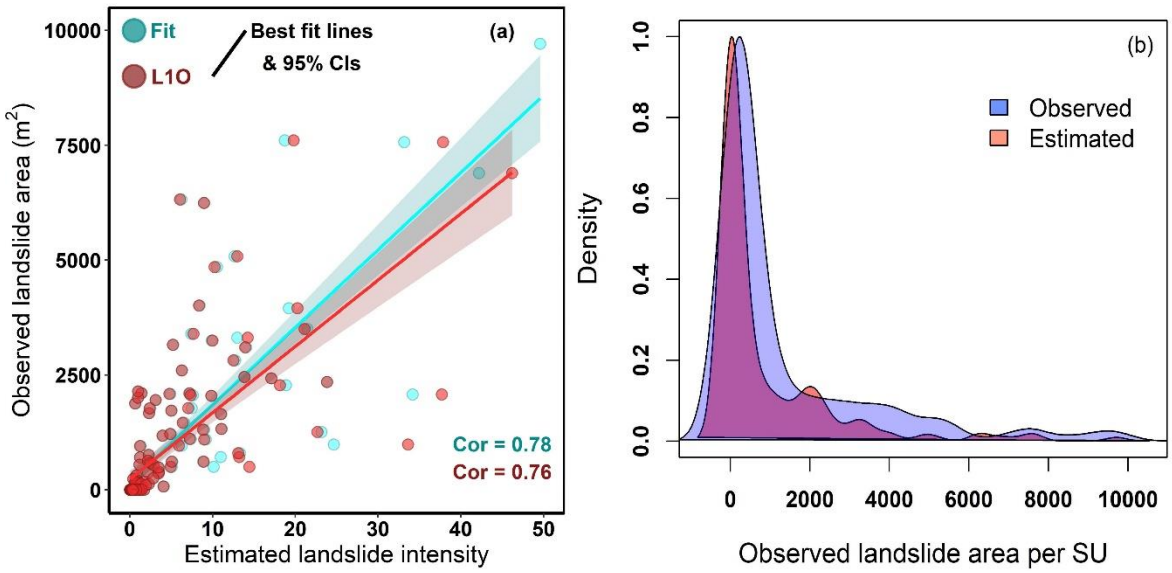

Figure 5.26 Correlation analysis between estimated intensity vs. observed landslide area.

This has been achieved via a simple linear regression, where two parameters were obtained, namely intercept and angular coefficient. Furthermore, planimetric area information of the different SUs were also available. Thus, it was possible to estimate the landslide area density per each SUs expressed in percentage. This was simply achieved by dividing the obtained landslide area by the area of each SU.

In summary, Figure 5.27 groups all the results obtained with the proposed mapping procedure, i.e. the landslide intensity map at pixel scale and aggregated per SU, the predicted landslide area for each SU and lastly, the landslide density per SU. The figure highlights what has been derived for both fit and L1O. Firstly, it is worth emphasizing that the pattern of the fitted landslides count is extremely close to the pattern shown for the corresponding L1O cases, this is valid both on the continuous scale and in the aggregates for SUs ones. The results clearly show that the central parts of the *Vernazza* and *Monterosso* hamlets are the most prone to instability, reaching higher intensity values (colour in yellow). In addition, the intensity at pixel scale is displayed using continuous values, as frequently appointed in Italy in the framework of landslide risk management. Moreover, the wide areas with the greatest intensity fall within the *Vernazza* catchment, which is also confirmed by the highest number of landslides surveyed in the same territory. When the intensities are aggregated per SU, the instability of the central sectors is more emphasized. In particular, the estimated landslides areas reach values of about 7000-8000 m^2. Considering also the soil and debris covers thickness that could be mobilised, the involved volumes are considerable and the phenomena occurrence probability, such as October 2011 event, is very likely. The higher instability of the central portions, especially for the *Vernazza* basin, is also confirmed by the landslide density where the percentages are greater than 8% for the SU.

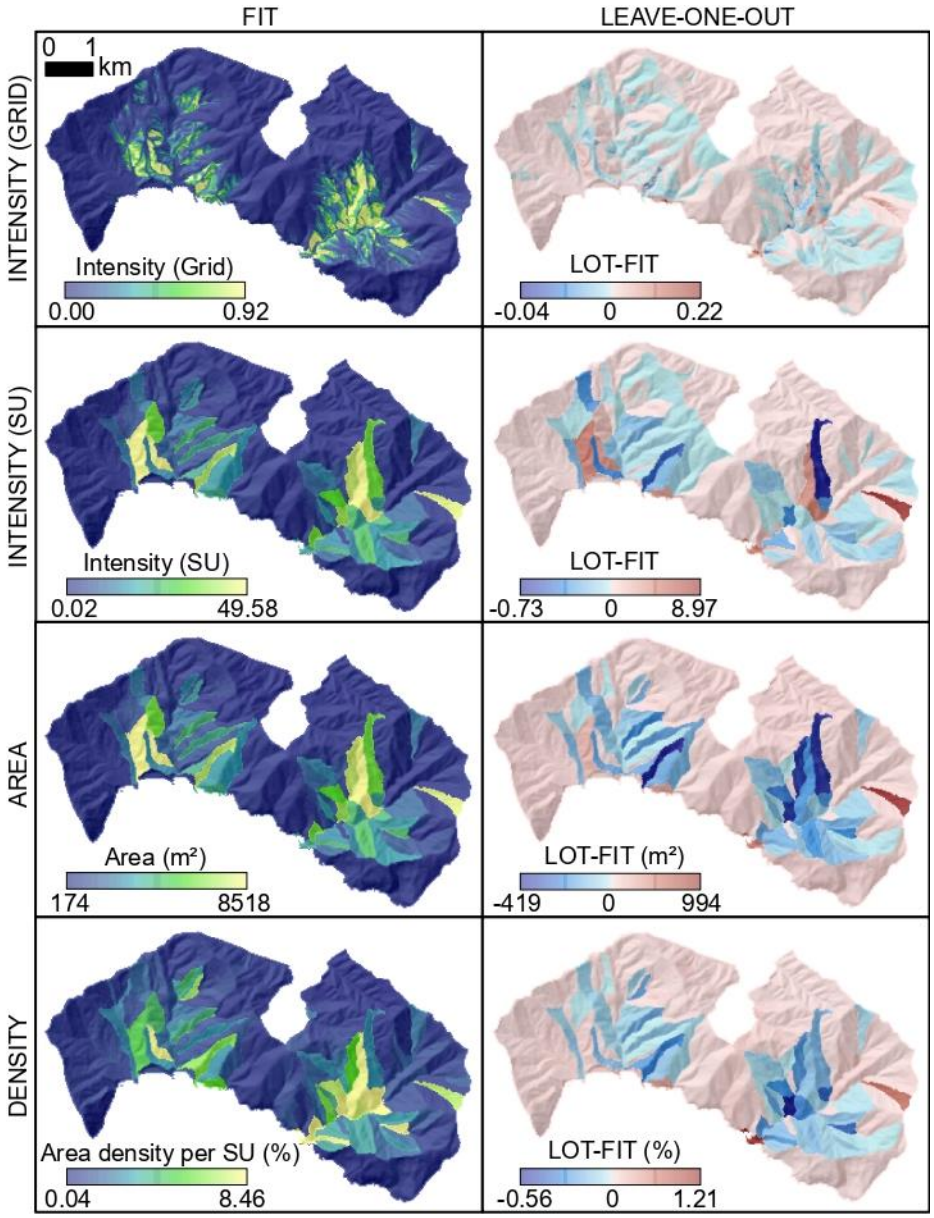

Figure 5.27 From top to bottom: landslide intensity map based on grid-scale resolution; landslide intensity map aggregated per SU; predicted landslide area map for each SU; landslide density area also aggregated per SU.

In addition, it must be stressed that the southern portions of the study area, characterised by coastal cliffs, do not fall within areas classified as high intensity because falls and topples were not taken into account, and the analysis focused only on rainfall-induced phenomena.

Finally, the linear and random effects contributions were analysed. Figure 5.28 plots the estimated coefficient of linear (or fixed) effects (except for the intercept) for the posterior mean and the 95% credible interval around it. The designated covariates, that have been rescaled to have mean 0 and variance 1, show relatively strong negative and positive influences on landslides. More specifically, out of 9 predisposing factors used linearly only 4 appeared to be significant for the model. Non-significance does not necessarily imply that the model is not influenced by these covariates. Significance indicates that the model is 95% certain of the role (either positive or

negative) of the given covariate concerning the landslide count distribution. As the covariates have been rescaled to be expressed in the same unitless range, the regression coefficient also follows this criterion, thus it is possible to rank the covariates from the most relevant to the least according to the absolute values of the posterior distributions.

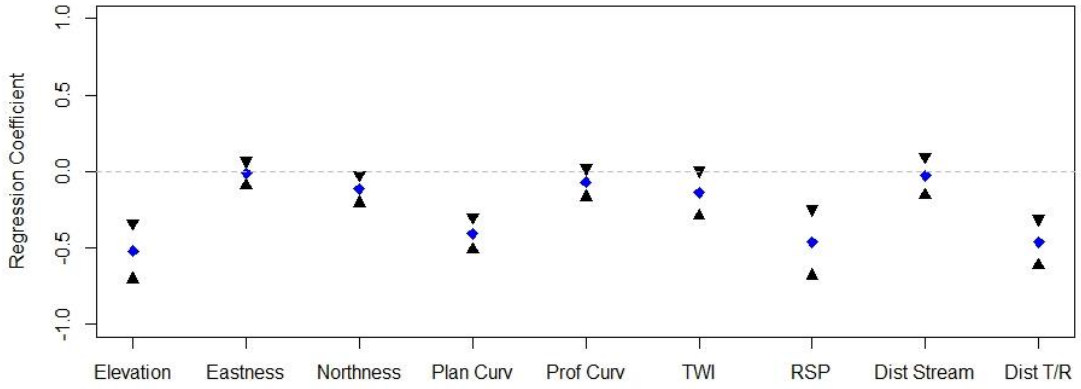

Figure 5.28 Posterior means (blue dots) of fixed linear effects (except the intercept) with 95% credible intervals (black arrows) for the model. The horizontal black dashed lines indicate no contribution to the landslide sizes. From left to right are plotted the following covariates: Elevation, Eastness, Northness, Planform Curvature, Profile Curvature, Topographic Wetness Index, Relative slope Position, Distance to Stream, Distance to Train and Road.

Figure 5.29 displays all the non-linear (or random) covariates' effects featured in the model, by plotting the estimated coefficients in terms of posterior mean and the 95% credible intervals. The panel reports environmental factors that have been used in a purely categorical form, i.e., with class effects being mutually independent a priori (except for the LSE). The slope covariate has been employed as an ordinal variable with an adjacent inter-class dependency driven by a random walk (see section 3.4.1).

A reassuring covariate contribution can be seen for the slope. The variation of the steepness inside a given SU can be intuitively interpreted as a proxy for topographic roughness. Slope values assume a twofold behaviour, in which negative values are noted up to about 20° - 25°, then assume increasing positive values up to about 35° - 40° up to settle at constant values for greater acclivity classes. This behaviour is in line with the type of landslide considered, i.e. superficial and rapid landslides, since these phenomena are mobilized around 25° up to a maximum of about 40° (Cevasco 2007; Cevasco et al. 2013a, 2014). In addition, slope appears as a positively contributing variable in studies assessing the susceptibility of rainfall- and earthquake-induced landslides (Guzzetti et al. 2005; Tanyas et al. 2019).

Concerning land use, LU7 and LU8, namely vineyards and abandoned vineyards respectively, contribute highly to increasing the instability area degree. This is in agreement with what has already been widely reported in the previous chapters of the thesis and literature (Cevasco et al. 2013a; Brandolini et al. 2018a, b; Pepe et al. 2019; Di Napoli et al. 2021), in which terraced and,

especially, abandoned terraces areas are more prone to instability and landslide phenomena detachment. Furthermore, Pepe ad co-authors conducted a detailed investigation on land-use transformations from the early 1950s to 2011, analysing the influence that the abandonment of cultivated terraced slopes have assumed on the distribution and magnitude of rainfall-induced shallow landslides. The outcomes highlighted that the documented transformation has played a crucial role in influencing hydro-geomorphological processes and the terraces abandoned for a short time exhibited the highest proneness to slope instability. The assurance of what has just been described was given by the state of activity of the terraces covariate. The terraced abandoned slope areas with limited greenery (labelled as T3) and, therefore recently abandoned, have assumed noticeable importance in the implemented model. The state of activity of the terraces represents a fundamental parameter in the study area. In fact, it is widely documented in the literature that if the terraces are adequately preserved they guarantee soil conservation, while, otherwise, if they are abandoned promote the instability phenomena occurrence (Cevasco et al. 2014; Pepe et al. 2019; Di Napoli et al. 2021).

The geological aspect is not to be considered secondary in these analyses. D'Amato Avanzi et al. (2004) admitted the importance of geological influence on the landslide distribution and the importance as a predisposing factor in susceptibility investigation. The soil and debris slope cover thickness, which could be concerned by mass movements, depends on land use and geological setting. Furthermore, the high geological heterogeneity determines the high bedrock inhomogeneity, affecting the permeability conditions. Different permeability conditions may have played a role in predisposing the slopes to instability (Cevasco et al. 2014). Therefore, although the slope failures took place in colluvial and anthropically reworked deposits, the distribution of the landslides follow the bedrock lithology. Most of the slope failures took place in the fine-grained sandstones (*Macigno* Formation, G1), while, a slightly lower percentage of landslides occurred in the limestones (*Canetolo* Shales and Limestones and *Mt. Veri* Limestone, G2 and G5, respectively). However, the highest landslide occurrence was observed for the impermeable claystone and limestone, differently for fine-grained sandstones. There are several reasons for this: *i*) a greater degree of permeability of fine-grained sandstones compared to clay lithotypes, or *ii*) sandstones principally outcropping in wooded areas that were not affected as much by slope failures.

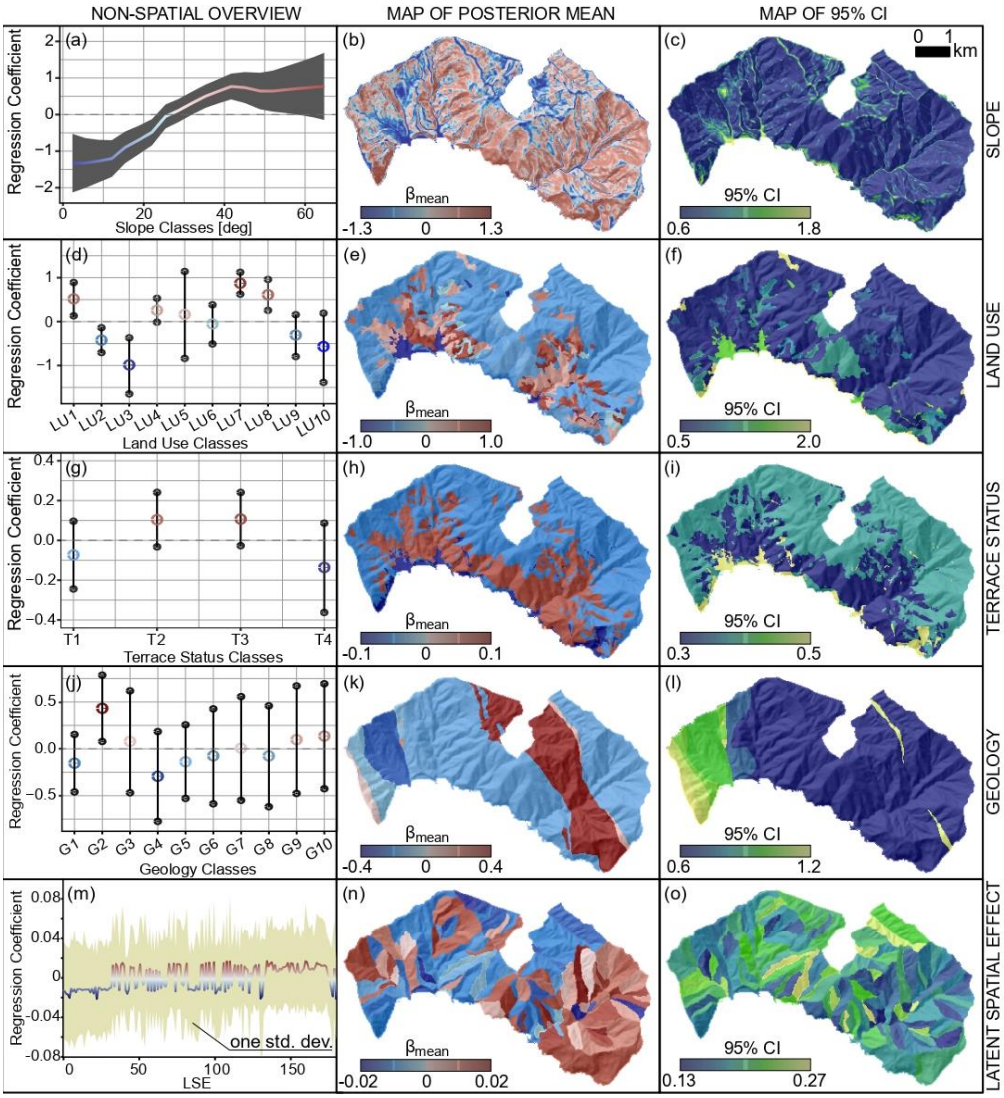

Figure 5.29 Random effects for the performed model, from top to bottom: slope ranging from 0 to 90 degrees, land use classes, terrace status, geology and latent Spatial Effect. For code classification refers to Table 5.5.

5.3.8. Conclusions

The standard definition of landslide hazard requires the expectation of "where", "when" or "how" frequently a landslides group may take place, as well as "how" large the landslide population may be. The common way is to evaluate the event landslide "magnitude", an index of how many and how large the total number of landslides may be for a whole study area. As a result, the community only provides a single number to represent the landslide-event magnitude, neglecting the geographic characteristic of the landslide size information. To put it differently, maps able to evaluate statistically the predicted extent of an unstable slope are not achievable today. The first attempt to fill this gap was realized by Lombardo et al. 2021 and this study represents an extension or alternative to their work.

The extremely interesting novelty of this application is that if the extent of the average landslides is known, in a given investigated area, it is possible to predict the landslide area by analysing the relationship that exists with the estimated intensity. Indeed, a further step was taken as the relationship between landslide intensity and the planimetric area was used to generate maps that predict the aggregated size of landslides per mapping unit, and the proportion they may affect.

The estimated landslide intensity has been processed through a novel Bayesian modelling framework for spatial landslides prediction. The procedure exploits a Log-Gaussian Cox Process (LGCP), which assumes that individual landslides in an area are the result of a stochastic point process driven by an unknown intensity function. The modelling framework was tested in the *Cinque Terre* National Park area, *Liguria*, Northern Italy, for which a detailed landslide inventory, redacted immediately after the October 2011 event, and other crucial predisposing factors are available.

Nowadays, governmental agencies manage the territory for landslide risk prevention by using susceptibility maps, which communicate the information about where landslides are expected to trigger. Therefore, the implemented procedure could be considered a complementary resource to improve operational decisions in territorial management protocols.

CHAPTER 6: OVERALL DISCUSSION AND CONCLUSIONS

The objective of this Ph.D. dissertation is to deal with methodological aspects of landslide predictive modelling within the *Cinque Terre* National Park. Several algorithms, procedures and datasets were implemented and exploited to investigate the spatial and temporal distribution of landslides from the local to the entire park scale. The *Cinque Terre* area was selected because of its uniqueness in terms of geology, geomorphology, landscape, land use, just as unique are the problems that this area is experiencing as a result of *i*) the social and economic changes that have taken place since the middle of the last century, which have led to the abandonment of agricultural activities on the terraced slopes; *ii*) the changes due to urbanisation, which have led to the culverting/deviation of the final stretch of the main watercourses; *iii*) the enormous increase in tourism, which, since 2000, has led to a sharp increase in risk (particularly of human beings).

The first step of this study was carried out in a test area (5.4 km^2 wide), including some small coastal basins near *Monterosso al Mare*, in order to test Machine Learning techniques. The main objective of this case study was to estimate, for the first time, advanced statistical techniques in a peculiar geological, geomorphological and environmental setting. Precisely, three different Machine Learning algorithms were tested to determine the landslide susceptibility scenario within the study area. After that, the elevated stand-alones' prediction variability was reduced by performing ensemble models. The obtained ensemble outcomes seem to be encouraging and improve the stand-alone methods, showing elevated performance values. The frameworks highlighted how landslide distribution in the small catchments near *Monterosso al Mare* is mainly located in areas characterized by high susceptibility. By taking into account this novel approach, the impact of landslides and associated losses can be reduced. This last aspect should not be underestimated, especially considering the high-risk condition affecting this area.

Consequently, because of the high model performance and accuracy, the methodology described above was applied to the entire *Cinque Terre* National Park. In particular, a combined procedure, considering simultaneously the susceptibility of shallow landslide failure, by using Machine Learning techniques, and runout, by using GIS-based tools, was developed. This step of the study was conducted because frequently, after severe rainfalls, the shallow landslides may evolve into potentially catastrophic flow-like movements. The consequences of shallow landslides and flow-like phenomena are typically more dangerous in inhabited centres located at the foot of slopes, where the hydrographic network is well developed. This was the case of the tragic event affecting *Cinque Terre* in October 2011. Unfortunately, despite its importance, runout evaluation is not as widespread in the data-driven literature compared to the analysis of the potential landslide detachment. Indeed, most of the available landslide zoning maps only examine susceptibility to

landslide detachment, having a great impact on final hazard models and urban planning. As known, the consequences of incorrect urban and land-use planning can be disastrous. Not coincidentally, the comparison between landslide detachment and landslide detachment, transit and runout susceptibility maps highlights how specific portions of the study area show an opposite degree of susceptibility. This especially occurs in flat areas located at the base of the slopes, that despite a low landslide detachment degree, could be affected by the flow-like slope failures runout. Information in this sense were obtained comparing the propagation areas of shallow landslides occurred on 25th October 2011, at *Vernazza* with the degree of susceptibility resulting from the landslide detachment and landslide detachment, transit and runout susceptibility maps. The outcomes of this comparison were very encouraging, indicating a higher performance of landslide detachment, transit and runout susceptibility map concerning landslide detachment map (percentages of landslide deposits falling in areas with high and very high susceptibility of 82% and 48%, respectively). So, the novelty of this work consists of a processing chain that considers both the detachment and runout susceptibility assessment. The availability of future events data could provide further information about the reliability and effectiveness of the landslide detachment, transit and runout susceptibility map obtained in this study.

To conclude, the last approach used in this study deviates from the previously implemented models, which are based on binary presence/absence data. In particular, a Bayesian hierarchical Cox point process model that describes landslide counts has been utilized. Precisely, a Log-Gaussian Cox Process, only recently employed in landslide applications, was built by considering landslide intensity and not susceptibility. Landslide intensity represents an alternative measure, depicting the expected number of landslides in any given terrain mapping unit. In addition, to cope with the landslide issue, the landslide size is believed to be in the same way significant. Regrettably, contemporary studies, besides ignoring the probable landslides number inside a given mapping unit, they also neglect the spatial estimation of the expected planimetric area or volume associated with landslides triggered within the same unit. The natural result, information about the landslide size is independently estimated and it refers to the landslide event magnitude. Recently, Lombardo et al. (2021) have proposed an innovative approach to build statistical models capable of predicting the planimetric area (expressed in logarithmic scale) of event-triggered landslides. In addition. Lombardo et al. (2020) have proved that intensity is closely correlated to the cumulated landslide area per mapping unit. In this application, the standard procedures used to evaluate landslide susceptibility were extended, and the more recent approach proposed to estimate landslide intensity and to model the size (area) of the landslides were employed. Moreover, a further step was taken as the relationship between landslide intensity and the planimetric area was used to generate maps that

predict the aggregated size of landslides per mapping unit, and the portion they may affect. This chain of landslide intensity, hazard and density may lead to substantially improve decision-making processes related to landslide risk. Maps able to evaluate statistically the predicted extent of an unstable slope are not achievable today. This study attempts to extend the framework described above while keeping the estimated landslide are in their linear form rather than producing a model that estimates it on the logarithmic scale. The extremely interesting novelty of this application is that if the extent of the average landslides is known in a given investigated area, it is possible to asses the landslide area by analysing the relationship that exists with the estimated intensity.

CHAPTER 7: REFERENCES

Abbaszadeh Shahri A, Spross J, Johansson F, Larsson S (2019) Landslide susceptibility hazard map in southwest Sweden using artificial neural network. CATENA 183:104225. https://doi.org/10.1016/j.catena.2019.104225

Abbate E, Fanucci F, Benvenuti M, et al (2005) Carta Geologica d'Italia alla scala 1:50.000-Foglio 248-La Spezia con note illustrative.

Abedini M, Ghasemyan B, Mogaddam MHR (2017) Landslide susceptibility mapping in Bijar city, Kurdistan Province, Iran: a comparative study by logistic regression and AHP models. Environmental Earth Sciences 76:

Agnoletti M (2007) The degradation of traditional landscape in a mountain area of Tuscany during the 19th and 20th centuries: Implications for biodiversity and sustainable management. Forest Ecology and Management 249:5–17. https://doi.org/10.1016/j.foreco.2007.05.032

Alvioli M, Marchesini I, Reichenbach P, et al (2016) Automatic delineation of geomorphological slope units with <tt>r.slopeunits v1.0</tt> and their optimization for landslide susceptibility modeling. Geoscientific Model Development 9:3975–3991. https://doi.org/10.5194/gmd-9-3975-2016

Amano T, Sutherland WJ (2013) Four barriers to the global understanding of biodiversity conservation: wealth, language, geographical location and security. Proceedings of the Royal Society B: Biological Sciences 280:20122649. https://doi.org/10.1098/rspb.2012.2649

Anderson RP, Lew D, Peterson AT (2003) Evaluating predictive models of species' distributions: criteria for selecting optimal models. Ecological Modelling 162:211–232. https://doi.org/10.1016/S0304-3800(02)00349-6

Arabameri A, Chen W, Lombardo L, et al (2020) Hybrid Computational Intelligence Models for Improvement Gully Erosion Assessment. Remote Sensing 12:140. https://doi.org/10.3390/rs12010140

Arabameri A, Pal SC, Rezaie F, et al (2021) Decision tree based ensemble machine learning approaches for landslide susceptibility mapping. Geocarto International 0:1–35. https://doi.org/10.1080/10106049.2021.1892210

Arabameri A, Pradhan B, Lombardo L (2019) Comparative assessment using boosted regression trees, binary logistic regression, frequency ratio and numerical risk factor for gully erosion susceptibility modelling. CATENA 183:104223. https://doi.org/10.1016/j.catena.2019.104223

Araújo MB, Pearson RG, Thuiller W, Erhard M (2005) Validation of species–climate impact models under climate change. Global Change Biology 11:1504–1513. https://doi.org/10.1111/j.1365-2486.2005.01000.x

Ardizzone F, Cardinali M, Carrara A, et al (2002) Impact of mapping errors on the reliability of landslide hazard maps. Natural Hazards and Earth System Sciences 2:3–14. https://doi.org/10.5194/nhess-2-3-2002

Ardizzone F, Cardinali M, Galli M, et al (2007) Identification and mapping of recent rainfall-induced landslides using elevation data collected by airborne Lidar. Natural Hazards and Earth System Sciences 7:637–650. https://doi.org/10.5194/nhess-7-637-2007

Arnáez J, Lana-Renault N, Lasanta T, et al (2015) Effects of farming terraces on hydrological and geomorphological processes. A review. CATENA 128:122–134. https://doi.org/10.1016/j.catena.2015.01.021

Arnaez J, Lasanta T, Errea MP, Ortigosa L (2011) Land abandonment, landscape evolution, and soil erosion in a Spanish Mediterranean mountain region: The case of Camero Viejo. Land Degradation & Development 22:537–550. https://doi.org/10.1002/ldr.1032

Arnone E, Francipane A, Scarbaci A, et al (2016) Effect of raster resolution and polygon-conversion algorithm on landslide susceptibility mapping. Environmental Modelling & Software 84:467–481. https://doi.org/10.1016/j.envsoft.2016.07.016

Aronica GT, Brigandı G, Morey N (2012) Flash floods and debris flow in the city area of Messina, north-east part of Sicily, Italy in October 2009: the case of the Giampilieri catchment. Nat Hazards Earth Syst Sci 15

ARPAL-CFMI-PC (2012) Uno tsunami venuto dai monti - Provincia della Spezia 25 ottobre 2011 rapporto di evento meteo-idrologico

Ayalew L, Yamagishi H (2005) The application of GIS-based logistic regression for landslide susceptibility mapping in the Kakuda-Yahiko Mountains, Central Japan. Geomorphology 65:15–31. https://doi.org/10.1016/j.geomorph.2004.06.010

Baddeley A, Turner R, Møller J, Hazelton M (2005) Residual analysis for spatial point processes (with discussion). Journal of the Royal Statistical Society: Series B (Statistical Methodology) 67:617–666. https://doi.org/10.1111/j.1467-9868.2005.00519.x

Baeza C, Corominas J (2001) Assessment of shallow landslide susceptibility by means of multivariate statistical techniques. Earth Surface Processes and Landforms 26:1251–1263. https://doi.org/10.1002/esp.263

Bakka H, Rue H, Fuglstad G-A, et al (2018) Spatial modeling with R-INLA: A review. WIREs Computational Statistics 10:e1443. https://doi.org/10.1002/wics.1443

Battistini, A., Segoni, S., Manzo, G., Catani, F., & Casagli, N. (2013). Web data mining for automatic inventory of geohazards at national scale. Applied Geography, 43, 147-158.

Baum RL, Godt JW, Highland L (2008) Landslides and Engineering Geology of the Seattle, Washington, Area. Geological Society of America

Beguería S (2006) Validation and Evaluation of Predictive Models in Hazard Assessment and Risk Management. Natural Hazards 3:315–329. https://doi.org/10.1007/s11069-005-5182-6

Bellugi DG, Milledge DG, Cuffey KM, et al (2021) Controls on the size distributions of shallow landslides. PNAS 118:. https://doi.org/10.1073/pnas.2021855118

Besag J (1975) Statistical Analysis of Non-Lattice Data. Journal of the Royal Statistical Society: Series D (The Statistician) 24:179–195. https://doi.org/10.2307/2987782

Beven KJ, Kirby MJ (1979) A physically based, variable contributing area model of basin hydrology. Hydrological Sciences Bulletin 24:43–69. https://doi.org/10.1080/02626667909491834

Blangiardo M, Cameletti M (2015) Spatial and Spatio-temporal Bayesian Models with R - INLA. John Wiley & Sons

Bordoni M, Galanti Y, Bartelletti C, et al (2020) The influence of the inventory on the determination of the rainfall-induced shallow landslides susceptibility using generalized additive models. CATENA 193:104630. https://doi.org/10.1016/j.catena.2020.104630

Bordoni M, Persichillo MG, Meisina C, et al (2015) Developing and testing a data-driven methodology for shallow landslide susceptibility assessment: preliminary results. ROL 35:25–28. https://doi.org/10.3301/ROL.2015.55

Brabb EE (1985) Innovative approaches to landslide hazard and risk mapping. pp 17–22

Brabb EE, Pampeyan EH, Bonilla MG (1972) Landslide susceptibility in San Mateo County, California. U.S. Geological Survey, Reston, VA

Brancucci G, Paliaga G (2006) The Hazard Assessment in a Terraced Landscape: Preliminary Result of the Liguria (Italy) Case Study in the Interreg III Alpter Project. 9

Brandolini P (2017) The Outstanding Terraced Landscape of the Cinque Terre Coastal Slopes (Eastern Liguria). In: Soldati M, Marchetti M (eds) Landscapes and Landforms of Italy. Springer International Publishing, Cham, pp 235–244

Brandolini P, Cevasco A (2015) Geo-hydrological Risk Mitigation Measures and Land-Management in a Highly Vulnerable Small Coastal Catchment. In: Lollino G, Manconi A, Guzzetti F, et al. (eds) Engineering Geology for Society and Territory - Volume 5. Springer International Publishing, Cham, pp 759–762

Brandolini P, Cevasco A, Capolongo D, et al (2018a) Response of Terraced Slopes to a Very Intense Rainfall Event and Relationships with Land Abandonment: A Case Study from Cinque Terre (Italy). Land Degradation & Development 29:630–642. https://doi.org/10.1002/ldr.2672

Brandolini P, Pepe G, Capolongo D, et al (2018b) Hillslope degradation in representative Italian areas: Just soil erosion risk or opportunity for development? Land Degradation & Development 29:3050–3068. https://doi.org/10.1002/ldr.2999

Brunori E, Salvati L, Antogiovanni A, Biasi R (2018) Worrying about 'Vertical Landscapes': Terraced Olive Groves and Ecosystem Services in Marginal Land in Central Italy. Sustainability 10:1164. https://doi.org/10.3390/su10041164

Bueechi E, Klimeš J, Frey H, et al (2019) Regional-scale landslide susceptibility modelling in the Cordillera Blanca, Peru—a comparison of different approaches. Landslides 16:395–407. https://doi.org/10.1007/s10346-018-1090-1

Burnham KP, Anderson DR (2002) A practical information-theoretic approach, 2nd edn. Springer, New York, 2

Calcaterra D, De Riso R, Evangelista A, et al (2003a) Slope instabilities in the pyroclastic deposits of the Phlegraean district and the carbonate Apennine (Campania, Italy). Proceedings of an International Workshop on Occurrence and Mechanisms of Flows in Natural Slopes and Earthfills held in Sorrento, Ital 14–16

Calcaterra D, Parise M, Palma B (2003b) Combining historical and geological data for the assessment of the landslide hazard: a case study from Campania, Italy. Natural Hazards and Earth System Science 3:3–16

Calcaterra D, Parise M, Palma B, Pelella L (2000) The Influence of Meteoric Events in Triggering Shallow Landslides in Pyroclastic Deposits of Campania, Italy. In: Landslides in Research, Theory and Practice. Thomas Telford Publishing, p 1: 209-214

Camera C, Masetti M, Apuani T (2012) Rainfall, infiltration, and groundwater flow in a terraced slope of Valtellina (Northern Italy): field data and modelling. Environ Earth Sci 65:1191–1202. https://doi.org/10.1007/s12665-011-1367-3

Camera CAS, Apuani T, Masetti M (2014) Mechanisms of failure on terraced slopes: the Valtellina case (northern Italy). Landslides 11:43–54. https://doi.org/10.1007/s10346-012-0371-3

Cammeraat E, van Beek R, Kooijman A (2005) Vegetation Succession and its Consequences for Slope Stability in SE Spain. Plant Soil 278:135–147. https://doi.org/10.1007/s11104-005-5893-1

Capitani M, Ribolini A, Bini M (2013) The slope aspect: A predisposing factor for landsliding? Comptes Rendus Geoscience 345:427–438. https://doi.org/10.1016/j.crte.2013.11.002

Cardinali M, Ardizzone F, Galli M, et al (2000) Landslides triggered by rapid snow melting: the December 1996-January 1997 event in Central Italy. 10

Carrara A (1988) Drainage and Divide Networks Derived from High-Fidelity Digital Terrain Models. In: Chung CF, Fabbri AG, Sinding-Larsen R (eds) Quantitative Analysis of Mineral and Energy Resources. Springer Netherlands, Dordrecht, pp 581–597

Carrara A, Cardinali M, Detti R, et al (1991) GIS techniques and statistical models in evaluating landslide hazard. Earth Surface Processes and Landforms 16:427–445. https://doi.org/10.1002/esp.3290160505

Carrara A, Cardinali M, Guzzetti F, Reichenbach P (1995) Gis Technology in Mapping Landslide Hazard. In: Carrara A, Guzzetti F (eds) Geographical Information Systems in Assessing Natural Hazards. Springer Netherlands, Dordrecht, pp 135–175

Catani F, Lagomarsino D, Segoni S, Tofani V (2013) Landslide susceptibility estimation by random forests technique: sensitivity and scaling issues. Natural Hazards and Earth System Sciences 13:2815–2831. https://doi.org/10.5194/nhess-13-2815-2013

Cevasco A (2007) I fenomeni d'instabilità nell'evoluzione della costa alta delle Cinque Terre (Liguria Orientale). 17

Cevasco A, Brandolini P (2015) Rapid debris volume estimation by LiDAR data derived DEMs: applications to the 25 October 2011 debris flood event at Vernazza (Cinque Terre, Italy). ROL 35/2015: https://doi.org/10.3301/ROL.2015.64

Cevasco A, Brandolini P, Scopesi C, Rellini I (2013a) Relationships between geo-hydrological processes induced by heavy rainfall and land-use: the case of 25 October 2011 in the Vernazza catchment (Cinque Terre, NW Italy). Journal of Maps 9:289–298

Cevasco A, Diodato N, Revellino P, et al (2015) Storminess and geo-hydrological events affecting small coastal basins in a terraced Mediterranean environment. Science of The Total Environment 532:208–219. https://doi.org/10.1016/j.scitotenv.2015.06.017

Cevasco A, Pepe G, Brandolini P (2012) Shallow landslides induced by heavy rainfall on terraced slopes: the case study of the October, 25, 2011 event in the Vernazza catchment (Cinque Terre, NW Italy). Rend Online Soc Geol It 21:384–386

Cevasco A, Pepe G, Brandolini P (2013b) Geotechnical and stratigraphic aspects of shallow landslides at Cinque Terre (Liguria, Italy). Rendiconti Online Società Geologica Italiana 24:52–54

Cevasco A, Pepe G, Brandolini P (2014) The influences of geological and land use settings on shallow landslides triggered by an intense rainfall event in a coastal terraced environment. Bull Eng Geol Environ 73:859–875. https://doi.org/10.1007/s10064-013-0544-x

Cevasco A, Pepe G, D'Amato Avanzi G (2017) Preliminary analysis of the November 10, 2014 rainstorm and related landslides in the lower Lavagna valley (Eastern Liguria). Italian Journal of Engineering Geology and Environment 5–15. https://doi.org/10.4408/IJEGE.2017-01.S-01

Chen W, Peng J, Hong H, et al (2018a) Landslide susceptibility modelling using GIS-based machine learning techniques for Chongren County, Jiangxi Province, China. Science of The Total Environment 626:1121–1135. https://doi.org/10.1016/j.scitotenv.2018.01.124

Chen W, Pourghasemi HR, Kornejady A, Zhang N (2017) Landslide spatial modeling: Introducing new ensembles of ANN, MaxEnt, and SVM machine learning techniques. Geoderma 305:314–327. https://doi.org/10.1016/j.geoderma.2017.06.020

Chen W, Shahabi H, Shirzadi A, et al (2018b) A novel ensemble approach of bivariate statistical-based logistic model tree classifier for landslide susceptibility assessment. Geocarto International 33:1398–1420. https://doi.org/10.1080/10106049.2018.1425738

Chen W, Sun Z, Han J (2019) Landslide Susceptibility Modeling Using Integrated Ensemble Weights of Evidence with Logistic Regression and Random Forest Models. Applied Sciences 9:171. https://doi.org/10.3390/app9010171

Ciampalini A, Raspini F, Lagomarsino D, et al (2016) Landslide susceptibility map refinement using PSInSAR data. Remote Sensing of Environment 184:302–315. https://doi.org/10.1016/j.rse.2016.07.018

Clerici A, Perego S, Tellini C, Vescovi P (2002) A procedure for landslide susceptibility zonation by the conditional analysis method. Geomorphology 48:349–364. https://doi.org/10.1016/S0169-555X(02)00079-X

Conoscenti C, Rotigliano E, Cama M, et al (2016) Exploring the effect of absence selection on landslide susceptibility models: A case study in Sicily, Italy. Geomorphology 261:222–235. https://doi.org/10.1016/j.geomorph.2016.03.006

Corominas J (1996) The angle of reach as a mobility index for small and large landslides. Can Geotech J 33:260–271. https://doi.org/10.1139/t96-005

Corominas J, Copons R, Vilaplana JM, et al (2003) Integrated Landslide Susceptibility Analysis and Hazard Assessment in the Principality of Andorra. Natural Hazards 30:421–435. https://doi.org/10.1023/B:NHAZ.0000007094.74878.d3

Corominas J, van Westen C, Frattini P, et al (2014) Recommendations for the quantitative analysis of landslide risk. Bull Eng Geol Environ 73:209–263. https://doi.org/10.1007/s10064-013-0538-8

Corsini A, Mulas M (2017) Use of ROC curves for early warning of landslide displacement rates in response to precipitation (Piagneto landslide, Northern Apennines, Italy). Landslides 14:1241–1252. https://doi.org/10.1007/s10346-016-0781-8

Cox DR (1965) On the Estimation of the Intensity Function of a Stationary Point Process. Journal of the Royal Statistical Society: Series B (Methodological) 27:332–337. https://doi.org/10.1111/j.2517-6161.1965.tb01500.x

Crosta GB, Imposimato S, Roddeman DG (2003) Numerical modelling of large landslides stability and runout. Natural Hazards and Earth System Science 3:523–538

Cruden DM (1991) A simple definition of a landslide. Bulletin of the International Association of Engineering Geology 43:27–29. https://doi.org/10.1007/BF02590167

Cruden DM, Varnes DJ (1996) Landslides: Investigation and Mitigation. Chapter 3 - Landslide types and processes. Transportation Research Board Special Report

D’Amato Avanzi G, Galanti Y, Giannecchini R, et al (2013) Remarks on the 25 October 2011 rainstorm in Eastern Liguria and Northwestern Tuscany (Italy) and the related landslides. Rend Online Soc Geol It 24:76–78

D’Amato Avanzi G, Giannecchini R, Puccinelli A (2004) The influence of the geological and geomorphological settings on shallow landslides. An example in a temperate climate environment: the June 19, 1996 event in northwestern Tuscany (Italy). Engineering Geology 73:215–228. https://doi.org/10.1016/j.enggeo.2004.01.005

Dehnavi A, Aghdam IN, Pradhan B, Morshed Varzandeh MH (2015) A new hybrid model using step-wise weight assessment ratio analysis (SWARA) technique and adaptive neuro-fuzzy inference system (ANFIS) for regional landslide hazard assessment in Iran. CATENA 135:122–148. https://doi.org/10.1016/j.catena.2015.07.020

Del Monte M, Vergari F, Brandolini P, et al (2015) Multi-method Evaluation of Denudation Rates in Small Mediterranean Catchments. In: Lollino G, Manconi A, Clague J, et al. (eds) Engineering Geology for Society and Territory - Volume 1. Springer International Publishing, Cham, pp 563–567

Del Soldato M, Riquelme A, Bianchini S, et al (2018) Multisource data integration to investigate one century of evolution for the Agnone landslide (Molise, southern Italy). Landslides 15:2113–2128. https://doi.org/10.1007/s10346-018-1015-z

Di Martire D, De Rosa M, Pesce V, et al (2012) Landslide hazard and land management in high-density urban areas of Campania region, Italy. Nat Hazards Earth Syst Sci 12:905–926. https://doi.org/10.5194/nhess-12-905-2012

Di Napoli M, Carotenuto F, Cevasco A, et al (2020) Machine learning ensemble modelling as a tool to improve landslide susceptibility mapping reliability. Landslides. https://doi.org/10.1007/s10346-020-01392-9

Di Napoli M, Di Martire D, Bausilio G, et al (2021) Rainfall-Induced Shallow Landslide Detachment, Transit and Runout Susceptibility Mapping by Integrating Machine Learning Techniques and GIS-Based Approaches. Water 13:488. https://doi.org/10.3390/w13040488

Dietrich WE, Reiss R, Hsu M-L, Montgomery DR (1995) A process-based model for colluvial soil depth and shallow landsliding using digital elevation data. Hydrological Processes 9:383–400. https://doi.org/10.1002/hyp.3360090311

Dikau R, Cavallin A, Jäger S (1996) Databases and GIS for landslide research in Europe. Geomorphology 15:227–239. https://doi.org/10.1016/0169-555X(95)00072-D

Eeckhaut MVD, Poesen J, Verstraeten G, et al (2007) Use of LIDAR-derived images for mapping old landslides under forest. Earth Surface Processes and Landforms 32:754–769. https://doi.org/10.1002/esp.1417

El-Gabbas A, Dormann CF (2018) Wrong, but useful: regional species distribution models may not be improved by range-wide data under biased sampling. Ecology and Evolution 8:2196–2206. https://doi.org/10.1002/ece3.3834

Elith J, Graham* CH, Anderson RP, et al (2006) Novel methods improve prediction of species' distributions from occurrence data. Ecography 29:129–151. https://doi.org/10.1111/j.2006.0906-7590.04596.x

Elith J, Graham CH, Valavi R, et al (2020) Presence-only and presence-absence data for comparing species distribution modeling methods. Biodiversity Informatics 15:69–80. https://doi.org/10.17161/bi.v15i2.13384

Elith J, Phillips SJ, Hastie T, et al (2011) A statistical explanation of MaxEnt for ecologists. Diversity and Distributions 17:43–57. https://doi.org/10.1111/j.1472-4642.2010.00725.x

EPOCH (1993) The temporal occurrence and forecasting of landslides in the European community

Ermini L, Catani F, Casagli N (2005) Artificial Neural Networks applied to landslide susceptibility assessment. Geomorphology 66:327–343. https://doi.org/10.1016/j.geomorph.2004.09.025

Esposito G, Marchesini I, Mondini AC, et al (2020) A spaceborne SAR-based procedure to support the detection of landslides. Natural Hazards and Earth System Sciences 20:2379–2395. https://doi.org/10.5194/nhess-20-2379-2020

Fairfield J, Leymarie P (1991) Drainage networks from grid digital elevation models. Water Resources Research 27:709–717. https://doi.org/10.1029/90WR02658

Fan L, Lehmann P, McArdell B, Or D (2017) Linking rainfall-induced landslides with debris flows runout patterns towards catchment scale hazard assessment. Geomorphology 280:1–15. https://doi.org/10.1016/j.geomorph.2016.10.007

Farina P, Colombo D, Fumagalli A, et al (2006) Permanent Scatterers for landslide investigations: outcomes from the ESA-SLAM project. Engineering Geology 88:200–217. https://doi.org/10.1016/j.enggeo.2006.09.007

Felicísimo ÁM, Cuartero A, Remondo J, Quirós E (2013) Mapping landslide susceptibility with logistic regression, multiple adaptive regression splines, classification and regression trees, and maximum entropy methods: a comparative study. Landslides 10:175–189. https://doi.org/10.1007/s10346-012-0320-1

Fell R (1994) Landslide risk assessment and acceptable risk. Can Geotech J 31:261–272. https://doi.org/10.1139/t94-031

Fell R, Corominas J, Bonnard C, et al (2008) Guidelines for landslide susceptibility, hazard and risk zoning for land-use planning. Engineering Geology 102:99–111. https://doi.org/10.1016/j.enggeo.2008.03.014

Fressard M, Thiery Y, Maquaire O (2014) Which data for quantitative landslide susceptibility mapping at operational scale? Case study of the Pays d'Auge plateau hillslopes (Normandy, France). Natural Hazards and Earth System Sciences 569–588. https://doi.org/10.5194/nhess-14-569-2014, 2014

Froude, M. J., & Petley, D. N. (2018). Global fatal landslide occurrence from 2004 to 2016. Natural Hazards and Earth System Sciences, 18(8), 2161-2181.

Galanti Y, Barsanti M, Cevasco A, et al (2018) Comparison of statistical methods and multi-time validation for the determination of the shallow landslide rainfall thresholds. Landslides 15:937–952. https://doi.org/10.1007/s10346-017-0919-3

Gallart F, Llorens P, Latron J (1994) Studying the role of old agricultural terraces on runoff generation in a small Mediterranean mountainous basin. Journal of Hydrology 159:291–303. https://doi.org/10.1016/0022-1694(94)90262-3

Gallart F, Llorens P, Latron J, Regüés D (2002) Hydrological processes and their seasonal controls in a small Mediterranean mountain catchment in the Pyrenees. Hydrology and Earth System Sciences 6:527–537. https://doi.org/10.5194/hess-6-527-2002

Galli M, Ardizzone F, Cardinali M, et al (2008) Comparing landslide inventory maps. Geomorphology 94:268–289. https://doi.org/10.1016/j.geomorph.2006.09.023

Gallien L, Douzet R, Pratte S, et al (2012) Invasive species distribution models – how violating the equilibrium assumption can create new insights. Global Ecology and Biogeography 21:1126–1136. https://doi.org/10.1111/j.1466-8238.2012.00768.x

Galve JP, Cevasco A, Brandolini P, et al (2016) Cost-based analysis of mitigation measures for shallow-landslide risk reduction strategies. Engineering Geology 213:142–157. https://doi.org/10.1016/j.enggeo.2016.09.002

Galve JP, Cevasco A, Brandolini P, Soldati M (2015) Assessment of shallow landslide risk mitigation measures based on land use planning through probabilistic modelling. Landslides 12:101–114. https://doi.org/10.1007/s10346-014-0478-9

García-Ruiz JM (2010) The effects of land uses on soil erosion in Spain: A review. CATENA 81:1–11. https://doi.org/10.1016/j.catena.2010.01.001

Gariano SL, Rianna G, Petrucci O, et al (2018) Regional-scale evaluation of past and future impacts of climate and environmental changes in rainfall-induced landslide occurrence. 20:12272

Giammarino S, Giglia G (1990) Gli elementi strutturali della piega di La Spezia nel contesto geodinamico dell'Appennino settentrionale. Boll Soc Geol Ital 109:683–692

Giammarino S, Giglia G, Capponi G, et al (2002) Carta Geologica della Liguria–Scala 1: 200000. Lab Cartografia digitale e GIS del Dipartimento di Scienze della Terra dell'Università di Siena, Litografia Artistica Cartografica, Firenze

Gigli G, Morelli S, Fornera S, Casagli N (2014) Terrestrial laser scanner and geomechanical surveys for the rapid evaluation of rock fall susceptibility scenarios. Landslides 11:1–14. https://doi.org/10.1007/s10346-012-0374-0

Giordan D, Cignetti M, Godone D, et al (2020) A New Procedure for an Effective Management of Geo-Hydrological Risks across the "Sentiero Verde-Azzurro" Trail, Cinque Terre National Park, Liguria (North-Western Italy). Sustainability 12:561. https://doi.org/10.3390/su12020561

Glade T (2003) Landslide occurrence as a response to land use change: a review of evidence from New Zealand. CATENA 51:297–314. https://doi.org/10.1016/S0341-8162(02)00170-4

Goetz JN, Brenning A, Petschko H, Leopold P (2015) Evaluating machine learning and statistical prediction techniques for landslide susceptibility modeling. Computers & Geosciences 81:1–11. https://doi.org/10.1016/j.cageo.2015.04.007

GRASS GIS Development Team (2020) Geographic Resources Analysis Support System (GRASS GIS) Software, Version 7.8

Guadagno FM, Forte R, Revellino P, et al (2005) Some aspects of the initiation of debris avalanches in the Campania Region: the role of morphological slope discontinuities and the development of failure. Geomorphology 66:237–254. https://doi.org/10.1016/j.geomorph.2004.09.024

Guerriero L, Confuorto P, Calcaterra D, et al (2019) PS-driven inventory of town-damaging landslides in the Benevento, Avellino and Salerno Provinces, southern Italy. Journal of Maps 15:619–625. https://doi.org/10.1080/17445647.2019.1651770

Guinau M, Vilajosana I, Vilaplana JM (2007) GIS-based debris flow source and runout susceptibility assessment from DEM data ? a case study in NW Nicaragua. Natural Hazards and Earth System Science 7:703–716

Guisan A, Thuiller W, Zimmermann NE (2017) Habitat Suitability and Distribution Models: with Applications in R. Cambridge University Press

Guo Q, Kelly M, Graham CH (2005) Support vector machines for predicting distribution of Sudden Oak Death in California. Ecological Modelling 182:75–90. https://doi.org/10.1016/j.ecolmodel.2004.07.012

Guzzetti, F. (2000). Landslide fatalities and the evaluation of landslide risk in Italy. Engineering Geology, 58(2), 89-107.

Guzzetti F, Cardinali M, Reichenbach P, et al (2004) Landslides triggered by the 23 November 2000 rainfall event in the Imperia Province, Western Liguria, Italy. Engineering Geology 73:229–245. https://doi.org/10.1016/j.enggeo.2004.01.006

Guzzetti F, Carrara A, Cardinali M, Reichenbach P (1999) Landslide hazard evaluation: a review of current techniques and their application in a multi-scale study, Central Italy. Geomorphology 31:181–216. https://doi.org/10.1016/S0169-555X(99)00078-1

Guzzetti F, Mondini AC, Cardinali M, et al (2012) Landslide inventory maps: New tools for an old problem. Earth-Science Reviews 112:42–66. https://doi.org/10.1016/j.earscirev.2012.02.001

Guzzetti F, Peruccacci S, Rossi M, Stark CP (2008) The rainfall intensity–duration control of shallow landslides and debris flows: an update. Landslides 1:3–17. https://doi.org/10.1007/s10346-007-0112-1

Guzzetti F, Reichenbach P, Ardizzone F, et al (2006) Estimating the quality of landslide susceptibility models. Geomorphology 81:166–184. https://doi.org/10.1016/j.geomorph.2006.04.007

Guzzetti F, Reichenbach P, Cardinali M, et al (2005) Probabilistic landslide hazard assessment at the basin scale. Geomorphology 72:272–299. https://doi.org/10.1016/j.geomorph.2005.06.002

Hair JFj, Black WC, Babin BJ, Anderson RE (2010) Multivariate Data Analysis: A Global Perspective (7th ed.). New Jersey: Pearson Education Inc.

Hanley JA, McNeil BJ (1982) The meaning and use of the area under a receiver operating characteristic (ROC) curve. Radiology 143:29–36. https://doi.org/10.1148/radiology.143.1.7063747

Hansen A (1984) Landslide hazard analysis. Slope instability 523–602

Heim A (1932) Bergsturz und Menschenleben. Fretz&Wasmuth:

Hengl T (2016) Global soil information facilities.

Hengl T, Heuvelink GBM, Rossiter DG (2007) About regression-kriging: From equations to case studies. Computers & Geosciences 33:1301–1315. https://doi.org/10.1016/j.cageo.2007.05.001

Hengl T, Jesus JM de, Heuvelink GBM, et al (2017) SoilGrids250m: Global gridded soil information based on machine learning. PLOS ONE 12:e0169748. https://doi.org/10.1371/journal.pone.0169748

Hervás J, Barredo JI, Rosin PL, et al (2003) Monitoring landslides from optical remotely sensed imagery: the case history of Tessina landslide, Italy. Geomorphology 54:63–75. https://doi.org/10.1016/S0169-555X(03)00056-4

Hervás J, Bobrowsky P (2009) Mapping: Inventories, Susceptibility, Hazard and Risk. In: Sassa K, Canuti P (eds) Landslides – Disaster Risk Reduction. Springer, Berlin, Heidelberg, pp 321–349

Highland L, Bobrowsky P (2008) The Landslide Handbook—A Guide to Understanding Landslides

Hijmans RJ (2012) Cross-validation of species distribution models: removing spatial sorting bias and calibration with a null model. Ecology 93:679–688. https://doi.org/10.1890/11-0826.1

Hirzel AH, Hausser J, Chessel D, Perrin N (2002) Ecological-Niche Factor Analysis: How to Compute Habitat-Suitability Maps Without Absence Data? Ecology 83:2027–2036. https://doi.org/10.1890/0012-9658(2002)083[2027:ENFAHT]2.0.CO;2

Hirzel AH, Helfer V, Metral F (2001) Assessing habitat-suitability models with a virtual species. Ecological Modelling 145:111–121. https://doi.org/10.1016/S0304-3800(01)00396-9

Ho J-Y, Lee KT, Chang T-C, et al (2012) Influences of spatial distribution of soil thickness on shallow landslide prediction. Engineering Geology 124:38–46. https://doi.org/10.1016/j.enggeo.2011.09.013

Hong H, Miao Y, Liu J, Zhu A-X (2019) Exploring the effects of the design and quantity of absence data on the performance of random forest-based landslide susceptibility mapping. CATENA 176:45–64. https://doi.org/10.1016/j.catena.2018.12.035

Hooper A (2008) A multi-temporal InSAR method incorporating both persistent scatterer and small baseline approaches. Geophysical Research Letters 35:. https://doi.org/10.1029/2008GL034654

Hortal J, Jiménez-Valverde A, Gómez JF, et al (2008) Historical bias in biodiversity inventories affects the observed environmental niche of the species. Oikos 117:847–858. https://doi.org/10.1111/j.0030-1299.2008.16434.x

Hsu KJ (1975) Catastrophic debris streams (Sturzstroms) generated by rockfalls. Geological Society of american Bulletin 86:129–140

Hungr O (2001) Review of the classification of landslides of the flow type. Environ Eng Geosci 221–238

Hungr O (1995) A model for the runout analysis of rapid flow slides, debris flows, and avalanches. Can Geotech J 32:610–623. https://doi.org/10.1139/t95-063

Hungr O, Fell R, Couture R, Eberhardt E (2005) Landslide Risk Management. CRC Press

Hungr O, Leroucil S, Picarelli L (2014) The Varnes classification of landslide types, an update. Landslides 11:167–194

Hutchinson JN (1988) General report : Morphological and geotechnical parameters of landslides in relation to geology and hydrogeology. pp 3–35

Infante D, Di Martire D, Confuorto P, et al (2019) Assessment of building behavior in slow-moving landslide-affected areas through DInSAR data and structural analysis. Engineering Structures 199:109638. https://doi.org/10.1016/j.engstruct.2019.109638

Isaac NJB, Pocock MJO (2015) Bias and information in biological records. Biological Journal of the Linnean Society 115:522–531. https://doi.org/10.1111/bij.12532

Iverson RM (2000) Landslide triggering by rain infiltration. Water Resources Research 36:1897–1910. https://doi.org/10.1029/2000WR900090

Iverson RM, Reid ME, LaHusen RG (1997) Debris-Flow Mobilization from Landslides. Annual Review of Earth and Planetary Sciences 25:85–138. https://doi.org/10.1146/annurev.earth.25.1.85

Jaboyedoff M, Oppikofer T, Abellán A, et al (2012) Use of LIDAR in landslide investigations: a review. Nat Hazards 61:5–28. https://doi.org/10.1007/s11069-010-9634-2

Jenks GF (1967) The data model concept in statistical mapping. Israel National Center Registry International Yearbook of Cartography 7, International Cartographic Association University of Ulm, ULMGermany 1967 186–190

Jurgiel B, Verchere P, Tourigny E, Becerra (2020) Profile Tool, QGIS Python Plugins Repository

Kavzoglu T, Sahİn EK, Colkesen I (2015) An assessment of multivariate and bivariate approaches in landslide susceptibility mapping: a case study of Duzkoy district. Natural Hazards 76:471–496

Kim HG, Lee DK, Park C, et al (2018) Estimating landslide susceptibility areas considering the uncertainty inherent in modeling methods. Stoch Environ Res Risk Assess 32:2987–3019. https://doi.org/10.1007/s00477-018-1609-y

Kim MS, Onda Y, Kim JK, Kim SW (2015) Effect of topography and soil parameterisation representing soil thicknesses on shallow landslide modelling. Quaternary International 384:91–106. https://doi.org/10.1016/j.quaint.2015.03.057

Kittur A (2007) Power of Few vs. Wisdom of Crowd : Wikipedia and the Rise of the Bourgeoisie. 25^<th> Annual ACM Conference on Human Factors in Computing Systems, San Jose, United States, April2007

Knoll L, Breuer L, Bach M (2019) Large scale prediction of groundwater nitrate concentrations from spatial data using machine learning. Science of The Total Environment 668:1317–1327. https://doi.org/10.1016/j.scitotenv.2019.03.045

Kornejady A, Ownegh M, Bahremand A (2017) Landslide susceptibility assessment using maximum entropy model with two different data sampling methods. CATENA 152:144–162. https://doi.org/10.1016/j.catena.2017.01.010

Koulouri M, Giourga Chr (2007) Land abandonment and slope gradient as key factors of soil erosion in Mediterranean terraced lands. CATENA 69:274–281. https://doi.org/10.1016/j.catena.2006.07.001

Lagomarsino D, Tofani V, Segoni S, et al (2017) A Tool for Classification and Regression Using Random Forest Methodology: Applications to Landslide Susceptibility Mapping and Soil Thickness Modeling. Environ Model Assess 22:201–214. https://doi.org/10.1007/s10666-016-9538-y

Lasanta T, Nadal-Romero E, Arnáez J (2015) Managing abandoned farmland to control the impact of re-vegetation on the environment. The state of the art in Europe. Environmental Science & Policy 52:99–109. https://doi.org/10.1016/j.envsci.2015.05.012

Lasanta-Martínez T, Vicente-Serrano SM, Cuadrat-Prats JM (2005) Mountain Mediterranean landscape evolution caused by the abandonment of traditional primary activities: a study of the

Spanish Central Pyrenees. Applied Geography 25:47–65. https://doi.org/10.1016/j.apgeog.2004.11.001

Lee S, Ryu J-H, Won J-S, Park H-J (2004) Determination and application of the weights for landslide susceptibility mapping using an artificial neural network. Engineering Geology 71:289–302. https://doi.org/10.1016/S0013-7952(03)00142-X

Lesschen JP, Cammeraat LH, Nieman T (2008) Erosion and terrace failure due to agricultural land abandonment in a semi-arid environment. Earth Surface Processes and Landforms 33:1574–1584. https://doi.org/10.1002/esp.1676

Lomba A, Pellissier L, Randin C, et al (2010) Overcoming the rare species modelling paradox: A novel hierarchical framework applied to an Iberian endemic plant. Biological Conservation 143:2647–2657. https://doi.org/10.1016/j.biocon.2010.07.007

Lombardo L, Bachofer F, Cama M, et al (2016) Exploiting Maximum Entropy method and ASTER data for assessing debris flow and debris slide susceptibility for the Giampilieri catchment (north-eastern Sicily, Italy). Earth Surface Processes and Landforms 41:1776–1789. https://doi.org/10.1002/esp.3998

Lombardo L, Bakka H, Tanyas H, et al (2019a) Geostatistical Modeling to Capture Seismic-Shaking Patterns From Earthquake-Induced Landslides. Journal of Geophysical Research: Earth Surface 124:1958–1980. https://doi.org/10.1029/2019JF005056

Lombardo L, Cama M, Maerker M, Rotigliano E (2014) A test of transferability for landslides susceptibility models under extreme climatic events: application to the Messina 2009 disaster. Natural Hazards: Journal of the International Society for the Prevention and Mitigation of Natural Hazards 74:1951–1989

Lombardo L, Opitz T, Ardizzone F, et al (2020a) Space-time landslide predictive modelling. Earth-Science Reviews 209:103318. https://doi.org/10.1016/j.earscirev.2020.103318

Lombardo L, Opitz T, Ardizzone F, et al (2020b) Space-time landslide predictive modelling. Earth-Science Reviews 209:103318. https://doi.org/10.1016/j.earscirev.2020.103318

Lombardo L, Opitz T, Huser R (2018) Point process-based modeling of multiple debris flow landslides using INLA: an application to the 2009 Messina disaster. Stoch Environ Res Risk Assess 32:2179–2198. https://doi.org/10.1007/s00477-018-1518-0

Lombardo L, Opitz T, Huser R (2019b) Numerical Recipes for Landslide Spatial Prediction Using R-INLA: A Step-by-Step Tutorial. In: Pourghasemi HR, Gokceoglu C (eds) Spatial Modeling in GIS and R for Earth and Environmental Sciences. Elsevier, pp 55–83

Lombardo L, Tanyas H, Huser R, et al (2021) Landslide size matters: A new data-driven, spatial prototype. Engineering Geology 293:106288. https://doi.org/10.1016/j.enggeo.2021.106288

MacDonald D, Crabtree JR, Wiesinger G, et al (2000) Agricultural abandonment in mountain areas of Europe: Environmental consequences and policy response. Journal of Environmental Management 59:47–69. https://doi.org/10.1006/jema.1999.0335

Malamud BD, Turcotte DL, Guzzetti F, Reichenbach P (2004) Landslides, earthquakes, and erosion. Earth and Planetary Science Letters 229:45–59. https://doi.org/10.1016/j.epsl.2004.10.018

Martha TR, Kerle N, Jetten V, et al (2010) Characterising spectral, spatial and morphometric properties of landslides for semi-automatic detection using object-oriented methods. Geomorphology 116:24–36. https://doi.org/10.1016/j.geomorph.2009.10.004

McPherson JM, Jetz W, Rogers DJ (2004) The effects of species' range sizes on the accuracy of distribution models: ecological phenomenon or statistical artefact? Journal of Applied Ecology 41:811–823. https://doi.org/10.1111/j.0021-8901.2004.00943.x

Melo R, Zêzere JL, Rocha J, Oliveira SC (2019) Combining data-driven models to assess susceptibility of shallow slides failure and run-out. Landslides 16:2259–2276. https://doi.org/10.1007/s10346-019-01235-2

Mergili M, Schwarz L, Kociu A (2019) Combining release and runout in statistical landslide susceptibility modeling. Landslides 16:2151–2165. https://doi.org/10.1007/s10346-019-01222-7

Mondini AC, Guzzetti F, Reichenbach P, et al (2011) Semi-automatic recognition and mapping of rainfall induced shallow landslides using optical satellite images. Remote Sensing of Environment 115:1743–1757. https://doi.org/10.1016/j.rse.2011.03.006

Moore ID, Wilson JP (1992) Length-slope factors for the Revised Universal Soil Loss Equation: Simplified method of estimation. Journal of Soil and Water Conservation 47:423–428

Moreno-de-las-Heras M, Lindenberger F, Latron J, et al (2019) Hydro-geomorphological consequences of the abandonment of agricultural terraces in the Mediterranean region: Key controlling factors and landscape stability patterns. Geomorphology 333:73–91. https://doi.org/10.1016/j.geomorph.2019.02.014

Morgan RPC (2009) Soil Erosion and Conservation. John Wiley & Sons

Nemčok A, Pašek J, Rybář J (1972) Classification of landslides and other mass movements. Rock Mechanics 4:71–78. https://doi.org/10.1007/BF01239137

Novellino A, Cesarano M, Cappelletti P, et al (2021) Slow-moving landslide risk assessment combining Machine Learning and InSAR techniques. CATENA 203:105317. https://doi.org/10.1016/j.catena.2021.105317

Parise M (2001) Landslide mapping techniques and their use in the assessment of the landslide hazard. Physics and Chemistry of the Earth, Part C: Solar, Terrestrial & Planetary Science 26:697–703. https://doi.org/10.1016/S1464-1917(01)00069-1

Park HJ, Jang JY, Lee JH (2019) Assessment of rainfall-induced landslide susceptibility at the regional scale using a physically based model and fuzzy-based Monte Carlo simulation. Landslides 16:695–713. https://doi.org/10.1007/s10346-018-01125-z

Peckham SD (2011) Profile, Plan and Streamline Curvature: A Simple Derivation and Applications. Proceedings of Geomorphometry 4

Peh KK, Lim CP, Quek SS, Khoh KH (2000) Use of Artificial Neural Networks to Predict Drug Dissolution Profiles and Evaluation of Network Performance Using Similarity Factor. Pharm Res 17:1384–1389. https://doi.org/10.1023/A:1007578321803

Pepe G, Mandarino A, Raso E, et al (2019) Investigation on Farmland Abandonment of Terraced Slopes Using Multitemporal Data Sources Comparison and Its Implication on Hydro-Geomorphological Processes. Water 11:1552. https://doi.org/10.3390/w11081552

Persichillo MG, Bordoni M, Meisina C, et al (2016) Shallow landslide susceptibility analysis in relation to land use scenarios. Landslides and Engineered Slopes Experience, Theory and Practice 8

Persichillo MG, Bordoni M, Meisina C, et al (2017a) Shallow landslides susceptibility assessment in different environments. Geomatics, Natural Hazards and Risk 8:748–771. https://doi.org/10.1080/19475705.2016.1265011

Persichillo MG, Bordoni M, Meisina C, et al (2017b) Remarks on the Role of Landslide Inventories in the Statistical Methods Used for the Landslide Susceptibility Assessment. In: Mikos M, Tiwari B, Yin Y, Sassa K (eds) Advancing Culture of Living with Landslides. Springer International Publishing, Cham, pp 759–766

Peterson AT, Papeş M, Soberón J (2008) Rethinking receiver operating characteristic analysis applications in ecological niche modeling. Ecological Modelling 213:63–72. https://doi.org/10.1016/j.ecolmodel.2007.11.008

Phillips SJ, Anderson RP, Schapire RE (2006) Maximum entropy modeling of species geographic distributions. Ecological Modelling 190:231–259. https://doi.org/10.1016/j.ecolmodel.2005.03.026

Piacentini T, Galli A, Marsala V, Miccadei E (2018) Analysis of Soil Erosion Induced by Heavy Rainfall: A Case Study from the NE Abruzzo Hills Area in Central Italy. Water 10:1314. https://doi.org/10.3390/w10101314

Piccarreta M, Pasini A, Capolongo D, Lazzari M (2013) Changes in daily precipitation extremes in the Mediterranean from 1951 to 2010: the Basilicata region, southern Italy. International Journal of Climatology 33:3229–3248. https://doi.org/10.1002/joc.3670

Pierson TC, Costa J (1987) A rheologic classification of subaerial sediment-water flows. Geological Society of America

Pijanowski BC, Brown DG, Shellito BA, Manik GA (2002) Using neural networks and GIS to forecast land use changes: a Land Transformation Model. Computers, Environment and Urban Systems 26:553–575. https://doi.org/10.1016/S0198-9715(01)00015-1

Poiraud A (2014) Landslide susceptibility–certainty mapping by a multi-method approach: A case study in the Tertiary basin of Puy-en-Velay (Massif central, France). Geomorphology 216:208–224. https://doi.org/10.1016/j.geomorph.2014.04.001

Pourghasemi HR, Kornejady A, Kerle N, Shabani F (2020) Investigating the effects of different landslide positioning techniques, landslide partitioning approaches, and presence-absence balances on landslide susceptibility mapping. CATENA 187:104364. https://doi.org/10.1016/j.catena.2019.104364

Pourghasemi HR, Yousefi S, Kornejady A, Cerdà A (2017) Performance assessment of individual and ensemble data-mining techniques for gully erosion modeling. Science of The Total Environment 609:764–775. https://doi.org/10.1016/j.scitotenv.2017.07.198

Poyatos R, Latron J, Llorens P (2003) Land Use and Land Cover Change After Agricultural Abandonment. mred 23:362–368. https://doi.org/10.1659/0276-4741(2003)023[0362:LUALCC]2.0.CO;2

Pradhan AMS, Kang H-S, Lee S, Kim Y-T (2017) Spatial model integration for shallow landslide susceptibility and its runout using a GIS-based approach in Yongin, Korea. Geocarto International 32:420–441. https://doi.org/10.1080/10106049.2016.1155658

Promper C, Puissant A, Malet J-P, Glade T (2014) Analysis of land cover changes in the past and the future as contribution to landslide risk scenarios. Applied Geography 53:11–19. https://doi.org/10.1016/j.apgeog.2014.05.020

R Core Team (2021) R: A language and environment for statistical computing

Raes N, Aguirre Gutierrez J (2018) A Modeling Framework to Estimate and Project Species Distributions in Space and Time. Wiley

Raso E, Cevasco A, Martire DD, et al (2019a) Landslide-inventory of the Cinque Terre National Park (Italy) and quantitative interaction with the trail network. Journal of Maps 15:818–830. https://doi.org/10.1080/17445647.2019.1657511

Raso E, Di Martire D, Cevasco A, et al (2020a) Evaluation of prediction capability of the MaxEnt and Frequency Ratio methods for landslide susceptibility in the Vernazza catchment (Cinque Terre, Italy). In: De Maio M, Tiwari AK (eds) Applied Geology: Approaches to Future Resource Management. Springer International Publishing, Cham, pp 299–316

Raso E, Mandarino A, Pepe G, et al (2020b) Geomorphology of Cinque Terre National Park (Italy). Journal of Maps 0:1–14. https://doi.org/10.1080/17445647.2020.1837270

Raso E, Mandarino A, Pepe G, et al (2019b) Landslide Inventory of the Cinque Terre National Park, Italy. In: Shakoor A, Cato K (eds) IAEG/AEG Annual Meeting Proceedings, San Francisco, California, 2018 - Volume 1. Springer International Publishing, Cham, pp 201–205

Raspini F, Bardi F, Bianchini S, et al (2017) The contribution of satellite SAR-derived displacement measurements in landslide risk management practices. Nat Hazards 86:327–351. https://doi.org/10.1007/s11069-016-2691-4

Rau J-Y, Jhan J-P, Rau R-J (2014) Semiautomatic Object-Oriented Landslide Recognition Scheme From Multisensor Optical Imagery and DEM. IEEE Transactions on Geoscience and Remote Sensing 52:1336–1349. https://doi.org/10.1109/TGRS.2013.2250293

Reddy S, Dávalos LM (2003) Geographical sampling bias and its implications for conservation priorities in Africa. Journal of Biogeography 30:1719–1727. https://doi.org/10.1046/j.1365-2699.2003.00946.x

Reichenbach P, Rossi M, Malamud BD, et al (2018) A review of statistically-based landslide susceptibility models. Earth-Science Reviews 180:60–91. https://doi.org/10.1016/j.earscirev.2018.03.001

Revellino P, Guadagno F, Hungr O (2008) Morphological methods and dynamic modelling in landslide hazard assessment of the Campania Apennine carbonate slope. Landslides 5:59–70. https://doi.org/10.1007/s10346-007-0103-2

Roberts DR, Bahn V, Ciuti S, et al (2017) Cross-validation strategies for data with temporal, spatial, hierarchical, or phylogenetic structure. Ecography 40:913–929. https://doi.org/10.1111/ecog.02881

Rollando G (2003) Vernazza nell'Ottocento. Notizie dagli Archivi del paese. Parco Nazionale delle Cinque Terre.

Rotigliano E, Agnesi V, Cappadonia C, Conoscenti C (2011) The role of the diagnostic areas in the assessment of landslide susceptibility models: a test in the sicilian chain. Natural Hazards: Journal of the International Society for the Prevention and Mitigation of Natural Hazards 58:981–999

Rue H, Martino S, Chopin N (2009) Approximate Bayesian inference for latent Gaussian models by using integrated nested Laplace approximations. Journal of the Royal Statistical Society: Series B (Statistical Methodology) 71:319–392. https://doi.org/10.1111/j.1467-9868.2008.00700.x

Rue H, Riebler A, Sørbye SH, et al (2017) Bayesian Computing with INLA: A Review. Annual Review of Statistics and Its Application 4:395–421. https://doi.org/10.1146/annurev-statistics-060116-054045

Sadr MP, Maghsoudi A, Saljoughi BS (2014) Landslide susceptibility mapping of komroud sub-basin using Fuzzy logic approach. In: Geodynamics Res Int Bulletin. 2

Sarno Basin Authority (2011) Hydrogeological Setting Plan (update) - General technical report with reference to the geological and geomorphological aspects of the territories in the province of Naples

Schilirò L, Cevasco A, Esposito C, Mugnozza GS (2017) Role of Land Use in Landslide Initiation on Terraced Slopes: Inferences from Numerical Modelling. In: Mikoš M, Casagli N, Yin Y, Sassa K (eds) Advancing Culture of Living with Landslides. Springer International Publishing, Cham, pp 315–320

Schilirò L, Cevasco A, Esposito C, Mugnozza GS (2018) Shallow landslide initiation on terraced slopes: inferences from a physically based approach. Geomatics, Natural Hazards and Risk 9:295–324. https://doi.org/10.1080/19475705.2018.1430066

Scopesi C, Olivari S, Firpo M, et al (2020) Land capability classification of Vernazza catchment, Cinque Terre National Park, Italy. Journal of Maps 16:357–362. https://doi.org/10.1080/17445647.2020.1750067

Scott KM, Vallance JW, Kerle N, et al (2005) Catastrophic precipitation-triggered lahar at Casita volcano, Nicaragua: occurrence, bulking and transformation. Earth Surface Processes and Landforms 30:59–79. https://doi.org/10.1002/esp.1127

Seeger M, Rodrigo-Comino J, Iserloh T, et al (2019) Dynamics of Runoff and Soil Erosion on Abandoned Steep Vineyards in the Mosel Area, Germany. Water 11:2596. https://doi.org/10.3390/w11122596

Segoni S, Lagomarsino D, Fanti R, et al (2015) Integration of rainfall thresholds and susceptibility maps in the Emilia Romagna (Italy) regional-scale landslide warning system. Landslides 12:773–785. https://doi.org/10.1007/s10346-014-0502-0

Segoni S, Pappafico G, Luti T, Catani F (2020) Landslide susceptibility assessment in complex geological settings: sensitivity to geological information and insights on its parameterization. Landslides 17:2443–2453. https://doi.org/10.1007/s10346-019-01340-2

Segoni S, Rossi G, Catani F (2012) Improving basin scale shallow landslide modelling using reliable soil thickness maps. Nat Hazards 61:85–101. https://doi.org/10.1007/s11069-011-9770-3

Seneviratne S, Nicholls N, Easterling D, et al (2012) Changes in climate extremes and their impacts on the natural physical environment. 109–230. https://doi.org/10.7916/d8-6nbt-s431

Sharma A, Tiwari KN, Bhadoria PBS (2011) Effect of land use land cover change on soil erosion potential in an agricultural watershed. Environ Monit Assess 173:789–801. https://doi.org/10.1007/s10661-010-1423-6

Sidle RC, Ochiai H (2006) Landslides: processes, prediction, and land use. American Geophysical Union, Washington, DC

Simpson D, Rue H, Riebler A, et al (2017) Penalising Model Component Complexity: A Principled, Practical Approach to Constructing Priors. https://doi.org/10.1214/16-STS576

Soeters R, van Westen CJ (1996) Slope instability recognition, analysis, and zonation. In: Landslides, investigation and mitigation (Transportation Research Board, National Research Council, Special Report ; 247). National Academy Press, pp 129–177

Somodi I, Lepesi N, Botta-Dukát Z (2017) Prevalence dependence in model goodness measures with special emphasis on true skill statistics. Ecology and Evolution 7:863–872. https://doi.org/10.1002/ece3.2654

Stanchi S, Freppaz M, Agnelli A, et al (2012) Properties, best management practices and conservation of terraced soils in Southern Europe (from Mediterranean areas to the Alps): A review. Quaternary International 265:90–100. https://doi.org/10.1016/j.quaint.2011.09.015

Steger S, Bell R, Petschko H, Glade T (2015) Evaluating the Effect of Modelling Methods and Landslide Inventories Used for Statistical Susceptibility Modelling. In: Lollino G, Giordan D, Crosta GB, et al. (eds) Engineering Geology for Society and Territory - Volume 2. Springer International Publishing, Cham, pp 201–204

Steger S, Brenning A, Bell R, Glade T (2016) The propagation of inventory-based positional errors into statistical landslide susceptibility models. Natural Hazards and Earth System Sciences 16:2729–2745. https://doi.org/10.5194/nhess-16-2729-2016

Steger S, Glade T (2017) The Challenge of "Trivial Areas" in Statistical Landslide Susceptibility Modelling. In: Mikos M, Tiwari B, Yin Y, Sassa K (eds) Advancing Culture of Living with Landslides. Springer International Publishing, Cham, pp 803–808

Steger S, Mair V, Kofler C, et al (2021) Correlation does not imply geomorphic causation in data-driven landslide susceptibility modelling – Benefits of exploring landslide data collection effects. Science of The Total Environment 776:145935. https://doi.org/10.1016/j.scitotenv.2021.145935

Stumpf A, Kerle N (2011) Object-oriented mapping of landslides using Random Forests. Remote Sensing of Environment 115:2564–2577. https://doi.org/10.1016/j.rse.2011.05.013

Süzen ML, Doyuran V (2004) A comparison of the GIS based landslide susceptibility assessment methods: multivariate versus bivariate. Env Geol 45:665–679. https://doi.org/10.1007/s00254-003-0917-8

Swets JA (1988) Measuring the accuracy of diagnostic systems. Science 240:1285–1293. https://doi.org/10.1126/science.3287615

Tanyas H, Rossi M, Alvioli M, et al (2019) A global slope unit-based method for the near real-time prediction of earthquake-induced landslides. Geomorphology 327:126–146. https://doi.org/10.1016/j.geomorph.2018.10.022

Tarolli P, Preti F, Romano N (2014) Terraced landscapes: From an old best practice to a potential hazard for soil degradation due to land abandonment. Anthropocene 6:10–25. https://doi.org/10.1016/j.ancene.2014.03.002

Tarolli P, Rizzo D, Brancucci G (2019) Terraced Landscapes: Land Abandonment, Soil Degradation, and Suitable Management. In: Varotto M, Bonardi L, Tarolli P (eds) World Terraced Landscapes: History, Environment, Quality of Life. Springer International Publishing, Cham, pp 195–210

Terranova R (1984) Aspetti geomorfologici e geologico-ambientali delle Cinque Terre: rapporti con le opere umane (Liguria orientale). Studi e ricerche di geografia Genova 7:39–89

Terranova R (1989) Il paesaggio costiero terrazzato delle Cinque Terre in Liguria

Terranova R (1987) Guida all'escursione lungo la costa della Liguria orientale (25/6/87)

Terranova R (2005) L'abbandono dei versanti montani terrazzati ei dissesti geomorfologici: una grave perdita di valori ambientali di grande pregio. a valorizzazione turistica dello spazio fisico come via alla salvaguardia ambientale Studi regionali e monografici Patron, Bologna 36:129–143

Terranova R, Brandolini P, Spotorno M, et al (2002) Patrimoni de marjades a la Mediterrania Occidental. Una proposta de catalogaciò. Commissio Europea DGX, Programa Raphael, Palma di Mallorca: Fodesma

Terranova R, Zanzucchi G, Bernini M, et al (2006) Geologia, geomorfologia e vini del parco Nazionale delle Cinque Terre (Liguria, Italia). Bollettino della Società Geologica Italiana Spec, 6, 115–128

Terzaghi K (1950) Mechanisms of landslides. Geological Society of America, Berkley Volume 83:83–123

Thuiller W, Georges D, Engler R, Breiner F (2016) Biomod2: ensemble platform for species distribution modeling

Thuiller W, Lafourcade B, Engler R, Araújo MB (2009) BIOMOD – a platform for ensemble forecasting of species distributions. Ecography 32:369–373. https://doi.org/10.1111/j.1600-0587.2008.05742.x

Trigila A, Iadanza C, Esposito C, Scarascia-Mugnozza G (2015) Comparison of Logistic Regression and Random Forests techniques for shallow landslide susceptibility assessment in Giampilieri (NE Sicily, Italy). Geomorphology 249:119–136. https://doi.org/10.1016/j.geomorph.2015.06.001

Trigila A, Iadanza C, Rischia I (2007) Metodologia di lavoro e struttura della banca dati (In Italian). 28

Turan ID, Özkan B, Türkeş M, Dengiz O (2020) Landslide susceptibility mapping for the Black Sea Region with spatial fuzzy multi-criteria decision analysis under semi-humid and humid terrestrial ecosystems. Theoretical and Applied Climatology 140:1233–1246. https://doi.org/10.1007/s00704-020-03126-2

Umar Z, Pradhan B, Ahmad A, et al (2014) Earthquake induced landslide susceptibility mapping using an integrated ensemble frequency ratio and logistic regression models in West Sumatera Province, Indonesia. CATENA 118:124–135. https://doi.org/10.1016/j.catena.2014.02.005

Van Den Eeckhaut M, Poesen J, Verstraeten G, et al (2005) The effectiveness of hillshade maps and expert knowledge in mapping old deep-seated landslides. Geomorphology 67:351–363. https://doi.org/10.1016/j.geomorph.2004.11.001

Van Den Eeckhaut M, Reichenbach P, Guzzetti F, et al (2009) Combined landslide inventory and susceptibility assessment based on different mapping units: an example from the Flemish Ardennes, Belgium. Natural Hazards and Earth System Sciences 9:507–521. https://doi.org/10.5194/nhess-9-507-2009

van Westen CJ, Castellanos E, Kuriakose SL (2008) Spatial data for landslide susceptibility, hazard, and vulnerability assessment: An overview. Engineering Geology 102:112–131. https://doi.org/10.1016/j.enggeo.2008.03.010

van Westen CJ, Rengers N, Soeters R (2003) Use of Geomorphological Information in Indirect Landslide Susceptibility Assessment. Natural Hazards 30:399–419. https://doi.org/10.1023/B:NHAZ.0000007097.42735.9e

van Westen CJ, Rengers N, Terlien MTJ, Soeters R (1997) Prediction of the occurrence of slope instability phenomenal through GIS-based hazard zonation. Geol Rundsch 86:404–414. https://doi.org/10.1007/s005310050149

van Westen CJ, van Asch TWJ, Soeters R (2006) Landslide hazard and risk zonation—why is it still so difficult? Bull Eng Geol Environ 65:167–184. https://doi.org/10.1007/s10064-005-0023-0

van Westen CJ, van Duren IC, Kruse HMG, Terlien MTJ (1993) GISSIZ : training package for Geographic Information Systems in slope instability zonation : Part 1. theory Part 2. exercises. International Institute for Geo-Information Science and Earth Observation

Varnes DJ (1978) Slope movement types and processes. Landslides : Analysis and Control

Vorpahl P, Elsenbeer H, Märker M, Schröder B (2012) How can statistical models help to determine driving factors of landslides? Ecological Modelling 239:27–39. https://doi.org/10.1016/j.ecolmodel.2011.12.007

Wang Q, Wang D, Huang Y, et al (2015) Landslide Susceptibility Mapping Based on Selected Optimal Combination of Landslide Predisposing Factors in a Large Catchment. Sustainability 7:16653–16669. https://doi.org/10.3390/su71215839

Watts N, Amann M, Arnell N, et al (2021) The 2020 report of The Lancet Countdown on health and climate change: responding to converging crises. The Lancet 397:129–170. https://doi.org/10.1016/S0140-6736(20)32290-X

Wilson JP, Gallant JC (2000) Digital terrain analysis

Wistuba M, Malik I, Wójcicki K, Michałowicz P (2015) Coupling between landslides and eroding stream channels reconstructed from spruce tree rings (examples from the Carpathians and Sudetes – Central Europe). Earth Surface Processes and Landforms 40:293–312. https://doi.org/10.1002/esp.3632

WP/WLI (1991) A suggested method for a landslide summary. Bulletin of the International Association of Engineering Geology 43:101–110. https://doi.org/10.1007/BF02590177

WP/WLI (1993) A suggested method for describing the activity of a landslide. Bulletin of the International Association of Engineering Geology 47:101–110

Xiao T, Yin K, Yao T, Liu S (2019) Spatial prediction of landslide susceptibility using GIS-based statistical and machine learning models in Wanzhou County, Three Gorges Reservoir, China. Acta Geochim 38:654–669. https://doi.org/10.1007/s11631-019-00341-1

Yalcin A (2008) GIS-based landslide susceptibility mapping using analytical hierarchy process and bivariate statistics in Ardesen (Turkey): Comparisons of results and confirmations. CATENA 72:1–12. https://doi.org/10.1016/j.catena.2007.01.003

Yalcin A, Reis S, Aydinoglu AC, Yomralioglu T (2011) A GIS-based comparative study of frequency ratio, analytical hierarchy process, bivariate statistics and logistics regression methods for landslide susceptibility mapping in Trabzon, NE Turkey. CATENA 85:274–287. https://doi.org/10.1016/j.catena.2011.01.014

Yao X, Tham LG, Dai FC (2008) Landslide susceptibility mapping based on Support Vector Machine: A case study on natural slopes of Hong Kong, China. Geomorphology 101:572–582. https://doi.org/10.1016/j.geomorph.2008.02.011

Yilmaz I (2010) Comparison of landslide susceptibility mapping methodologies for Koyulhisar, Turkey: conditional probability, logistic regression, artificial neural networks, and support vector machine. Environ Earth Sci 61:821–836. https://doi.org/10.1007/s12665-009-0394-9

Zaniewski AE, Lehmann A, Overton JM (2002) Predicting species spatial distributions using presence-only data: a case study of native New Zealand ferns. Ecological Modelling 157:261–280. https://doi.org/10.1016/S0304-3800(02)00199-0

Zhao C, Zhang Q, He Y, et al (2016) Small-scale loess landslide monitoring with small baseline subsets interferometric synthetic aperture radar technique—case study of Xingyuan landslide, Shaanxi, China. JARS 10:026030. https://doi.org/10.1117/1.JRS.10.026030

Zhu A-X, Miao Y, Yang L, et al (2018) Comparison of the presence-only method and presence-absence method in landslide susceptibility mapping. CATENA 171:222–233. https://doi.org/10.1016/j.catena.2018.07.012

Zingaro M, Refice A, Giachetta E, et al (2019) Sediment mobility and connectivity in a catchment: A new mapping approach. Science of The Total Environment 672:763–775. https://doi.org/10.1016/j.scitotenv.2019.03.461

Zurada JM (1992) Introduction to artificial neural network systems. West Publishing Company 58